SOLVENT EFFECTS ON PUSH PULL ETHYLENES

AN NMR STUDY

ON

SOLVENT EFFECTS ON THE CHEMICAL EXCHANGE OF A PUSH PULL ETHYLENES

By

MAYSOON KHASAWNEH, B. A.

A Thesis

Submitted to the school of graduate studies

in Partial fulfillment of the requirements

for the degree

Master of science

McMaster University

September 20, 2004

MASTER OF SCIENCE (2004)	**MCMASTER UNIVERSITY**
(CHEMISTRY)	HAMILTON, ON.
TITLE:	An NMR study on solvent effects on chemical exchange of a push-pull ethylene
AUTHOR:	Maysoon Khasawneh, B.Sc. (Kent State University)
SUPERVISOR:	Professor A.D. Bain
NUMBER OF PAGES:	x, 154

ABSTRACT

Solvent effects on the chemical exchange of a push pull Ethylenes

Chemical exchange rates provide a sensitive probe of solvent effects in solution. The push–pull ethylene methyl 3-dimethylamino-2-cyanocrotonate (MDACC) has three exchange processes E-Z (the same as E'-Z'), E-E', and Z-Z', and we have measured these rates in acetone-d_6, chloroform-d, tetrahydrofuran-d_8, toluene-d_8, methanol-d_4, acetonitrile-d_3, and methylene chloride-d_2 through 1D ^{1}H.NMR at different temperatures. From this we obtain $\Delta G^{\ddagger}$, $\Delta H^{\ddagger}$, $\Delta S^{\ddagger}$ of activation for each solvent by employing an Eyring plot. As the solvent changes, $\Delta H^{\ddagger}$ is approximately constant whereas $\Delta S^{\ddagger}$ follows the solvent polarity .

Since the equilibrium constant is less than one, we would expect it to increase with temperature, but it decreases. This is seen in the Van't Hoff plot where the slope is positive indicating that the process of going from the major site to the minor site is exothermic, so not only is the rate governed by entropy effects, but also the equilibrium constant between E and Z.

The rotation between the C-N and the C=C bond occurs through a non-concerted mechanism. Two reasons why this occurred was apparent through EXSY, since the intensity of the off diagonal peak varies with different mixing time and second, the rates from C=C rotation (E-Z) and C-N rotations (E-E' and Z-Z') are different at the same temperature

ACKNOWLEDGEMENTS

I would like to extend my sincerest appreciation to my supervisor, Dr. Alex D. Bain, for his patience, support, and encouragement over the years that I had the privilege to work with him. I would also like to thank Dr. Donald Hughes and Mr. Brian Sayer for their support and assistance in the NMR lab. I would like to thank Mrs. Carol Dada for her understanding, great support and advice, Dr. Gillian Goward, for her great assistance and valuable discussions, Dr. Giuseppe Melacini, for his assistance, Dr. Barbara Russer for her assistance and advice, and the people of the chemistry department at McMaster University. I would like to thank Ms. Marzia Bianchi for her great help, hard work, and excellent support, and Ms. Blythe Erin Fortier-McGill for her excellent help, and hard work. I would also like to extend a warm thank you to Dr. Peter L. Rinaldi for inspiring me to pursue spectroscopy and having taught me NMR.

I would also like to thank my parents and my family who have never failed to support me through my university career.

Finally, I would like to express my deepest appreciation to my husband Adnan, my kids; Thamer, Adam, and Imran for their patience, understanding and support, and it is to them I dedicate this work.

TABLE OF CONTENTS

LIST OF TABLES

LIST OF FIGURES

Chapter 1

INTRODUCTION

Nuclear magnetic resonance, or NMR as it is abbreviated by scientists, is a phenomenon which occurs when the nuclei of certain atoms are immersed in a static magnetic field and exposed to a second oscillating magnetic field.[1] Some nuclei experience this phenomenon, and others do not, dependent upon whether they possess a property called spin. Because all nuclei are positively charged and we know from physics that moving charged particles produce a magnetic field, these nuclei must have an associated magnetic field (Figure 1).

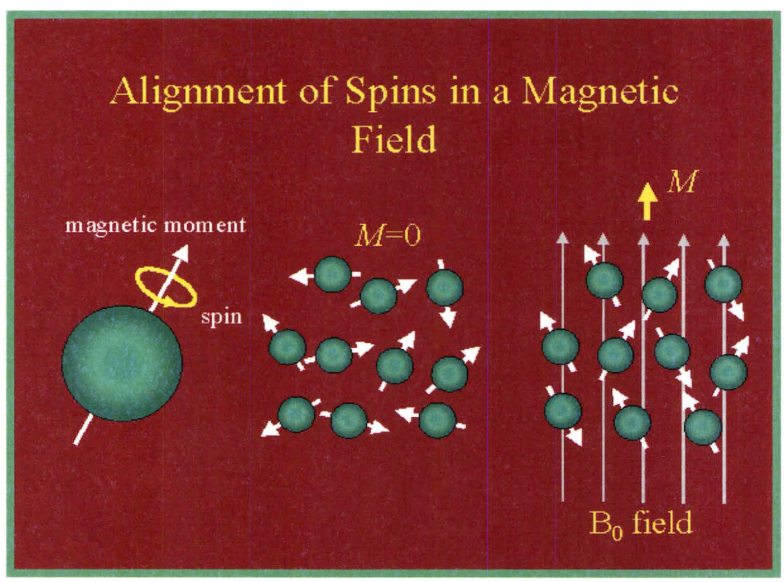

Figure 1. How the nuclei behave in the presence and absence of a magnetic field

Most of the matter we can examine with NMR is composed of molecules. Molecules are composed of atoms, for example,[2] water molecules. Each water molecule has one oxygen and two hydrogen atoms. If we zoom into one of the hydrogens (Figure 2) past the electron cloud we see a nucleus composed of a single proton.

Figure 2. H_2O molecule

The proton possesses a property called spin which can be thought of as a small magnetic field, and will cause the nucleus to produce an NMR signal (Figure 3).

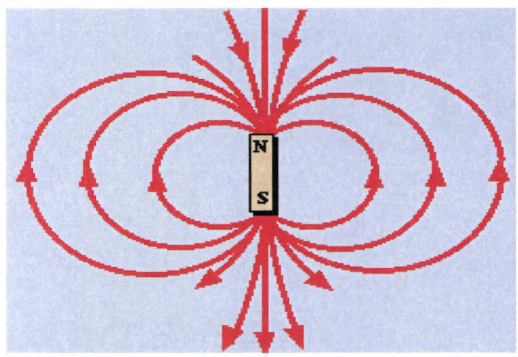

Figure 3. Magnetic field produced by proton

A convenient measure of this field is its magnetic moment, which seems to arise when the spins of the protons and neutrons in the nucleus are not paired. When the number of protons is an even number and is equal to the number of neutrons in the nucleus, the spins are paired and the nucleus has no magnetic moment. The spin quantum number, which characterizes the magnetic moment, is then zero and the nucleus cannot absorb energy in a magnetic field. For other nuclei, the spin quantum number can have any value that is a multiple of ½. (table 1) For example, the ^{13}C nucleus, ^{119}Sn, ^{31}P, and ^{19}F nuclei all have a spin quantum number of 1/2 , whereas the ^{14}N nucleus has a quantum number of 1, ^{11}B is 3/2, and ^{73}Ge is 9/2. Fortunately, each different isotope with a spin quantum number of 1/2 or greater absorbs radiation of a different frequency in a constant magnetic field.

Mass Number	Atomic Number	Spin Number
Odd	Even or odd	$\frac{1}{2}, \frac{3}{2}, \frac{5}{2}$
Even	Even	0
Even	Odd	1,2,3

Table 1. Relation among Mass, Atomic and Spin number

Spectroscopy is the study of the interaction of electromagnetic radiation with matter. Nuclear magnetic resonance spectroscopy is the use of the NMR phenomenon to study physical, chemical, and biological properties of matter. As a consequence, NMR spectroscopy finds applications in several areas of science. NMR spectroscopy is a powerful tool and routinely used in most field of chemistry (organic, inorganic, analytical, physical biochemistry and physics), and has increased application in polymer chemistry, pharmaceutical applications, biological, biomedical and material science.

Several NMR techniques involve combinations of radio-frequency pulses, time delays, selective irradiation of peaks and polarization transfer. NMR techniques are used to study chemical structure and to probe kinetic and thermodynamic data using simple one-dimensional techniques. The only information that can be easily obtained from one-dimensional (The basic 1D NMR experiment consists of exciting the nuclei with a single pulse then receiving the free induction decay (FID). The FID is then Fourier transformed to yield the spectrum. This is usually the type of experiment used for ^{1}H Proton NMR) are chemical shifts, scalar coupling constants and integrals. For

example, the one dimensional ^{1}H NMR spectrum for ethanol (Figure 4) contains a wealth of information that can help us to elucidate the structure. As we can see from the spectrum there are three signals, two of which are in part split up into several lines. The three signals at 1.26ppm, 3.75ppm, and 4.88 ppm can be assigned to the CH_3, CH_2, and OH protons, respectively. The assignment was done based on the chemical shifts.[3] In other words, the electrons in a molecule surround the nuclei and create a small magnetic field which shields the nuclei slightly from the external field. Therefore, the Larmor frequencies of different nuclei vary due to their chemical environment.[4;5] This effect is called "chemical shift" (Figure 5). It is one of the major parameters of NMR spectroscopy since it causes the different positions of the signals in a NMR spectrum (Table 2 and 3).[2;6]

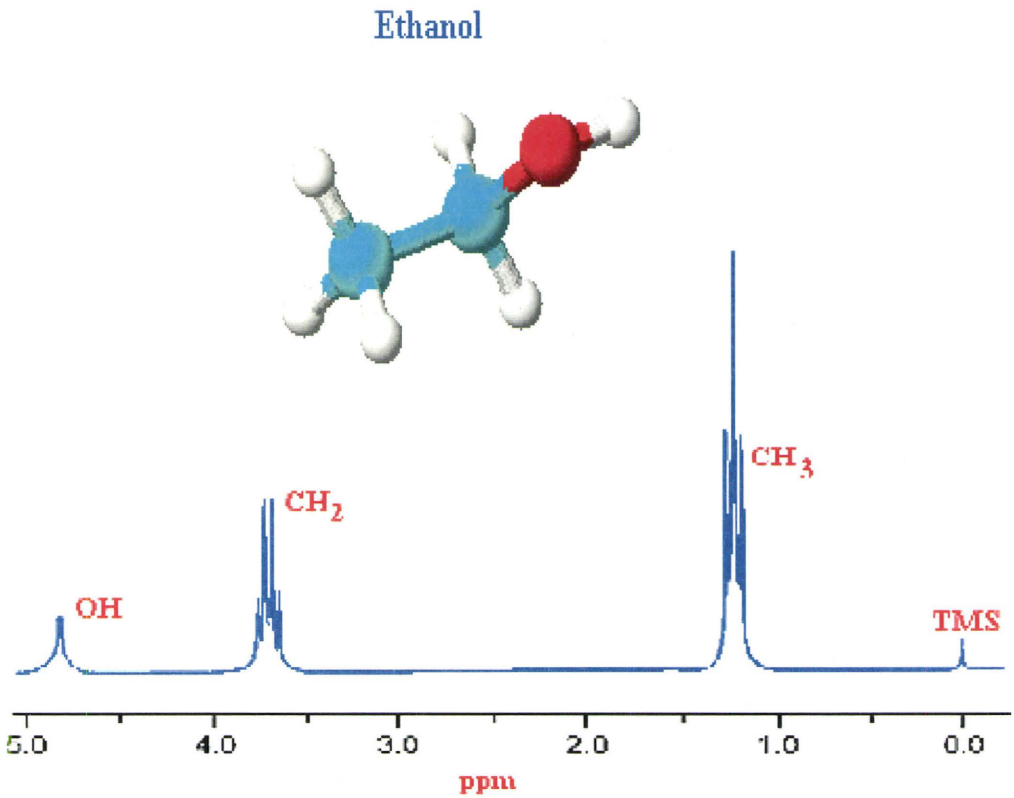

Figure 4. 1D ^{1}H NMR spectrum for Ethanol

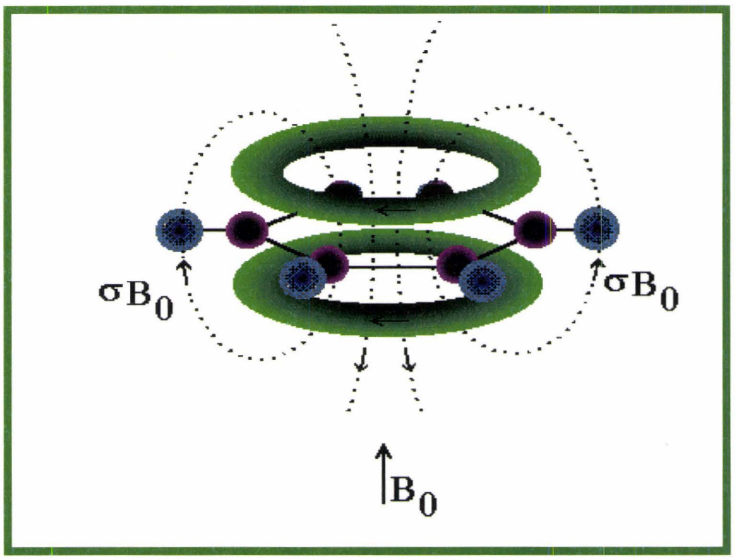

Figure 5. Chemical Shift

Type of carbon atom	Chemical shift (δ ppm)
Alkyl, R**C**H_3	0-40
Alkyl, R**C**H_2R	10-50
Alkyl, R**C**HR_2	15-50
Alkyl halide or amine , $(CH_3)_3$**C**-X (X = Cl, Br, NR_2)	10-65
Alcohol or ether, R_3**C**OR	50-90
Alkyne, -**C**=	60-90
Alkene, R_2**C**=	100-170
Benzylic carbon	100-170
Nitriles, -**C**=N	120-130
Amides, -**C**NR_2	150-180
Carboxylic acids, esters, -**C**OOH	160-185

Table 2. ^{13}C chemical shifts for some systems

Type of proton.	Chemical shift (δ ppm)
Alkyl, R**C**H_3	0.8-1.0
Alkyl, R**C**H_2CH$_3$	1.2-1.4
Alkyl, R_3C**H**	1.4-1.7
Allylic, R_2C=CRCH_3	1.6-1.9
Benzylic, ArCH_3	2.2-2.5
Alkyl chloride, RCH_2Cl	3.6-3.8
Alkyl bromide, RCH_2Br	3.4-3.6
Alkyl iodide , RCH_2I	3.1-3.3
Ether, ROCH_2R	3.3-3.9
Alcohol, HOCH_2R	3.3-4.0
Ketone, RCOCH_3	2.1-2.6
Aldehyde, RCO**H**	9.5-9.6
Vinylic, R_2C=CH_2	4.6-5.0
Vinylic, R_2C=CR**H**	5.2-5.7
Aromatic, Ar**H**	6.0-9.5
Acetylenic, RC=C**H**	2.5-3.1
Alcohol hydroxyl, RO**H**	0.5-6.0[a]
Carboxylic, RCOO**H**	10-13[a]
Phenolic, ArO**H**	4.5-7.7[a]
Amino, R-NH_2	1.0-5.0[a]

Table 3. ^{1}H NMR chemical shift for some systems

Two-dimensional techniques are used to determine the structure of more complicated molecules.[7;8] These techniques are complementary to x-ray crystallography for the determination of protein structure. The NMR signal depends on the local molecular structure and motion experienced by spins. For a more detailed explanation of NMR spectroscopy, the following references are recommended. [7;9-14]

Chemical exchange refers to any process in which a nucleus exchanges between two or more environments in which its NMR parameters (e.g. chemical shift, scalar

coupling, or relaxation) differ. Dynamic NMR deals with the effects in a broad sense of chemical exchange processes on NMR spectra; and conversely with the information about the changes in the environment of magnetic nuclei that can be derived from observation of NMR spectra.[15-20] The underlying exchange process may also be chemical exchange, such as exchange between the hydroxyl protons and protons from dissolved water. Alternatively, it could be conformational exchange. All these processes are frequently encountered in NMR (Figure 6).

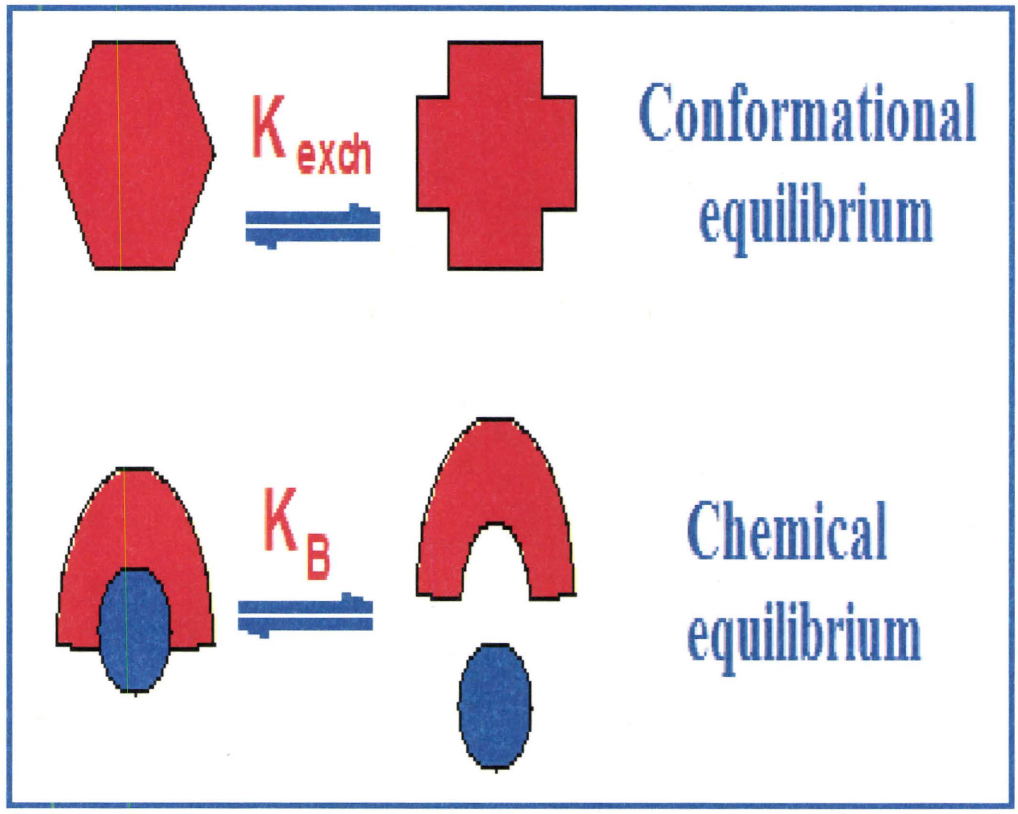

Figure 6. Conformational versus Chemical Equilibrium

We characterize a site by some unique physical and chemical conditions that make it different from another site. The frequency of these motions are usually comparable to the Larmor frequency of the spins.

In NMR, a spin moving from one site to another will experience different fields at different times. The frequency, ω, of a spin in a static magnetic field B_0 is given by the Larmor equation,

$$\omega = \gamma \mathbf{B}_0 \qquad [1]$$

where γ is the gyromagnetic ratio of the spin. However, if the spin experiences a time varying magnetic field in addition to the static field, the Larmor frequency will be a function of time:

$$\omega(\tau) = \gamma\left[B_o + B'(t)\right] \qquad [2]$$

where B'(t) is the time varying field due to the spins motion from one another. What does this do to the NMR spectra? To answer this we need to consider the rates of the exchange process and how it compares to the NMR timescale.

When the partial bond is formed, e.g. aldehyde group in furfural, the exchange is to be intramolecular, which can be further classified into mutual or non-mutual exchange. An example of mutual exchange is illustrated in Figure 7,[21] the methyl proton environment is changed by rotation about the bond from the nitrogen to the ring. As the temperature of the sample is raised, the methyl signals broaden, move together, coalesce, and will eventually join to make a single sharp line (Figure 7). Although there is only one distinguishable molecule, in this chemical exchange, the equilibrium constant is exactly 1, and the NMR parameters before and after the exchange are identical (Figure 7).

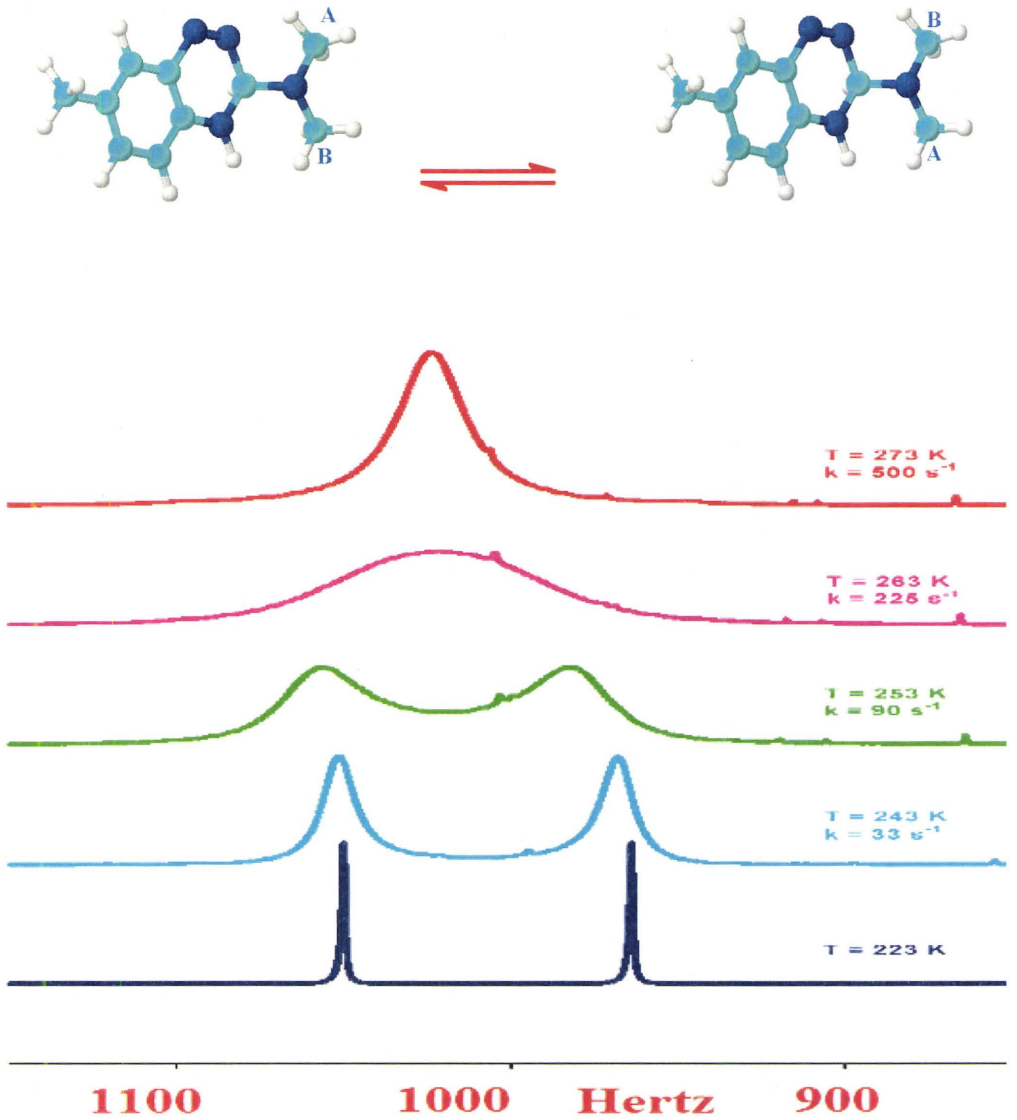

Figure 7. 3-dimethylamino-7-methyl-1, 2, 4-benzotriazine

In the non-mutual case (Figure 8 and 9), internal rotation will convert one site to another. The aldehyde (Figure 9) group has two unequally-populated conformations which can be observed by varying temperatures. Note that the equilibrium constant is not one. In some cases, we can see both conformations, and witness the effect of exchange between them. There are two different reaction rates, both the forward and reverse and the ratio is given by the equilibrium constant. The rate of the major- to-minor process must be the smaller of the two rates, by the principle of detailed balance.[22]

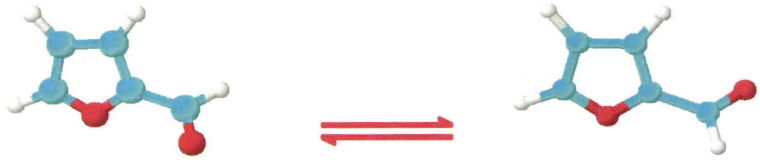

Figure 8. Internal rotation in furfural

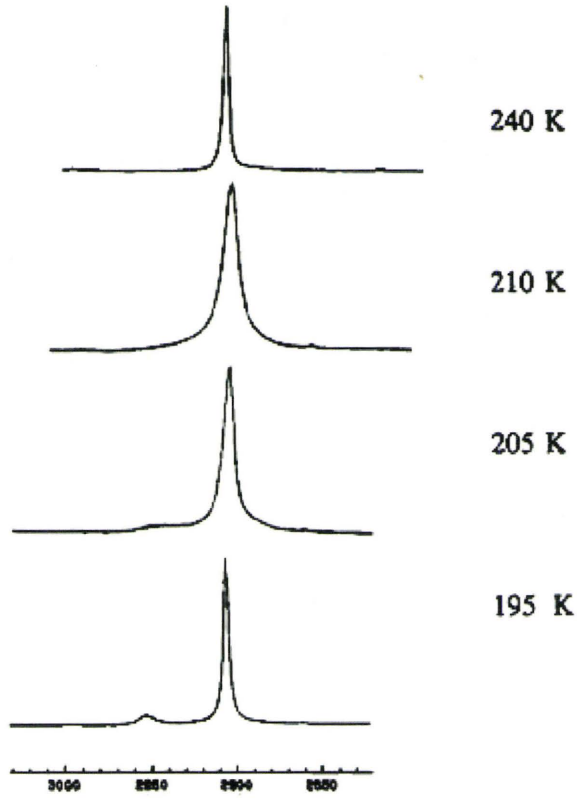

Figure 1

Figure 9. Furfural - Two unequally populated conformations seen in the aldehyde group at different temperatures

In order to understand the timescale of these exchange processes, it is important to define the limiting cases. Three different states can be distinguished (Figure 10)

1.) Slow exchange - two sets of resonances with reasonable sharp lines.

2.) Fast exchange - a single, sharp line positioned somewhere between the two lines.

3.) Intermediate exchange - a single very broad or invisible line.

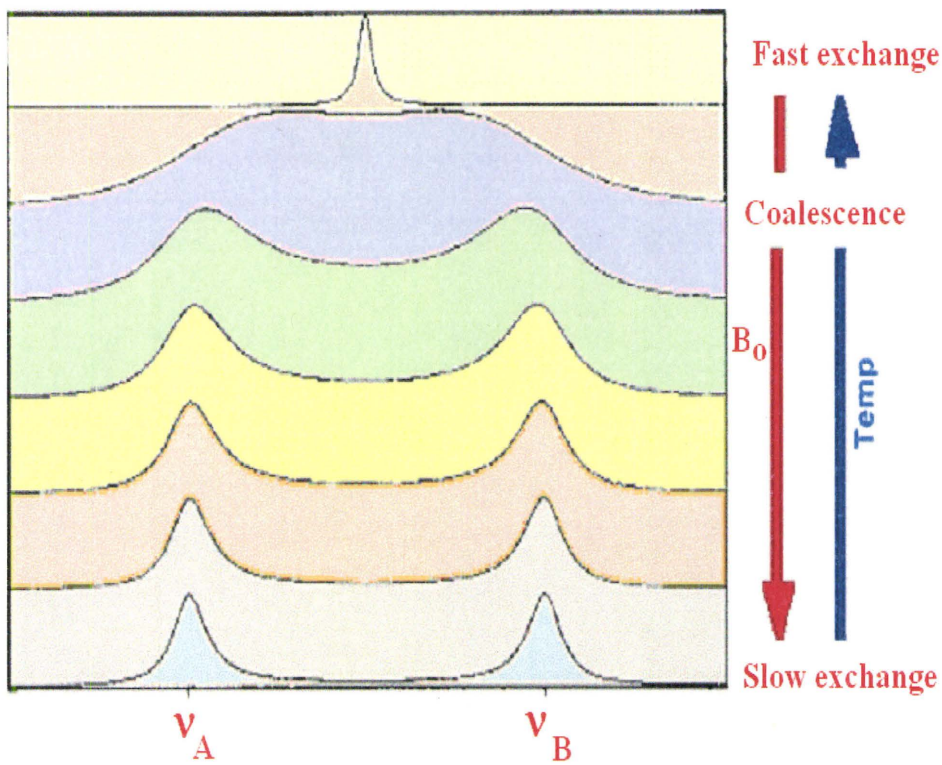

Figure 10. Exchange Processes

Relaxation processes

Relaxation refers to all processes which regenerate the Boltzmann distribution of nuclear spin on their precession states and the resulting equilibrium magnetization along the static magnetic field.[23;24] The concept of "relaxation time" was introduced to NMR by Bloch in his famous equations of motion:

$$\frac{dM_z}{dt} = \frac{M_o - M_z}{T_1} \quad [3]$$

$$\frac{dM_{x,y}}{dt} = -\frac{M_{x,y}}{T_2} \quad [4]$$

Bloch equations assume the magnetization component along B_o (the longitudinal magnetization M_z) to relax exponentially to its equilibrium value, M_o.[25;26] The time constant for the process is called the spin-lattice or longitudinal relaxation time, and is denoted T_1. The inverse of relaxation time, $1/T_1$, is the rate for the decay process. Furthermore, there are two types of 1D ^1H T_1 experiment for two sites chemical exchange:

1.) A non- selective inversion that inverts both sites equally will mask most of the exchange effects and the relaxation will be dominated by T_1.

2.) Selective inversion recovery involves the inversion of one of the two sites of the isomers, selectively. The site can then regain equilibrium by either T_1 processes or by exchanging with the other site that was left at equilibrium. The inverted signal will relax at roughly the sum of the exchange and spin –lattice relaxation rate, while the signal that was unperturbed at start of the experiment shows a characteristic transient. These one dimensional selective – inversion experiments have been widely used in systems without scalar coupling such as the methyl group.

The magnetization components perpendicular to B_o (the transverse magnetization, $M_{x, y}$) are also assumed to relax in an exponential manner to their equilibrium value of zero. The time constant for this process is called the spin – spin or transverse relaxation time and is denoted by T_2.

Push-pull ethylenes

Push-Pull Ethylenes are molecules that contain one or more electron donating groups (typically amino groups) at one end of the C=C bond and one or more electron-accepting groups at the other (Figure 11). [16;27-29]

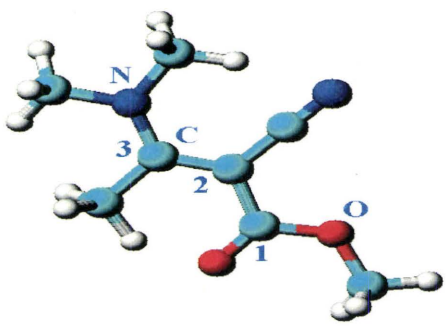

Figure 11. Crotonic acid, 2-cyano-3-(dimethyl amino)-, methyl ester

When the donor and acceptor groups have suitable structures, they often show hindered rotations with substantial torsional barriers. These properties, low C=C barriers and high C-N barriers, are in general ascribed to:

- Electronic/resonance effects
- Steric interactions between the donor and acceptor groups
- A combination of both.

Delocalization of the amino nitrogen lone pair into the C=C π system results in an increased barrier to rotation about C-N bond(s) adjacent to the C=C bond. A classic case of a push-pull ethylene compound is crotonic acid,2-cyano-3-(dimethyl amino)-,methyl ester or originally, known as methyl 3-dimethylamino-2-cyanocrotonate and conveniently abbreviated as MDACC (which is what I am going to use).[30] Registry number: 26978-71-2

The thesis emphasizes the study of the dynamic processes of MDACC by using variable temperature solution NMR spectroscopy. The kinetic processes occurring in MDACC are diagramed in Figure 12. The letters A-F refer to the unique magnetic environment of the methyl groups involved in the exchange processes. There are three different rate constants. [30]The rate constants k_{EZ} and k_{ZE} as well as $k_{E'Z'}$ and $k_{Z'E'}$ refer to rotation about the C=C bond in MDACC, whereas $k_{E'E}$, or $k_{EE'}$ and $k_{ZZ'}$ or $k_{Z'Z}$ correspond to the rotation about the C-N bond in the E and Z isomers, respectively.

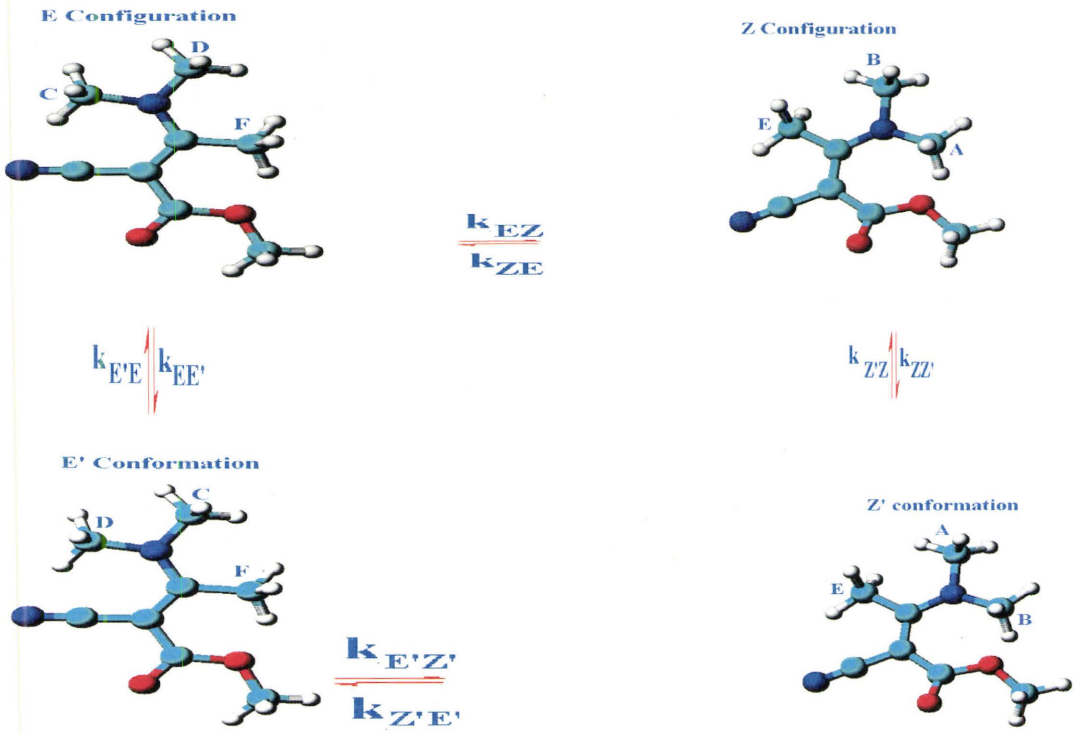

Figure 12. Kinetic processes occurring in MDACC

Solvent Effects

The interaction between the solvent polarity and thermodynamic quantities using line shape analysis through 1D ^{1}HNMR is still not clear.[31] These quantities $\Delta G^{\ddagger}$, $\Delta H^{\ddagger}$, and $\Delta S^{\ddagger}$ can be defined as the standard Gibbs free energy - the difference between the transition state of a reaction (either an elementary reaction or a stepwise reaction) and the ground state of the reactants; the enthalpy of activation – the standard enthalpy difference between the transition state and the ground state of the reactants at the same temperature and pressure; and the standard entropy difference between the transition state and the ground state of the reactants, at the same temperature and pressure, respectively.

These terms are related to each other by the following equation:

$$\Delta G^{\ddagger} = \Delta H^{\ddagger} - T \Delta S^{\ddagger} \qquad [5]$$

Our investigation will show that there is no obvious relationship between $\Delta G^{\ddagger}$ and the solvent's polarity. However, there is a linear relationship between $\Delta S^{\ddagger}$ and the solvent polarity. This will be discussed in more depth in Section 4.4.

The choice of solvent will affect chemical shifts, coupling constants, relaxation times, NOE and the ability to observe exchangeable protons. For example, R-OH, R_2-NH, R-NH_2, R-CO_2H, R-SH. Solvent effects occur by the following mechanisms:

1.) Polar solvent (electric field) effects.

2.) Solvent anisotropy.

3.) Specific solvent-solute interactions.

Polar solvent (electric field) effects:

Polar solvent molecules will align themselves in a specific orientation around solute molecules containing polar groups (Figure 13).[32] This will enhance any shielding caused by inductive effects within the solute molecule for example, protons at one end of a molecule or bond dipole in a solute such as $\mathbf{CH_3\text{-}C^{\delta+}\equiv N^{\delta-}}$ will experience an additional deshielding.[33;34]

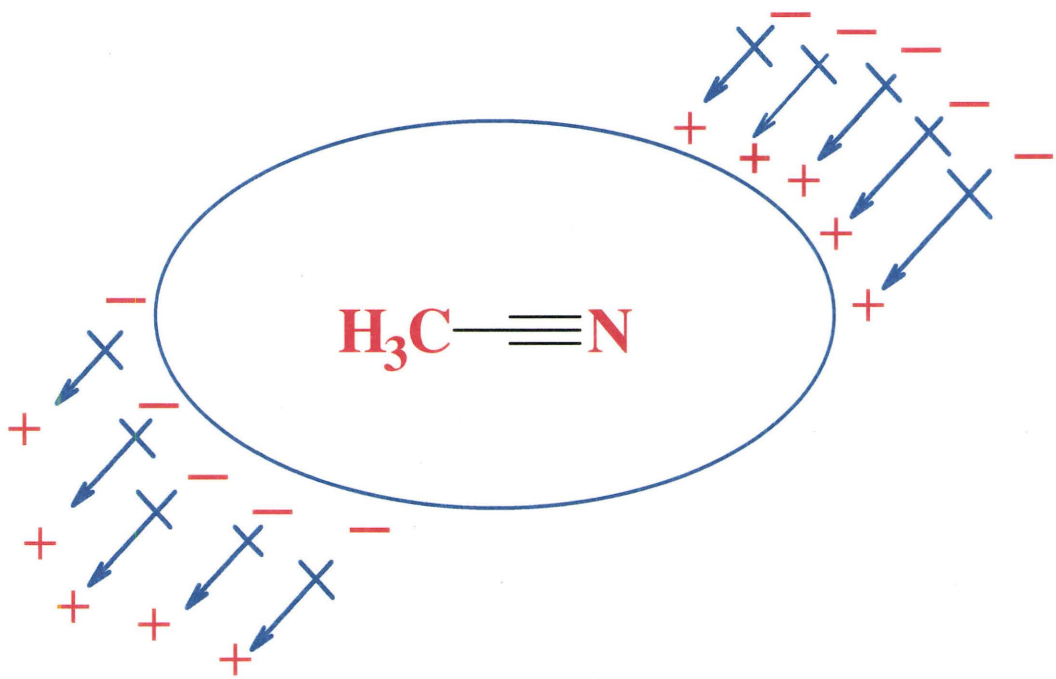

Figure 13. Alignment of polar solvent dipoles

Solvent Anisotropy:

Molecules with anisotropy of a particular solvent such as benzene will cause changes in chemical shifts. This procedure involves comparing chemical shifts in aromatic solvents such as benzene, toluene, pyridine, and substituted naphthalenes with shifts observed in solvents such as $CDCl_3$ or CCl_4. In molecules containing amides, unsaturated ketones, nitriles, aldehydes, and ketones there are very specific aromatic solvent induced shifts (ASIS) effects owing to the relative position of the solvent and solute when they associate to form a collision complex (Figure 14). In this case the following is observed:

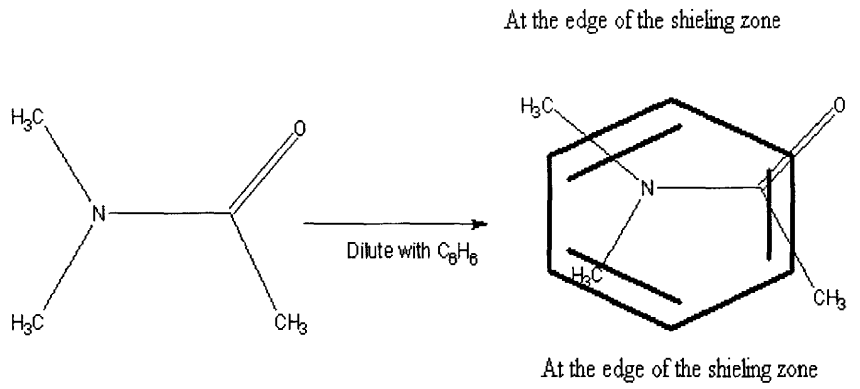

Figure 14. Solvent Anisotropy

1.) $\Delta G^{\ddagger}$ for a solvent/solute complex formation is ~0.8-2.0 kJ/mol.

2.) The observed effect is averaged over all possible solvent-solute molecular associations.

3.) There is a specific interaction between ketones and benzene.

4.) The collision complex is formed in which the benzene molecule is positioned as far away as possible from the partial negative charge on the carbonyl oxygen (Figure 15).

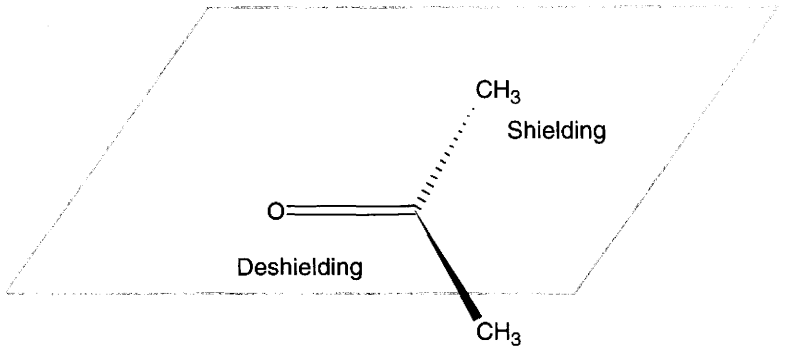

Figure 15. Collision complex

5.) In cyclohexanone the α-axial and γ-axial protons are most affected by ASIS, however the equatorial proton shows little or no change since it is positioned close to the plane containing the carbonyl group (Figure 16).

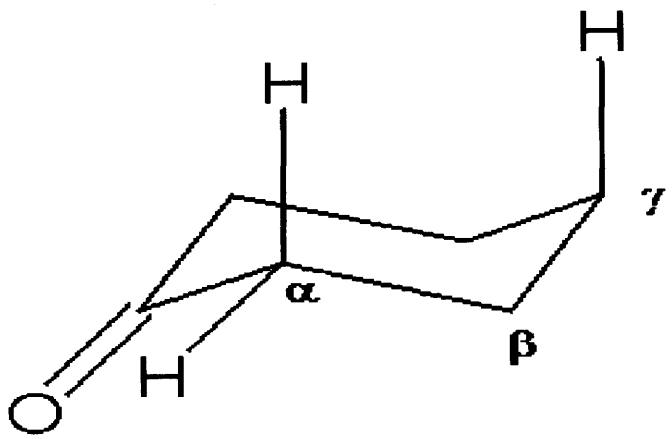

Figure 16. Cyclohexanone

Specific solvent-solute interactions:

The most frequently observed solvent-solute interaction is hydrogen bonding. Hydrogen bonding is useful since it allows the direct observation of exchangeable protons. For example, -OH, -NH, and –SH, exchange is stopped by the formation of hydrogen bonds:

R - O - H ---------- $^{-}$O - S^{+} - $(CD_3)_2$

The anisotropy of the sulfoxide bond is similar to **C ≡ C,** therefore the chemical shifts of protons at specific spatial locations near the hydrogen bonding group will also be affected by DMSO.

Two-Site exchange:

Let us consider the following reaction

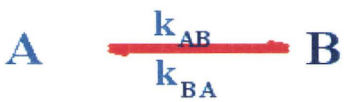

The kinetics are described by the set of two equations:

$$\frac{dA}{dt} = -k_{AB}A + k_{BA}B \qquad [6]$$

$$\frac{dB}{dt} = k_{AB}A - k_{BA}B \qquad [7]$$

They satisfy the conservation law:

$$\frac{d\ (\ A\ +\ B\ )}{d\ t}\ =\ 0 \qquad [8]$$

The solution is

$$A=\left(\frac{A_0+B_o}{k}\right)k_{BA}+\frac{k_{AB}A_0-k_{BA}B_o}{k}e^{-kt} \qquad [9]$$

$$B\ =\ \frac{A_0\ +\ B_0}{k}k_{AB}\ -\ \frac{k_{AB}A_0\ -\ k_{BA}B_o}{k}e^{-kt} \qquad [10]$$

Here

$$k=k_{AB}+k_{BA} \qquad [11]$$

is the rate of equilibration. The equilibrium concentrations are

$$A_e\ =\ C\frac{k_{BA}}{k},B_e\ =\ C\frac{k_{AB}}{k},C\ =\ A_o\ +\ B_o \qquad [12]$$

The corresponding equilibrium magnetization can be also calculated

$$M_{eA}=m_oC\frac{k_{BA}}{k},M_{eB}=m_oC\frac{k_{AB}}{k} \qquad [13]$$

1. The lifetime of state A is:

$$\tau_A\ =\ \frac{1}{k_{+1}} \qquad [14]$$

Where k_{+1} is the forward rate

and of state B is:

$$\tau_B\ =\ \frac{1}{k_{-1}} \qquad [15]$$

Where k_{-1} is the reversed rate

The NMR parameters that characterize both states are:

- The chemical shift
- Scalar spin, spin coupling
- The line width (transverse relaxation time). The NMR time scale is defined by the relation of the exchange rate with respect to the magnitude of the accompanying change in the corresponding NMR parameter.

Exchange rates			
Time scale	Slow	Intermediate	Fast
Chemical shift	$K << \delta_A - \delta_B$	$K = \delta_A - \delta_B$	$K >> \delta_A - \delta_B$
Scalar coupling	$K << J_A - J_B$	$K = J_A - J_B$	$K >> J_A - J_B$
Transverse Relaxation	$K \approx \frac{1}{T_{2A}} - \frac{1}{T_{2B}}$	$K = \frac{1}{T_{2A}} - \frac{1}{T_{2B}}$	$K \approx \frac{1}{T_{2A}} - \frac{1}{T_{2B}}$

Table 4

The exchange time scale is defined by the separation of the two signals relative to the exchange rate. The ratio is influenced by:

- Increasing the temperature. This causes acceleration in the exchange reaction and therefore pushes the system into the fast exchange regime.[35]
- Increasing the static field which causes an increase in the line separation and therefore drives the system into the slow exchange regime.

The effect of chemical or conformational exchange on the chemical shift is shown below. Therein, a signal in the fast exchange regime is pushed into the slow exchange regime by decreasing the temperature or increasing the field strength (Figure 4). At the coalescence temperature, a very broad line with a plateau is observed.

In fast exchange the spectrum consists of one line at the average position is determined by the Boltzmann probabilities:

$$\delta_{ave} = p_A \delta_A + (1 - p_A)\delta_B \qquad [16]$$

Where p_A and (1- p_A) are The probabilities to find the molecule in the states 1 and 2 respectively.

It is obvious from the equation above that the resonance position of the averaged signal may not be simply the arithmetic mean of the resonance position of the two slow exchanging lines. This is due to the fact that the population of the two states has to be taken into account.

In fast exchange, the exchange reaction causes an additional contribution to the linewidth:

$$\Delta\nu_{\frac{1}{2}} = \frac{1}{2}\frac{(\nu_A - \nu_B)^2}{\pi k_{+1}} \qquad [17]$$

Where k_{+1} is the forward rate.

Thereby, the faster the reaction or the smaller the frequency difference (provided that a single line is observed, fast exchange regime) the narrower the line. Such an increase in reaction rate can be accomplished via a temperature increase and decrease in frequency separation by lowering the magnitude of the static field.

A similar situation exists with averaging of couplings:

$$J_{ave} = p_A J_A + (1 - p_A) J_B \qquad [18]$$

An important example for averaging of couplings is found for hydroxyl protons of alcohols that exchange with solvent water protons. In the figure below, the boxed proton feels the vicinal proton to be in the α–state (left side). Through chemical exchange that proton is substituted by a proton that comes from water and is in the β–state (Figure17). When the exchange is slow both lines of the doublet are visible but for the fast case only the average singlet will be observed. This mechanism has been termed self-decoupling and the reason why OH protons in alcohols usually appear as (broad) singlets:

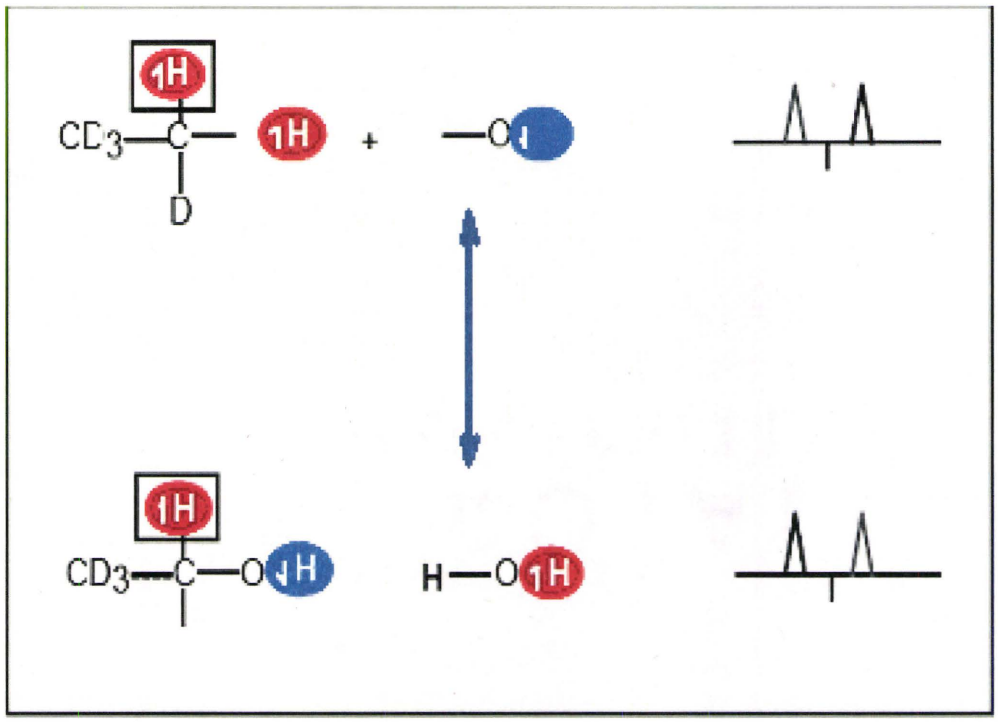

Figure 17. Exchange of the hydroxyl proton with a proton from water may lead to a change in the spin state of the OH proton. If this process is fast, only the averaged line at the center without splitting due to coupling is visible.

In slow exchange, the exchange rate ($1/\tau_e$) is much less than the resonance frequency separation ($\delta\omega$) between the two sites. So, a spin moving from one site to another loses all phase coherence by the time it returns. The NMR spectrum will show two distinct peaks centered on the resonance frequency (figure 10). When two separate signals are observed the additional contribution to the linewidth due to exchange is:

$$\Delta \nu = \frac{k + 1}{\pi} \qquad [19]$$

Hence, temperature decrease will lead to a sharpening of the lines. A typical example where both situations (slow and fast exchange) are simultaneously encountered is exchange of amide and hydroxyl protons of peptides with solvent in aqueous solution.[4;5;36] At a slightly acidic pH, the amide protons give rise to separate, sharp lines and the

exchange rate is on the order of 1-10 sec^{-1}. In contrast, exchange between hydroxyl and water protons is so fast that the hydroxyl protons coincide with the water chemical shift and cannot be observed separately. [15]

Intermediate exchange resembles a single, very broad or invisible line. The lineshape of the signals changes upon passing from the slow into the fast exchange regime. A detailed investigation shows that it may be described as:

$$g(\nu) = \frac{2\tau_A(\nu_A - \nu_x)^2}{\left[\nu - (\nu_A + \nu_x)\right]^2 + \pi^2\tau^2{}_A(\nu - \nu_A)^2(\nu - \nu_\chi)^2} \qquad [20]$$

The following figure shows calculated lineshapes for two signals 10 Hz apart (top trace) depending on the lifetime (which is the inverse of the reaction rate) or for two signals with 0.1 sec lifetime depending on the frequency separation (given in Hz):

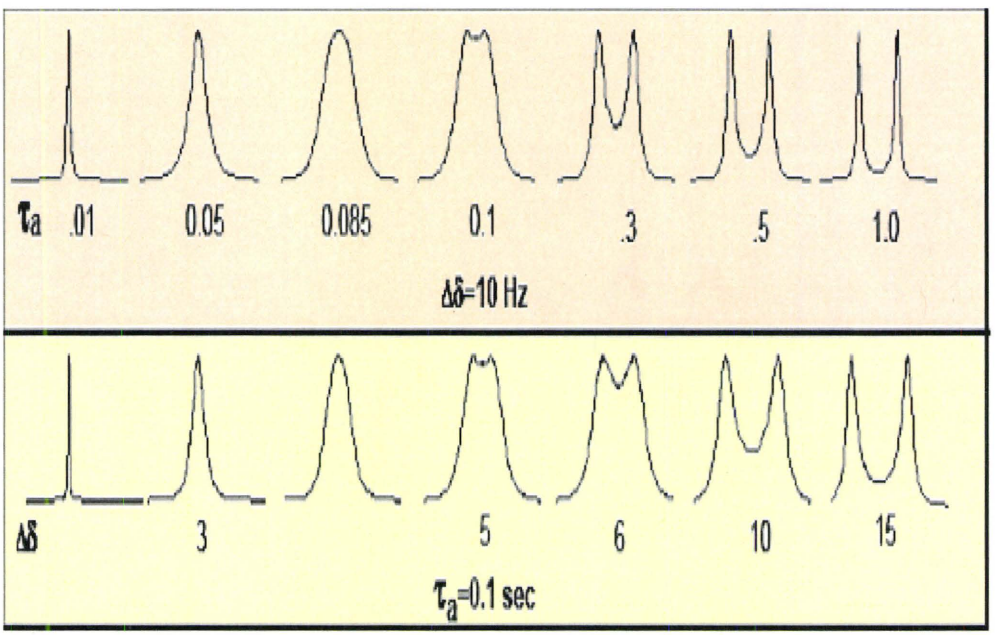

Figure 18. Top: Two lines, 10 Hz separated appears as a singlet, if the lifetime of the separate states is short (0.01S) or as two separate lines, when the lifetime is long (1 s). Bottom: Calculated for a lifetime of 0.1 s with varying frequency separations (1-15 Hz).

At coalescence the lineshape is characterized by a flat top Figure 18. The corresponding lifetime at coalescence is given by:

$$\tau_{A}^{C} = \frac{\sqrt{2}}{\pi}(\nu_{A} - \nu_{X}) \qquad [21]$$

Summary

Molecules, like push-pull ethylenes are so very interesting since a large amount of data, both thermodynamic and kinetic can be obtained. Through the use of variable temperature solution NMR, the dynamic processes of MDACC were studied. Our investigation shows that there is no relationship between $\Delta G^{\ddagger}$ and the solvent's polarity and most interestingly, there is a linear relationship between $\Delta S^{\ddagger}$ and the solvent polarity. In the next section, a closer look at the theory behind NMR will be discussed.

Chapter 2

THEORY

2.1 Basic Principles

After an introduction to basic NMR, a discussion of some aspects of NMR relevant to this work will be elaborated. General references on NMR are listed. Magnetization, the NMR signal, can be easily detected and manipulated to produce the NMR spectrum. Various NMR parameters can be measured to elucidate solvent effects on the chemical exchange of a push pull ethylenes. These NMR parameters are spin-lattice relaxation time constants, linewidths and chemical shifts; in addition, the variation of the temperature can provide additional information. Also the success of obtaining our result could not be done without using the simulation line shape program MEXICO,[37;37;38] which gives valuable and reliable kinetic information before coalescence temperature and CIFIT program,[39] which gives an excellent kinetic data at low temperature. Both programs were developed in this lab by Alex. D. Bain. Also, the principles behind these programs will be discussed. Wherever possible reference to literature will be given to provide an indication of how each of the aspects have been used or could be used to understand the dynamic of solvent effect on push pull ethylene systems.

Nuclear magnetic resonance involves transitions between nuclear spin energy levels (Figure 19):

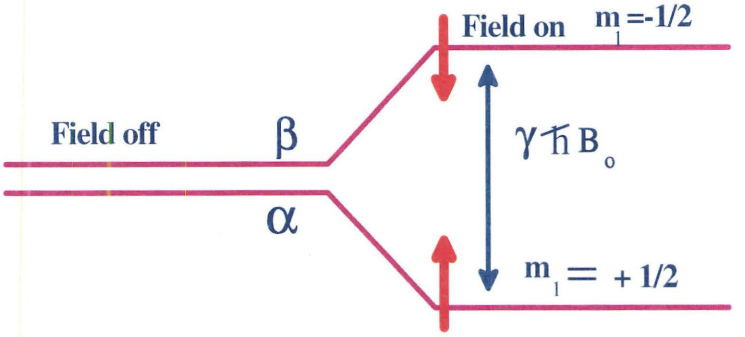

Figure 19. The two energy levels of the nuclear spin transition for spin ½.

The transition arises because the nuclei of some atoms have magnetic moments and these magnetic moments have different quantized orientations relative to the applied field for different nuclear spin states (see Figure 19). Actually any atomic nucleus which possess either odd mass or odd atomic number, or both, has a quantized angular momentum and a magnetic moment (Figure 20).[9 40]

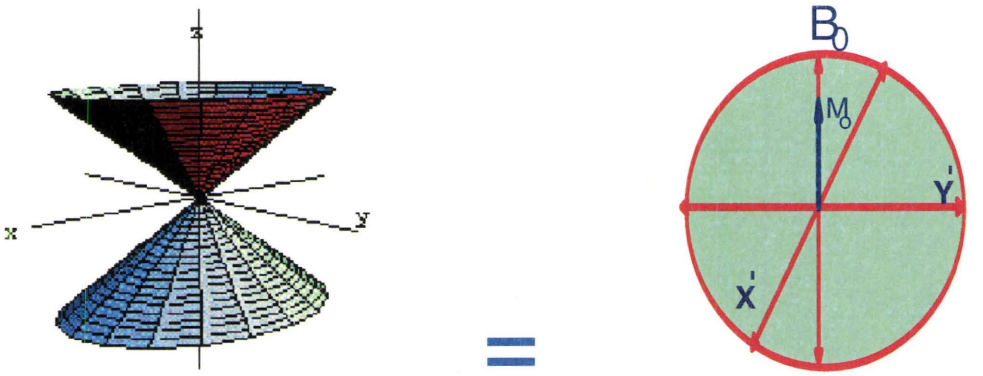

Figure 20. Different orientation of a spin ½ nucleus (left) and the equivalent vector model (right).

In NMR we apply a magnetic field (B_o) along a particular direction, by convention, the Z axis. For nuclei with spin, the magnetic moment vector appears to rotate around the Z axis with a quantized angular momentum. In the magnetic field B_o

there is a preference for one orientation of angular momentum to align with the field B_o, and one orientation to align against the field. This difference in relative orientation of spins can be represented as a vector quantity. This vector, called magnetization (M) is defined as the total magnetic moment of the sample (Figure 20). Magnetization will be discussed later in the relaxation and chemical exchange sections. As displayed in Figure 19 the two nuclear spin states for spin ½ nucleus are normally described in term of their Z-component of angular momentum. For example, for nuclear spin (I=1/2) there are two nuclear spin states, namely the Z-component of angular momentum ½ and – ½. In general, for each of the nuclei with spin, the number of allowed spin states which it may adopt is quantized and determined by its nuclear spin quantum number I. For a nucleus of spin quantum number I, there are 2I+1 allowed nuclear spin states. Both ^{1}H and ^{13}C have spin ½ and therefore only have two allowed energy levels. Deuterium ^{2}H however has spin 1 and has three energy levels, their Z-component of the angular momentum are +1, 0, and -1. For more detailed discussion see.[19, 41]

For a spin ½ nucleus the energy difference between the two nuclear spin states is:

$$\Delta E = h\nu = \gamma \left(\frac{h}{2\pi} \right) B_0 \qquad [22]$$

h is Planck's constant

ν is frequency of radiation

γ is the magnetogyric ratio of the nucleus of interest

B_o is the strength of the magnetic field

The magnetogyric ratio γ is a constant for each nucleus, and it is the ratio of magnetic moment to the angular momentum. For example the magnetogyric ratio of ^{1}H, ^{19}F, ^{13}C and many others are shown in Table 5 below. [2;42]

The negative sign for electrons indicates that the direction of rotation about the z axis is opposite to that for nuclei of positive γ.

Isotope	Natural Abundance (%)	Magnetogyric Ratio ($\gamma/10^7$, rad $T^{-1}s^{-1}$)	Relative Receptivity[a] (D^C)
^{1}H	99.985	26.7510	5.68×10^{3}
^{3}H		28.5335	
^{3}He	1.3×10^{-4}	-20.378	3.26×10^{-3}
^{13}C	1.108	6.7263	1.000
^{15}N	0.37	-2.7107	2.19×10^{-2}
^{19}F	100.0	25.1665	4.73×10^{3}
^{29}Si	4.70	-5.3141	2.09
^{31}P	100.0	10.829	3.77×10^{2}
^{57}Fe	2.19	0.8644	4.19×10^{-3}
^{77}Se	7.58	5.101	2.98
^{89}Y	100.0	-1.3106	0.668
^{103}Rh	100.0	-0.8420	0.177
^{107}Ag	51.82	-1.0828	0.197
^{109}Ag	48.18	-1.2449	0.276
^{111}Cd	12.75	-5.6720	6.97
^{113}Cd	12.26	-5.9330	7.59

Table 5. Properties of NMR-Active Nuclei A. I = 1/2 Nuclei

2.1.a Chemical shift

In order to see the great advantage of NMR, consider a simple nucleus like the proton. The power of NMR arises because not every proton in a molecule has its transition between nuclear spin states at exactly the same frequency. This change in frequency is due to the fact that the various protons in a molecule are surrounded by a slightly different electronic environment. The protons are said to be shielded by the electrons which surrounded them. The magnitude of this shielding increases with increasing electron density around the protons.[43] The resulting magnetic field that a nucleus experiences is lowered by the field. (Figure 21).

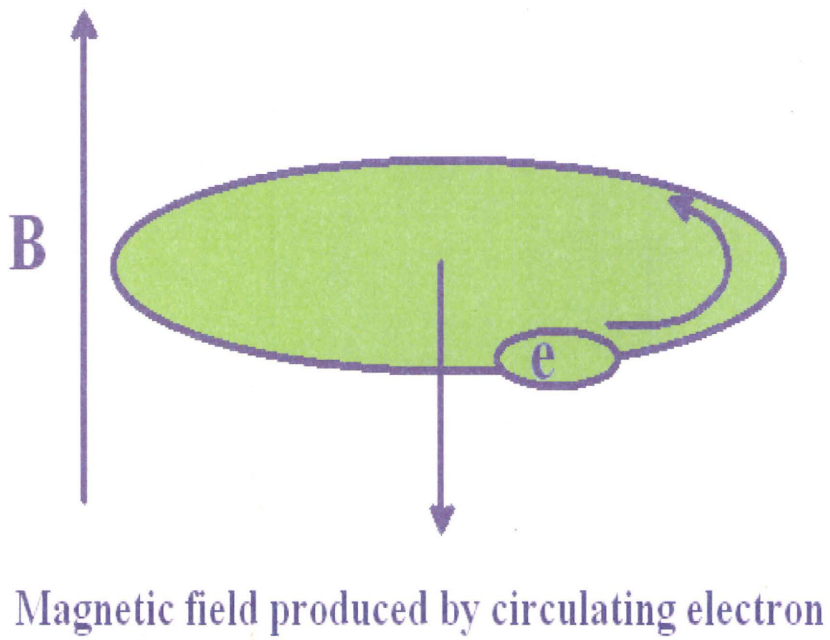

Figure 21. Pictorial representation of the magnetic field produced by a circulating electron.

The nucleus experiences a slightly lower field and thus a lower transition frequency (Table 2 and 3).[42] This allows a means of distinguishing between various

types of protons within a molecule, if the lines are very narrow. The difference in frequencies for different types of protons is very small. In practice the exact frequency is usually not determined, but measured relative to a frequency of a reference compound. The normal way this frequency difference is expressed is in terms of chemical shifts (δ). The chemical shift is defined by the shift (in ppm) of the sample (ν_{sample}) from the reference compound ($\nu_{reference}$) divided by the reference frequency (in MHz).

$$\delta = \left[\frac{\nu_{sample} - \nu_{reference}\,(Hz)}{\nu_{reference}\,(MHz)} \right] \times 10^{-6} \qquad [23]$$

As shown above, chemical shifts arise due to the nucleus of interest being in a slightly different electronic environment than the reference compound.

2.1.b Magnetization

Macroscopically, we look at the vector sum of all magnetic dipoles in the sample (Figure 22).[9] This vector sum, M, called Magnetization, aligns with B_o at thermal equilibrium and is proportional to the population difference of the two energy levels (Figure 22). By convention the direction of B_o is called the z-axis. In NMR the signal in the XY plane is always detected. To see this signal in FT-NMR (Fourier Transform NMR) the spin system must be modified or perturbed. To perturb the spin system a time dependent radiofrequency (RF) field B_1, or a pulse, is applied perpendicular to B_o. Now this results in M being flipped away from B_o (z-axis) and can be represented as a longitudinal (z) component (M_Z) and a transverse (XY) component (M_{XY}) (Figure 22). An NMR signal

is detected in the form of an oscillating current induced by M_{xy} through a receiver coil wound about an axis perpendicular to the z-axis or B_0. the signal detected is called a free-induction decay (FID) (Figure 23). [1]The time-domain is Fourier transformed into a frequency-domain NMR spectrum.[44]

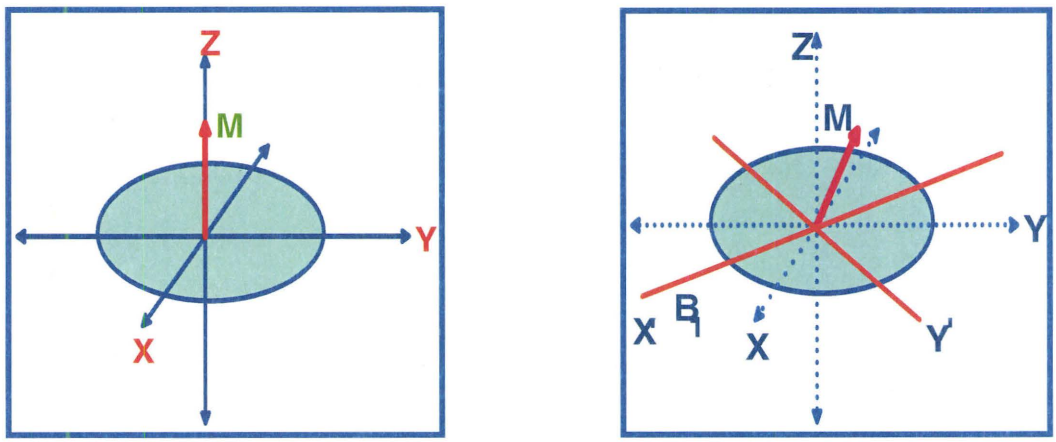

Figure 22. Total magnetization vector as viewed as a M_Z and M_{xy} component.

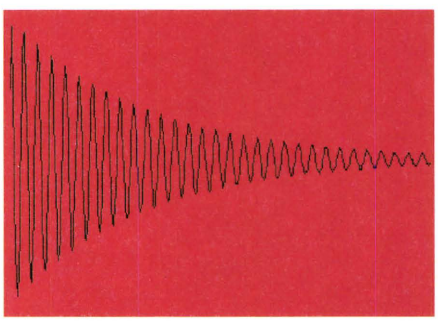

Figure 23. Free induction decay

2.1.c Relaxation

After a pulse is applied, M can be conveniently visualized as having two components M_Z and M_{XY}. These magnetizations then begin to return to equilibrium at a rate usually assumed to be a first-order exponential.[45] These relaxations are called spin-

lattice (longitudinal) relaxation and spin-spin (transverse) relaxation for the M_Z and M_{xy} components respectively. The time constants for these exponential relaxations are called T_1 for spin lattice and T_2 for spin –spin relaxation. Spin-lattice relaxation is described by the following equation:

$$M_z(t) - M_z(\infty) = (M_z(0) - M(\infty))e^{-\frac{t}{T_1}} \qquad [24]$$

M_Z (t) is the magnetization at time t

M_Z (∞) is the magnetization at equilibrium

M_Z (0) is the magnetization at t = 0 seconds

t is the variable delay time

T_1 is the spin –lattice relaxation time constant

Interaction	Range of interaction (Hz)	relevant parameters
1- Dipolar coupling	10^4 - 10^5	- abundance of magnetically active nuclei - size of the magnetogyric ratio
2- Quadrupolar coupling	10^6 - 10^9	- size of quadrupolar coupling constant - electric field gradient at the nucleus
3- Paramagnetic	10^7 -10^8	concentration of paramagnetic impurities
4- Scalar coupling	10 - 10^3	size of the scalar coupling constants
5-Chemical Shift Anisotropy (CSA)	10 - 10^4	- size of the chemical shift anisotropy - symmetry at the nuclear site
6- Spin rotation		

Table 6.

Any process which produces a fluctuating magnetic field at the nucleus can result in a relaxation mechanism. The T_1 relaxation mechanism arises in a number of ways. For instance, through dipole-dipole interactions (dd), quadrupolar interactions (qd), chemical shifts anisotropy (CSA), scalar coupling (SC), spin rotation interaction (Sr) and the presence of paramagnetic species (PS) (Table 6). For nuclei with spin the presence of a fluctuating magnetic field due to the tumbling of nearby magnetic dipoles induces a transition pathway. This type of interaction is called dipole-dipole. For nuclei of spin > 1/2 the presence of the non symmetric electronic environment induces quadrupolar relaxation. Chemical shift anisotropy arises when the electron density around the nucleus is anisotropic (not evenly distributed). The uneven distribution of electron density causes uneven shielding at the nucleus and thus the magnetic field acting on the nucleus varies with the orientation of the molecule relative to the field. This anisotropy generates a fluctuating field at the nucleus and this can aid in relaxation.[46] In addition, scalar coupling relaxation can also aid in T_2 relaxation. If chemical exchange is present and the exchange frequency is greater than the frequency of spin coupling, then the exchange process creates a fluctuating field at the site of the exchange nucleus.

A molecular rotation generates a magnetic field which can couple with nuclear spin. This coupling involves a magnetic field at the nucleus and provides a relaxation mechanism called spin-rotation relaxation. The final mechanism of relaxation to be discussed here is due to the presence of paramagnetic species in the sample. This interaction is normally due to dipolar coupling of the nucleus and the unpaired electrons of the paramagnetic species. In order to determine the mechanisms of relaxation for a particular system, each mechanism must be considered as contributing to the overall relaxation.

As mentioned earlier any process which causes a fluctuating magnetic field can aid in relaxation. For a given system any number of the above mentioned processes may be present at any time. The relaxation rates due to different mechanisms add together to give the total relaxation in the following manner:

$$T_1^{-1} = T_{1dd}^{-1} + T_{1qd}^{-1} + T_{1csa}^{-1} + T_{sr}^{-1} + T_{1ps}^{-1} \qquad [25]$$

The relative contribution of these mechanisms to the total relaxation depends on the system. The smaller the value of the T_1 of a particular mechanism the more efficient this mechanism is in causing relaxation. If a selective excitation is used chemical exchange can substantially alter the apparent T_1 of the system.

2.1.d Chemical Exchange

Chemical exchange is a term that covers both conformational changes and chemical reaction. The following analysis can be used for an exchange between two conformers of a species or two species in equilibrium. Consider for example a two site exchange say sites A and B (Figure 24).[47]

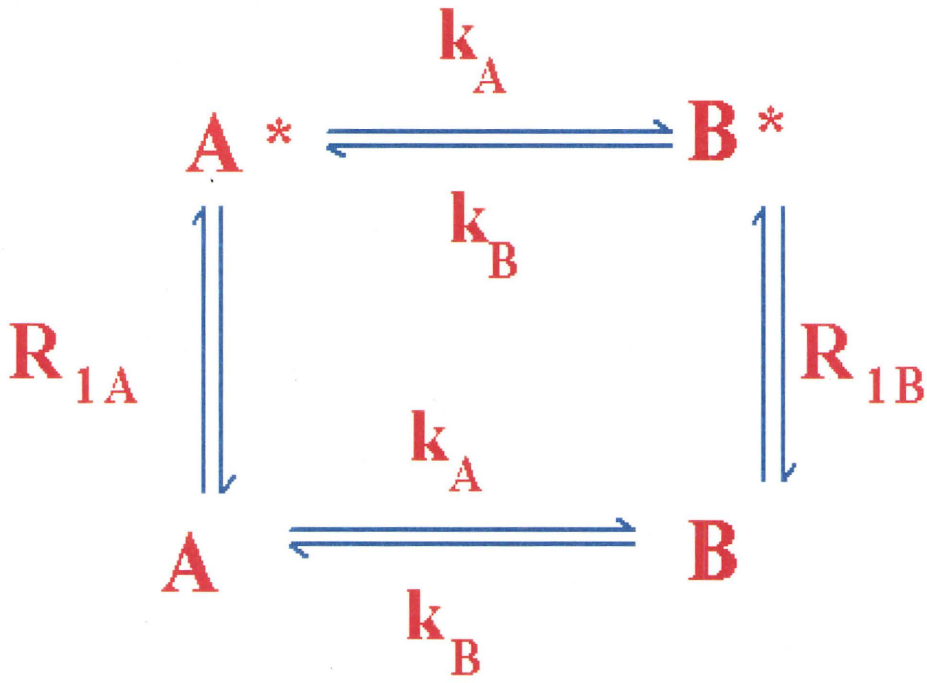

Figure 24. Schematic representation of a two site exchange/relaxation system.

A^* and B^* represent magnetically perturbed sites A and B.

A and B represent magnetization at equilibrium.

k_A and k_B are the rate for exchange from sites A to B and B to A respectively.

R_{1A} and R_{1B} are the relaxation rate constants with no exchange.

R_{1A} and R_{1B} are equal to $1/T_{1A}$ and $1/T_{1B}$ respectively.

The differential equations for the return to equilibrium for sites A and B are

$$\frac{d\left[M_{ZA}(t)-M_{ZA}(\infty)\right]}{dt}=-\left(\frac{1}{T_{1A}}+k_A\right)\left[M_{ZA}(0)-M_{ZA}(\infty)\right]+k_B\left[M_{ZB}(0)-M_{ZB}(\infty)\right] \qquad [26]$$

and

$$\frac{d\left[M_{ZB}(t)-M_{ZB}(\infty)\right]}{dt}=+k_A\left[M_{ZA}(0)-M_{ZA}(\infty)\right]-\left(\frac{1}{T_{1B}}+k_B\right)\left[M_{ZB}(0)-M_{ZB}(\infty)\right] \qquad [27]$$

respectively.

$M_{ZA}(t)$, $M_{ZB}(t)$ represent the magnetizations at any time t of sites A and B respectively immediately after a perturbation.

$M_{ZA}(\infty)$, $M_{ZB}(\infty)$ represent the equilibrium magnetization of A and B respectively. The values of T_{1A}, T_{1B}, k_A, and k_B can be determined readily by conducting inversion recovery experiments. There are two types of inversion recovery experiments which can be used, namely nonselective and selective inversion recovery.[15;48] These two types of experiments are designed to measure different aspect of the relaxation process.

First consider the non- selective inversion recovery experiment for a two site exchange system as described above. For a non –selective inversion recovery experiments common the pulse sequence used is:

(selective)$180^\circ - \tau$ – (non-selective)90° (Figure 25)

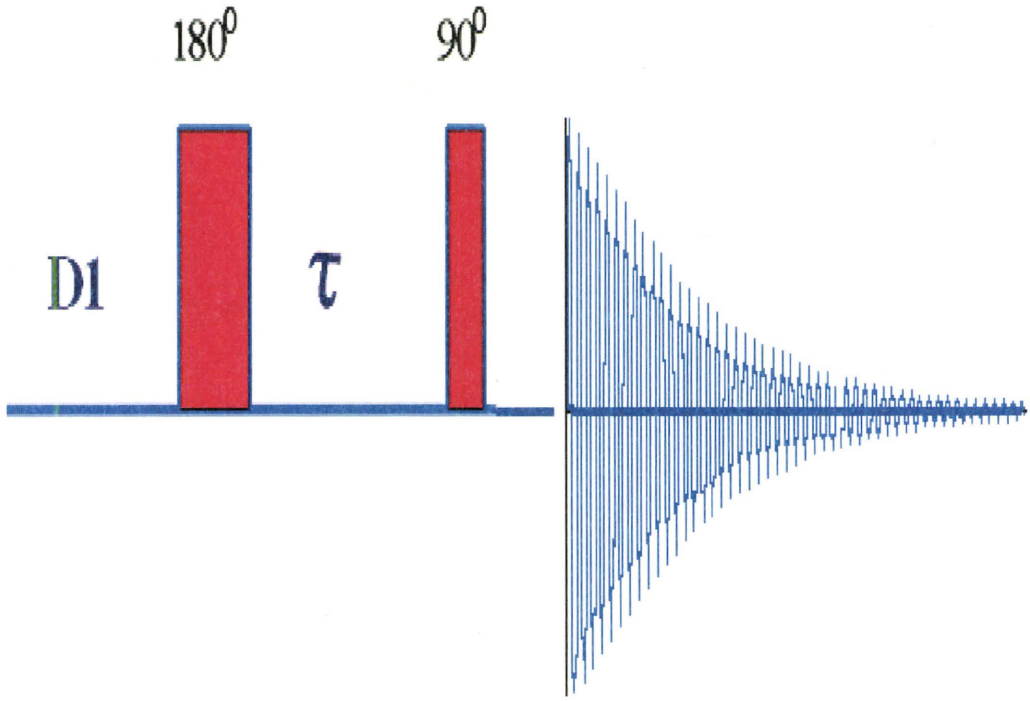

Figure 25. Pulse sequence for a selective/non-selective inversion recovery experiment.

When the selective 180° pulse is applied the magnetization that was along +Z is flipped down to –Z. For a spin lattice relaxation process this magnetization will relax along Z at a rate determined by the $1/T_1$'s and k's of the system. The initial magnetization of site (A) and (B) will be $M_{ZA}(0)$, $M_{ZB}(0)$ respectively, and the equilibrium magnetization for A and B will be $M_{ZA}(\infty)$, $M_{ZB}(\infty)$ respectively. If the inversion recovery pulse is exactly 180° then the initial condition of the relaxation are

$M_{ZA}(0) = - M_{ZA}(\infty)$ and $M_{ZB}(0) = - M_{ZB}(\infty)$. Using equations 25 and 26 and the conditions above the relaxation equation for site A is

$$\frac{d[M_{ZB}(t) - M_{ZB}(\infty)]}{dt} = -\left(\frac{1}{T_{1A}} + k_A\right)[2M_{ZA}(0)] + k_B[2M_{ZB}(0)] \qquad [28]$$

and similarly for site B. Actually in a T_1 experiment a series of measurements are conducted by using a variable delay τ (VD list in Bruker's NMR spectrometer language) between the 180^0 inversion pulse and 90^0 detection pulse . This $180^\circ - \tau - 90^\circ$ pulse sequence can be used for any number of exchanging sites (Figure 26).

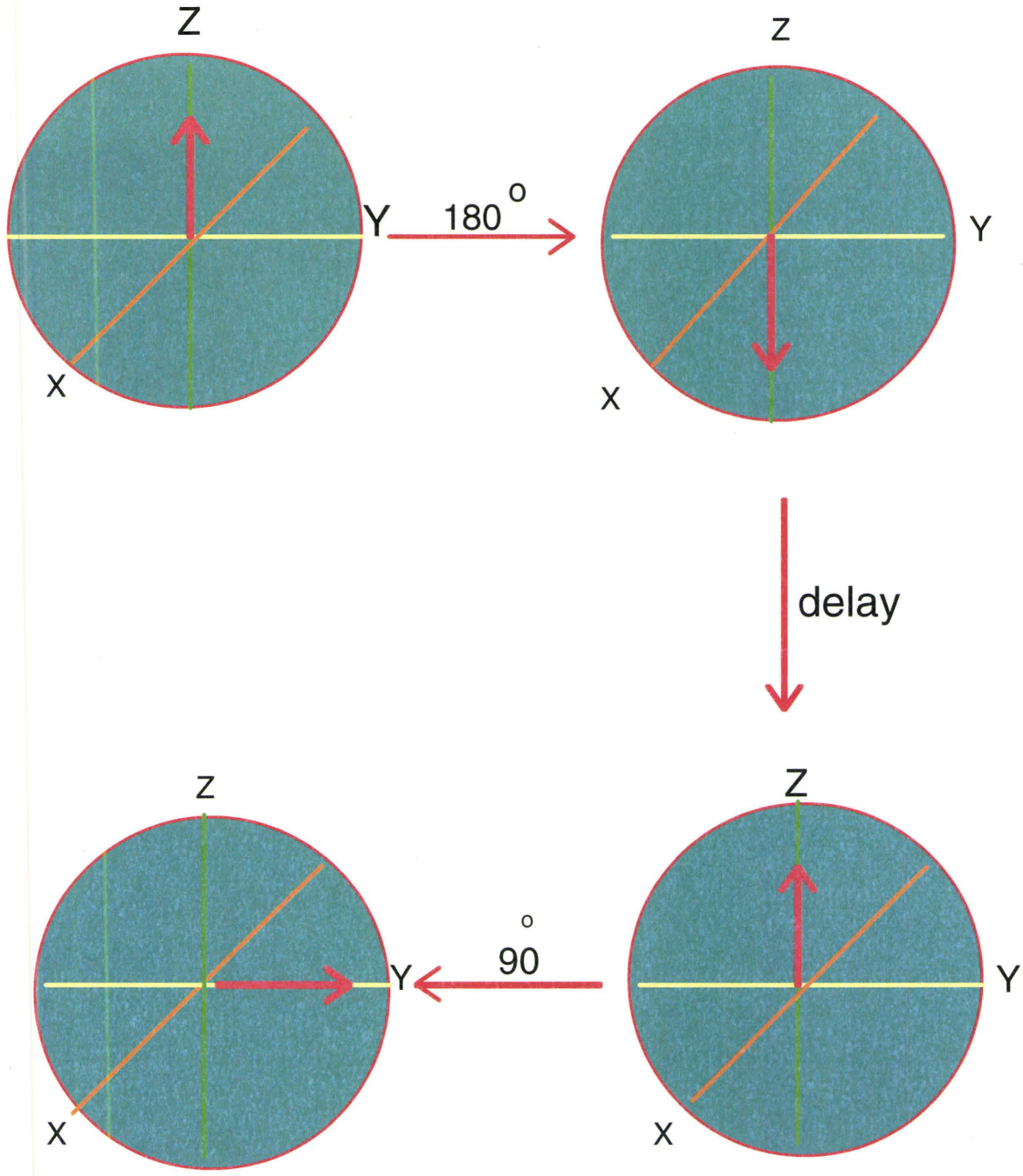

Figure 26. Vector model for 1D ^{1}H T_1 experiment

For a selective inversion recovery experiment the initial conditions are different. Again consider a two site exchange system, where A is inverted and B is not inverted (Figure 27).

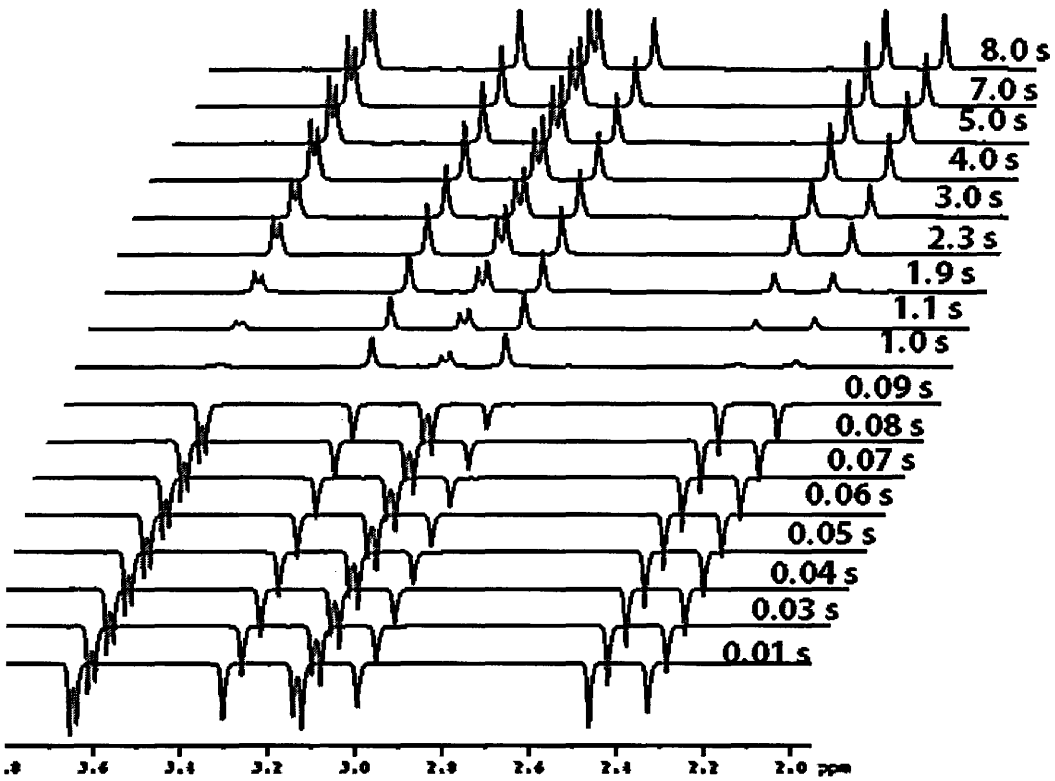

Figure 27. Non-Selective T_1 spectra

The initials conditions for A and B are then $M_{ZA}(0) = - M_{ZA}(\infty)$ and $M_{ZB}(0) = M_{ZB}(\infty)$ respectively. Again using equations above and the same conditions, the relaxation equations for site A and site B then becomes:

$$\frac{d[M_{zA}(t)-M_{zA}(\infty]}{dt} = -(1/T_{1A}+k_A)[M_{zA}(0)-M_{zA}(\infty)]+k_B[M_{zB}(0)-M_{zB}(\infty)] \quad [29]$$

and

$$\frac{d[M_{zB}(t)-M_{zB}}{dt} = +k_A[M_{zA}(0)-M_{zA}(\infty)]-1/T_{1B}+k_B)[M_{zB}(0)-M_{zB}(\infty)] \quad [30]$$

A similar situation would exist for a selective inversion on site B. A common pulse sequence for a selective inversion recovery is:

(Selective) $180^{\circ} - \tau -$ (non-selective) 90°.

The selective inversion pulse sequence is the same as the non-selective sequence except the180° is a selective pulse. [49,22] Figure 27 helps to illustrate a two site selective inversion experiment. The transmitter frequency is set equal to the frequency of the signal to be inverted. A delay consisted of several variable time values in seconds (VD list) between the 180^{0} and 90^{0} pulse. This delay allows the signals to get the 90^{0} out of phase as shown in Figure 28. The constants of T_{1A}, T_{1B}, k_A, and k_B can be determined by selective and non selective inversion recovery experiments. A multi site exchange fitting program Cifit developed in our lab by A. D. Bain was used to fit the experimental data.

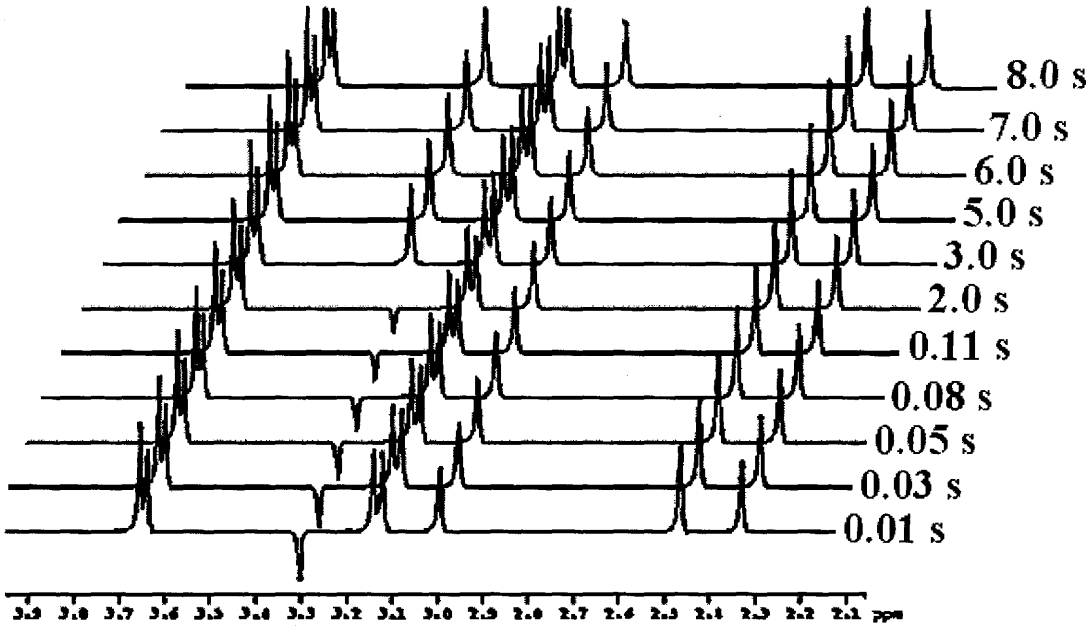

Figure 28. Selective Inversion Recovery (T_1) for MDACC in CD_2Cl_2 at -45°C.

2.2 Line widths

In analyzing linewidths there are two quite different types of broadening, coherent and incoherent line broadening. These two types of broadening are also known as homogenous (incoherent) broadening and inhomogeneous (coherent) broadening. The type of the broadening due to a superposition of many different sharp signals is called coherent line broadening. In contrast incoherent line broadening can simply be defined as the types of broadening that are not due to a distribution of sites. There are many sources of incoherent line broadening, namely chemical shift anisotropy and dipolar broadening. From the linewidths of a beak an estimate of T2 can be determined.[50] The line widths at half height (Δν 1/2) are inversely proportional to T2

$$\Delta\nu = \frac{1}{(\pi)(T_2^*)} \qquad [31]$$

Where T_2^* is the effective spin-spin lattice relaxation time constant.[51] The other sources of incoherent line broadening are slow motion and chemical exchange.

2.3 Push-Pull Ethylenes

Push-pull ethylenes can be represented by the general formula 1 where A and/or B represent electron-donating groups and X and/or Y represent electron –accepting groups. Other substituents may be aryl or alkyl groups.[30]

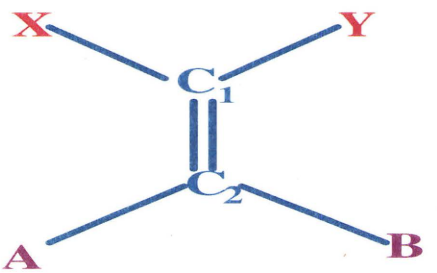

Figure 29. Push-pull ethylene

The conformational properties of such compound have been the subject of much interest, mostly centered on the low torsional barriers of the C_1=C_2 bond, which are sometimes below the limit for the DNMR technique, 20.0 k Joule/mol for this type of compound. When the donor and the acceptor groups have suitable structures, for example, acetyl and dimethylamino groups, they often show hindered rotations with substantial torsional barriers. These properties, low C=C barriers and C-A and C-B barriers, are in general ascribed to electron delocalization, illustrated by the limiting structures (Figure 30a and 30b).[16;30;52]

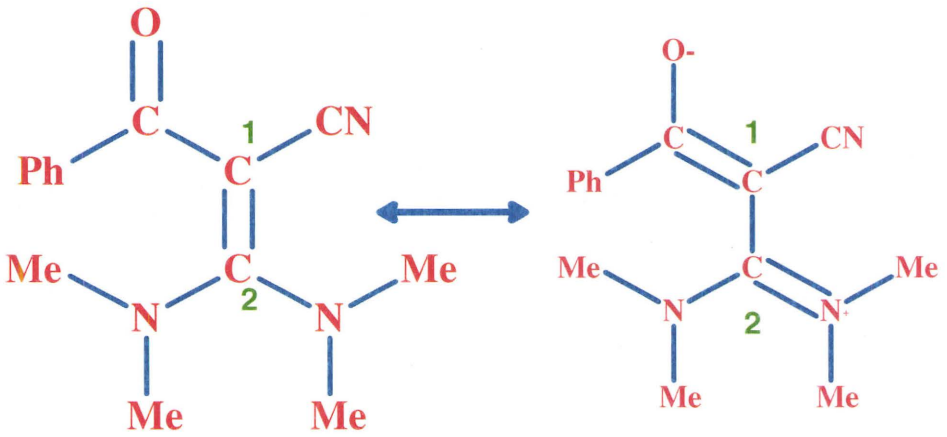

Figure 30a **Figure 30b**

Resonance structures for a push-pull ethylene.

In many cases, the barriers have been explained by high single –bond character of the C_1=C_2 bond and high double-bond character of the C-A and C-X bonds, respectively, due to considerable weight of such polar limiting structures as 30b .This is an example of the often fallacious "ground state thinking," trying to explain an energy difference in terms of the properties of the ground state only. In fact, these molecules have quite stable ground states when strong steric effects are absent , and the low C=C barriers must be due primarily to the capacity of the X-C-Y part to stabilize a negative charge and the A-C-B part to stabilize a positive charge in the 90° twisted transition states.

2.3.a Aminomethylene Compounds with two Acceptor Groups

In N, N-dialkylated members of this group, several authors[52-56] have observed fast thermal isomerizations at the double bond, using DNMR technique. Most compounds of this type also display hindered rotation about the C-N bond with substantial rotational barrier.[57]

Compounds of the general type, Figure 31a and 31b (R = H or CH_3) with a variety of aliphatic and aromatic N-substituents show several cases of double-bond rotation with barriers in the range of 79.5 to less than 37.7 kJ/mol, while NMe_2 torsional barriers are found in the range of 73.6 to less than 37.7 kJ/mol. When R = Me, all barriers are lower than when R = H, indicating a considerable ground state strain in the formercase.[27;28;58] When R1 (R2) is aromatic, a decrease in the C-N and an increase in the C=C barrier is observed.[28] According to Sandstrom[16] interesting substituent effects are observed, the CN barrier is in reverse order, a result obviously not expected from simple bond order arguments.

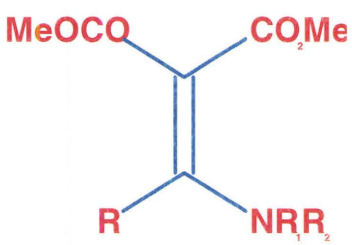

Figure 31a

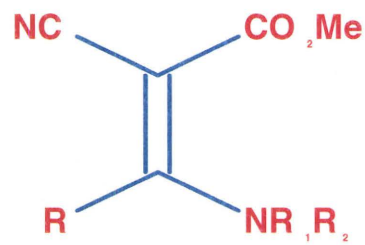

Figure 31b

General form of a push-pull ethylene

According to Dahlqvist,[32] molecule Figure 31b ,(R=R1=R2=Me) was subjected to a careful line-shape study over a wide range of temperature. The C-N barriers obtained in the two rotamers molecule 31a and 31b with respect to the C=C bond were quite different from those obtained by coalescence approximation. It was also found that the activation entropy for the C=C rotation was 41.7 to 75.6J/mol K. more negative than that for the C-N rotation.

Further line-shape work[59] has been performed on malonic ester derivatives figure 31a) (R=H; R1, R2=-(CH2)n-, with n increasing from 2 to 5). The C=C barriers showed a steady decrease from $\Delta G^{\ddagger}$ >97.1 kJ/mol for n=2 to 61.1 kJ/mol for n = 5, whereas the C-N barriers were less dependent on the ring size. An exception was the aziridine derivative, for which the C-N barrier, for which the C-N barrier was <30.5 kJ/mol.

β, β-Diacylenamines (Figure 32) have continued to be the subject of considerable interest. Barriers to C=C and C-N rotation have been reported from systems where the carbonyl groups are held more or less rigidly in the plane by ring closure.[60]

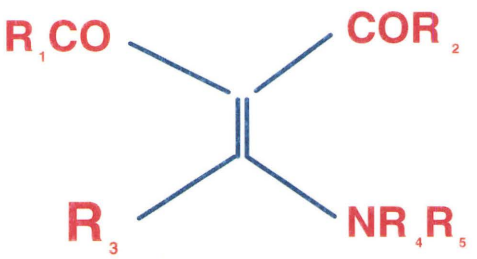

Figure 32. β, β-Diacylenamine

Some of these compound show remarkably high C-N barriers, which can be ascribed to superior resonance interaction in the planar system.[16] These barriers are in most cases higher in the compounds with 5-membered rings than in those with 6-membered rings, the reason probably being a larger ground state strain in the latter. The

relatively high C=C barriers in Figure 33 to 36 compared to that in Figure 37 are explained by the better resonance stabilization of the ground state in the planar compounds.

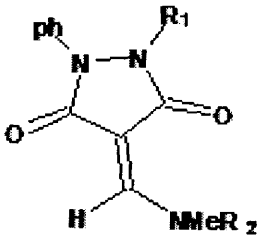

Figure 33.

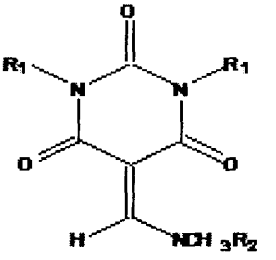

Figure 34

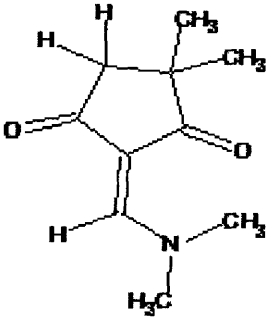

Figure 35.

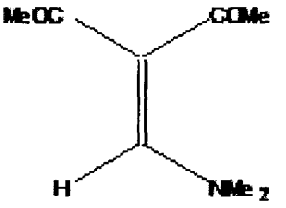

Figure 36.

In the transition state the capacity for stabilizing a negative charge is similar, except for Figure 36, where the high C=C barrier is explained by the competing donor effect of the nitrogen atom in the ring. In Figure 33 this is diminished by a urea-type conjugation of the nitrogen atoms with the third carbonyl group. The remarkably high C-N barriers in Figure 32 to Figure 34 indicate a very efficient ground state conjugation in the cyclic systems. This work presents a nice analysis of the interplay of stabilizing

conjugation and destabilizing steric interaction and their differential effects on the C=C and C-N barriers.[60]

A large and interesting group of diacylenamines has been studied by NMR and IR spectroscopy.[61] However, data have been recorded at room temperature only, and one of the conclusions seems questionable: the morpholino enamines (Figure 36) are assumed to exist entirely in the EE form:

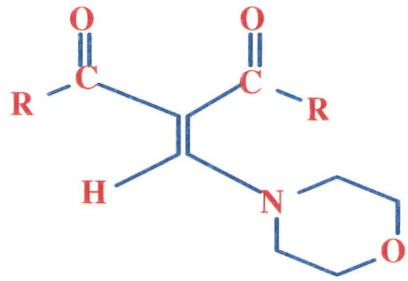

Figure 37. EE Configuration

This is a high-energy form, and a mixture of EZ forms and possibly the ZZ form is more likely.

Bakhmutov and Burmistrov [62] have studied a number of secondary enamines with a nitro group and a carbomethoxy group as acceptors (Figure 38a and 38b). These exist in two forms, both with strong hydrogen bonds.

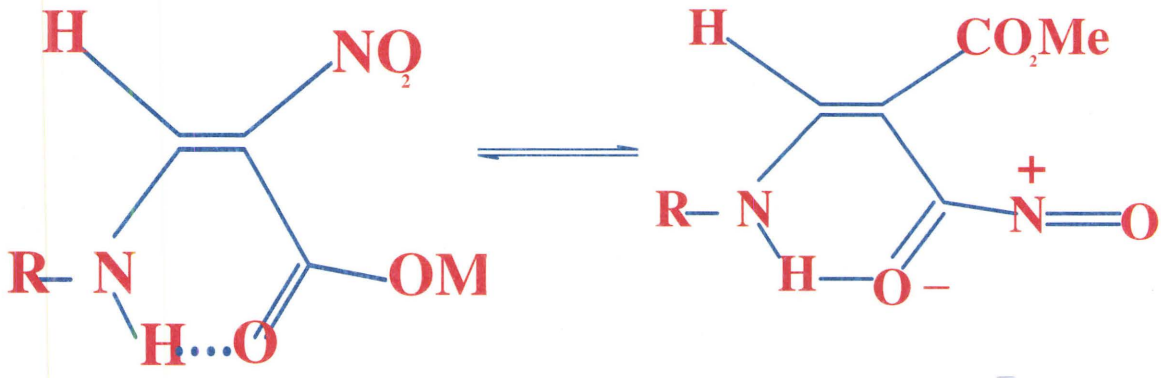

Figure 38a **Figure 38b**

Secondary enamines with a nitro group and a carbomethoxy group as acceptors

In solvents of very low basicity such as nitrobenzene, pure thermal rotation about C=C bond was demonstrated by the kinetic order of unity with respect to Figure 38a and 38b and by the persistence of the NH-CH coupling of 13 Hz to 15 Hz up to 200°C. In pyridine, on the other hand, the influence of X when R = p-XC_6H_4 indicated that formation of the anion of Figure 38a and 38b was the rate –determining step. The rate of NH exchange in pyridine solution was studied and the process was found to have a substantial negative activation entropy (-138 J/mol K), all indicating a bimolecular exchange mechanism. As for most acylenamines, the rotation is also subject to acid catalysis.

2.4 Line shape analysis

The Heisenberg uncertainty principle, although thought of in term of position and velocity of a particle, this principle can also be expressed in terms of the life time, Δt, and the uncertainty in the energy, ΔE ,of a state:

$$(\Delta t)(\Delta E) \approx \frac{h}{2\pi} \qquad [32]$$

According to this, if the life time of an excited state is infinite, there will be no uncertainty in its energy. However, if the life time is very short, the uncertainty in energy will be large. The uncertainty in energy is, in turn, manifested in an uncertainty in the frequency of a spectroscopic emission or absorption. Since

$$\Delta E = h\Delta\nu$$
$$(\Delta t)(h\Delta\nu) \approx \frac{h}{2\pi} \qquad [33]$$

and, therefore,

$$\Delta\nu \approx \frac{1}{(2\pi\Delta t)} \qquad [34]$$

so,

$$\Delta t \approx \frac{1}{(2\pi\Delta\nu)} \qquad [35]$$

Now, if a nucleus is exchanging between sites A and B, which have resonance frequency of ν_A and ν_B, a single broad line should appear when the uncertainty in the frequency, Δν, covers the range of frequencies between ν_A and ν_B. At this point, the time spent at each site is approximately Δt. For example, if the resonance frequencies are separated by 15 Hz, a single broad peak will result when the residence time is

$$\Delta t \sim \frac{1}{[2\pi\ (15\ Hz)]} \sim 10^{-2}\ s$$

Since the rate is the reciprocal of the residence time, the rate of exchange would be, therefore:

$$Rate \approx 2\pi\Delta\nu \qquad [36]$$

It is clear from this elementary treatment that the range of rates observable by NMR depends on the separation, in Hz, of the resonances of the nuclei involved in the dynamic process. The separation, in turn, depends on the strength of the magnetic field used to observe the nuclei, the nature of the nucleus (which determines the dispersion, or range, of chemical shifts) and, of course, the chemical environment of each nucleus involved in the dynamic process.

Although the uncertainty principle can be helpful in explaining the relationship between rate and $\Delta\nu$, the actual shape of the resonance lines can be completely described only by much more complex mathematical relationships. Usually these relationships are developed by modifying of a set both equations developed by Bloch.[63-65] The Bloch equations described the time dependence of the macroscopic magnetic moment in terms of the applied magnetic field, B_o, the radio frequency field, B_1, and the relaxation times, T_1 and T_2. These equations have been modified by others to include the effects of exchange. First, the first order chemical reactions describe such processes as isomerizations, conformation change, etc. The kinetics is described by the following equation:

$$\frac{dC_p}{dt} = \sum_r k_{pr} C_r \qquad [37]$$

Here C_p is the concentration of reagent P, k_{Pr} is the rate for the reaction

$$P \rightarrow r \qquad [38]$$

The following expression expresses the conversion law

$$0 = \frac{d}{dt}\sum_{p} C_p = \sum_{p,r} k_{pr} C_r \Rightarrow \sum_{p} k_{pr} = 0 \qquad [39]$$

as we see the total amount of matter in the other word the concentration does not change.

We can define the bulk magnetization

$$M = mc \qquad [40]$$

$$m = m_0 n \qquad [41]$$

So its time derivative is

$$\frac{dM}{dt} = C\frac{dm}{dt} + m\frac{dC}{dt} \qquad [42]$$

Combined kinetic equations

$$\frac{dM'_{+p}}{dt} = -\left(i\Omega_p - iw + \frac{1}{T_{2P}}\right) M_{+P}{}' + iM_Z\Omega_1 + \sum_r \frac{m_P}{m_r} k_{pr} M'_{+r} \qquad [43]$$

$$\frac{dM_{ZP}}{dt} = -M_y\Omega\frac{1}{T_{1P}}(M_{ZP} - M_{0p}) + \Sigma\frac{m_p}{m_r} k_{pr} M_{zr} \qquad [44]$$

where Ω is the resonance frequency.

As we see from the above equations we neglected the effect of magnetic field influence to chemical reaction:

$$\frac{m_P}{m_r} \approx \frac{m_{0p}}{m_{0r}} \approx 1 \qquad [45]$$

Usually this is a very good approximation because magnetic interactions are much less than chemical and other interactions. However, that under specific conditions

the magnetic field can affect chemical yield (magnetic effect)[66, 44] or chemical reactions produce reagents with non equilibrium magnetization. The above equations are called the modified Bloch equations. The resulting equations are quite complex but can be used to generate, usually by computer, line shapes for any set of nuclei inter-converted by some dynamics process.

The usual procedure for a total line shape analysis is to generate and plot a series of line shape, each of which corresponds to a different exchange rate. Each plot is then compared with the actual shape of the resonances at a particular temperature. The closest fit may be determined visually, by least squares comparisons or by some other technique designed to minimize the differences between certain features of the plotted and actual spectra. The mean lifetime, τ, is obtained from the plot that gives the best fit and is then converted to the rate constant at the temperature. If the same procedure is repeated at a number of different temperatures, an Eyring plot of ln k/T vs 1/T produces a straight line with the familiar form y = -mx + b (Figure 39), where:

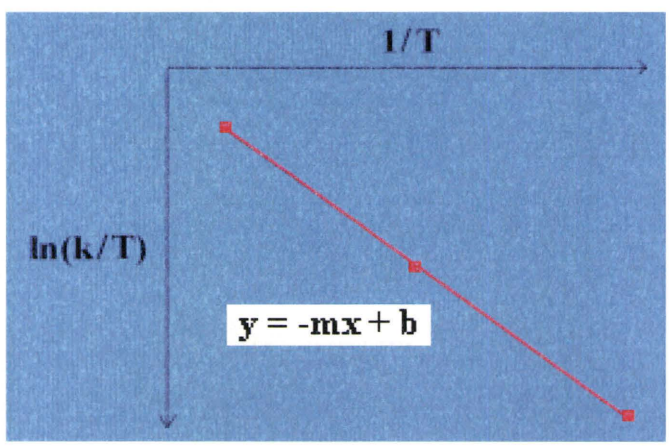

Figure 39. Eyring plot

$x = 1/T$

$y = \ln(k/T)$

$m = -\Delta H^{\ddagger}/R$

$b = y\ (x = 0)$

$\Delta H^{\ddagger}$ can be calculated from the slope m of this line: $\Delta H^{\ddagger} = -m \cdot R$. $\Delta S^{\#}$ can be determined using the y-intercept

$$y(x=0) = \ln\frac{k_B}{h} + \frac{\Delta S^{\ddagger}}{R} \qquad [46]$$

The free energy of activation can be obtained from the Eyring equation:

$$\ln k = \ln(\frac{k_B}{h}.T) - \frac{\Delta H^{\ddagger}}{R}.\frac{1}{T} + \frac{\Delta S^{\ddagger}}{R}$$
$$\ln\frac{k}{T} = -\frac{\Delta H^{\ddagger}}{R}.\frac{1}{T} + \ln\frac{k_B}{h} + \frac{\Delta S^{\ddagger}}{R} \qquad [47]$$

Where k_B = Boltzmann's constant [$1.381 \cdot 10^{-23}$ J · K^{-1}]

h = Plank constant [$6.626 \cdot 10^{-34}$ J · s]

2.4.a MEXICO Program

The McMaster program for Exchange lineshape calculations

Mexico is a one dimensional line-shape analysis tool used to acquire rates, and it is written in C computer language. Rates are varied until the simulated line of Mexico matches the experimental data. At very low temperatures, the NMR signals are distinct (Figure 40).

As the temperature is increased, the rate of rotation increases, the NMR signals broaden, move closer together, and coalesce into one single sharp peak.

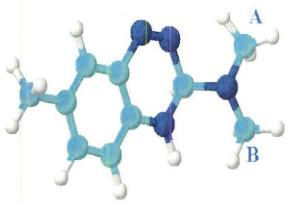

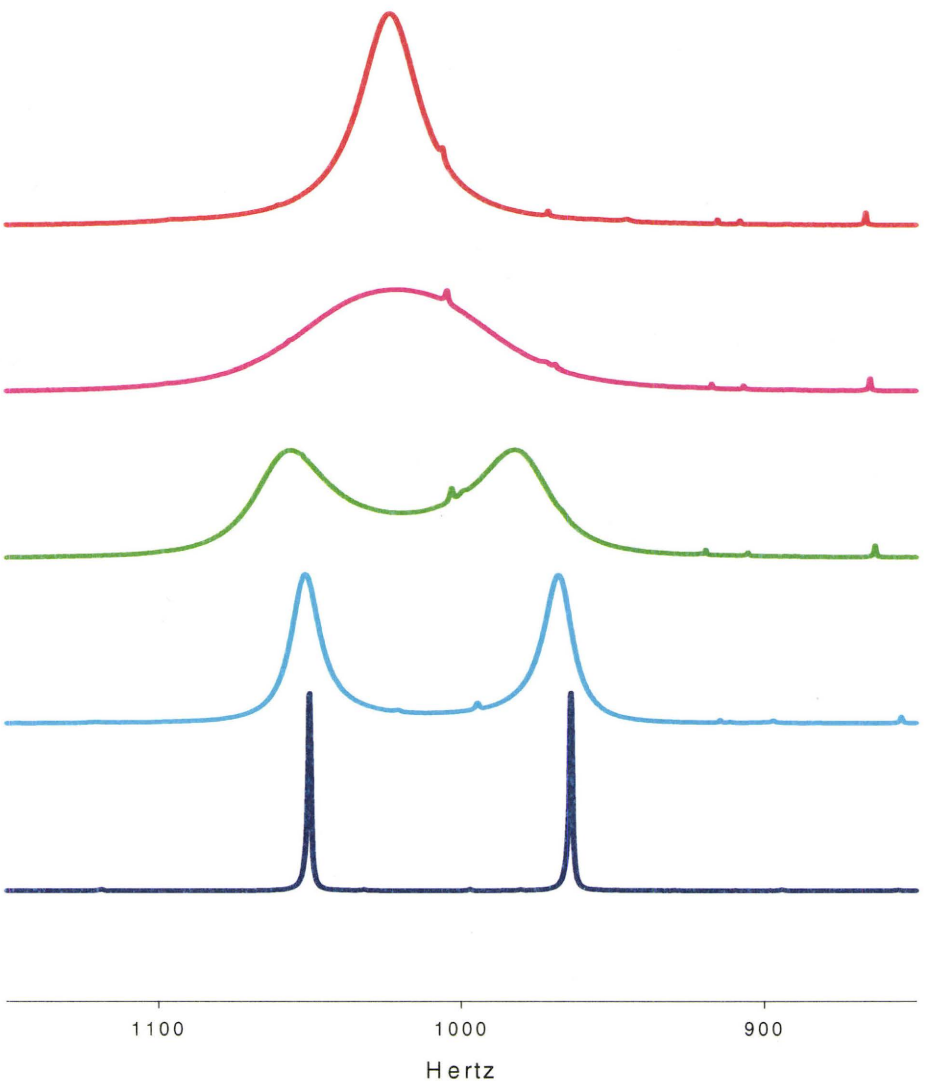

Figure 40

The calculation of the line shape in case of two equally-populated sites without coupling can be done by applying a modified set of Bloch equations. For the coupled system the same approach is used as the uncoupled simulation system, but the uncoupled simulation system is simpler, since there is a one-to-one correspondence between the sites and the lines in the spectrum. If the spectral parameters are different in the two sites of a coupled system a single transition in one site could map into parts of several transitions in the other site (Figure 41). And that needs a full density matrix calculation treatment.

MEXICO simulated spectrum is acquired by varying frequencies and rates some other parameters until a best fit is accomplished. For the best reference please see A. D. Bain review.[22]

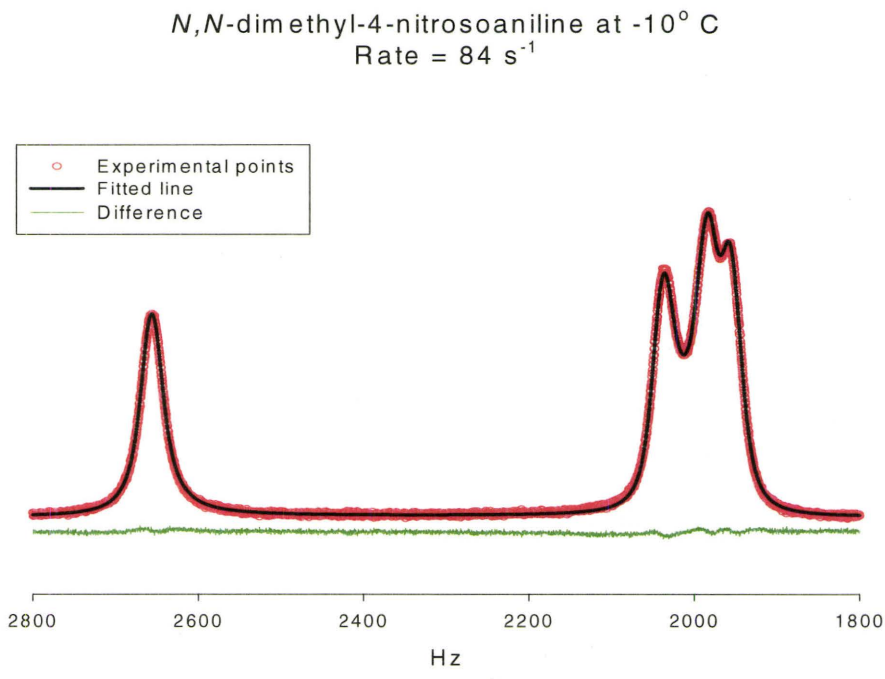

Figure 41. Simulated spectra versus experimental spectra of N,N-dimethyl-4-nitrosoaniline at -10°C

2.4.b CIFIT program

CIFIT is a program for fitting data from a selective inversion relaxation experiment on a system undergoing slow chemical exchange. In slow exchange, each different site is observable. They can be perturbed away from equilibrium, and observed as they return. This return to equilibrium is governed by a set of coupled differential equations. Given a table of observed intensities as a function of time, and a proposed mechanism, CIFIT will try to find the set of parameters (rates, relaxation times, initial and equilibrium intensities) that best fit the experimental data.[67;68]

Summary

The theory behind NMR was discussed in this chapter. When subjected to a magnetic field, nuclei orient themselves along the z-axis. A pulse disturbs the nuclei and the difference between the ground state and the excited state is measured. The pulse flips the magnetization vector from the z-axis to the transverse xy plane. The signal detected is the FID. The chemical shift is produced by different chemical and magnetic environments experienced by the nuclei. Rates were obtained from MEXICO and CIFIT programs. 1H 1D NMR spectra were obtained at differed temperatures. The rates were obtained by comparing the real and the fitted spectra and minimizing their differences.

Chapter 3

STRUCTURE DETERMINATION

3.1 Synthesis and mechanism

The push-pull ethylene system MDACC was synthesized according to a procedure given by Shvo and Shanan-Atidi reference.[28] [27] All reagents were purchased from Aldrich and used without further purification. Dimethylactamide dimethyl acetal (19.95 g; 0.15mol) and methyl cyanoacetate (14.85g; 0.15mol) were mixed. After 0.5 hour the resulting oil was vacuum distilled (bp 115-116 °C and 10^{-3}torr), and yielded orange-yellow distillate that crystallized when cool. The solid then re-crystallized from ethyl acetate-hexane in 80% yield with a melting point of 59 °C.[27;28] The proposed mechanism is shown below:

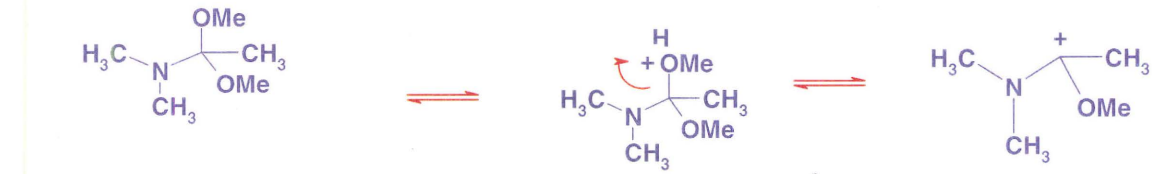

N,N-dimethylacetamide dimethyl acetal

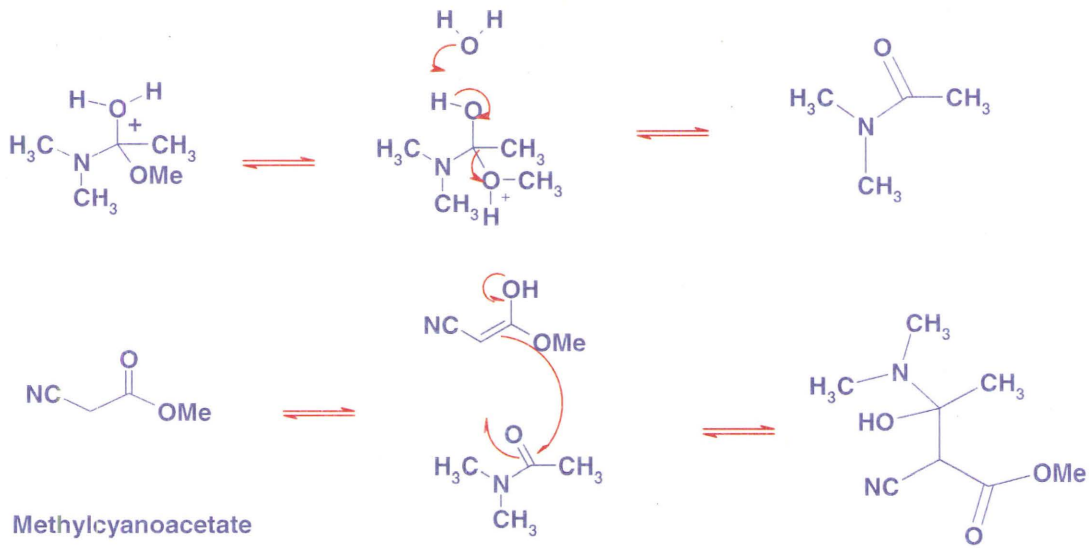

Methylcyanoacetate

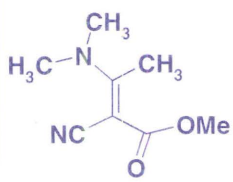

MDACC

Figure 42. Mechanism for formation of MDACC

3.2 Structure identification

Many NMR experiments have been employed at different temperature to be certain that we have the target molecule. The 1D ^{1}H-NMR spectrum of MDACC in CD_2Cl_2 was acquired using Bruker-AV500MHz (Figure 43) at -58°C. The low temperature spectrum exhibits pairs of signals for each equivalent group of protons, corresponding to the E and Z configuration, it should be noted that, at this temperature, rotation about the C-N bond is slow and the two N-methyl groups are nonequivalent. The relative populations of the two isomers are immediately obtained by integration of the two completely resolved C-methyl absorptions. The three sets of peaks are in the region of 2.2 - 3.8 ppm. The two signals at 3.66 and 3.64 correspond to the $-OCH_3$ protons of the carbomethoxy group in the E and Z isomers, respectively. As the temperature is raised, three distinct coalescences of the four N-methyl absorptions occur which must correspond to three different kinetic processes, namely rotation about the C-N bonds in E and Z configuration, and rotation about the carbon-carbon double bond.

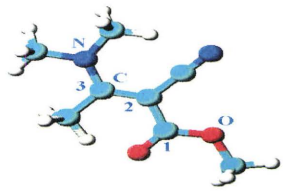

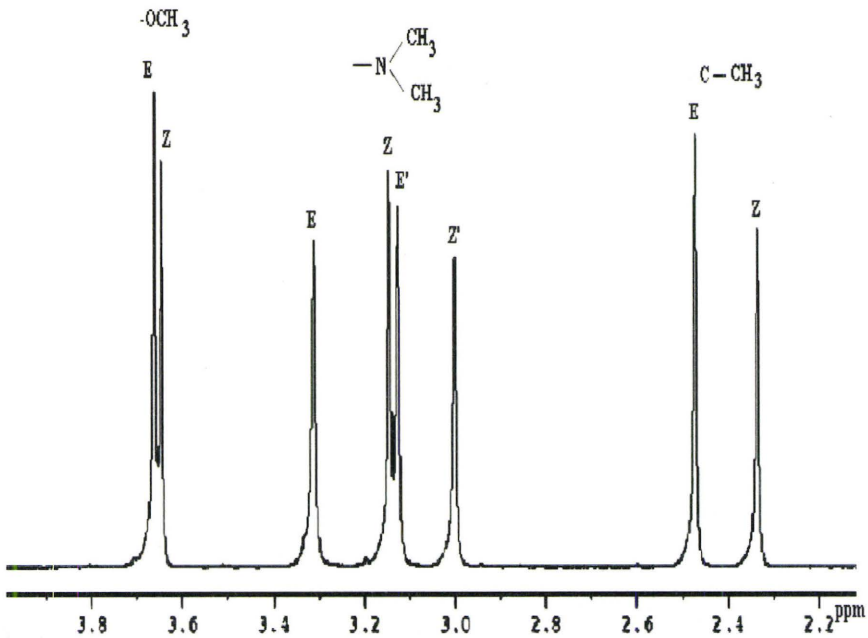

Figure 43. 1D ^{1}H NMR for MDACC in Cd_2Cl_2 at -58°C.

The peaks at 3.3 (E-configuration), 3.17 (Z-configuration), 3.1 (E'-conformation) and 3.0 (Z'-conformation) ppm arise from the –N $(CH_3)_2$ protons. The peaks at 2.47 and 2.33 ppm correspond to the C-CH_3 protons in the E and Z configuration, respectively (Table 7).

The explanation of this assignment will be discussed later. The spectrum was acquired at 500MHz using a zg30 pulse program. The spectrum was collected with P_1=7.70μs, SFO1=500.1326316MHz, NS=8 scans, D1=2.5 sec, DE=6.0μs, DW=73.8μs, AQ=2.4sec, SWH=6775.07Hz, DS=0 and TD=32k. The 1D ^{1}H-NMR spectrum of MDACC in CD_2Cl_2 was acquired using Bruker-AV500MHz (Figure 44) at 25°C .Unfortunately, overlapping spectrum was observed (Figure 44).

^{1}H number	Chemical shift in ppm
O-CH_3 E	3.66
O-CH_3 Z	3.64
–N-CH_3 E	3.31
–N-CH_3 Z	3.17
–N-CH_3 E'	3.11
–N-CH_3 Z'	3.01
C-CH_3 E	2.47
C-CH_3 Z	2.44

Table 7. Proton Chemical Shifts for MDACC

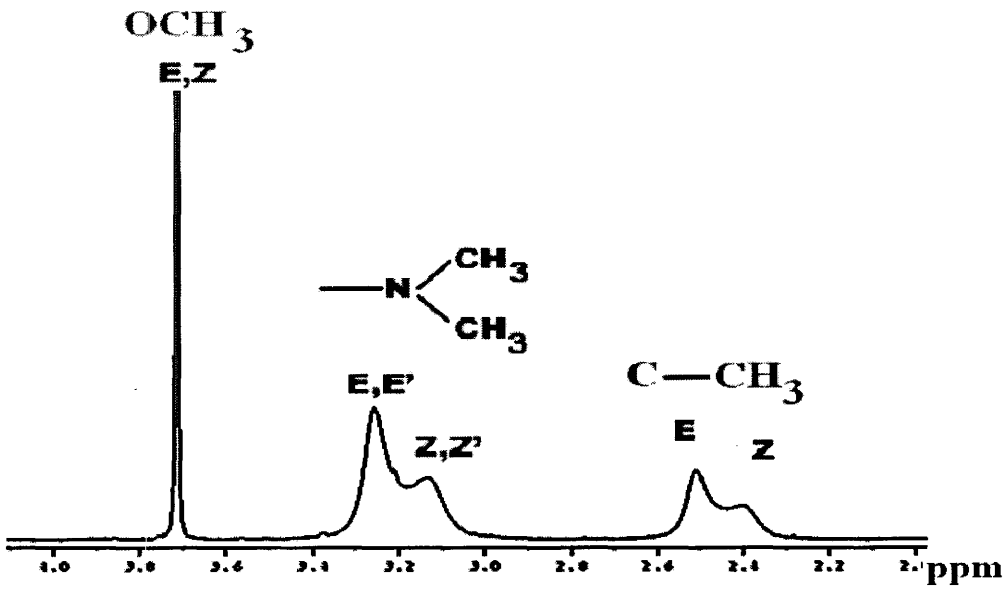

Figure 44. 1D ^{1}H NMR for MDACC in $CdCl_3$-at 25°C.

The 1D ^{1}H-NMR spectrum of MDACC in toluene-d_8 was acquired using Bruker-AV500MHz (Figure 45) at -68°C. As can be seen from Figure 45 the ^{1}H chemical shifts are different than ^{1}H NMR of MDACC in CD_2Cl_2 at -58°C.

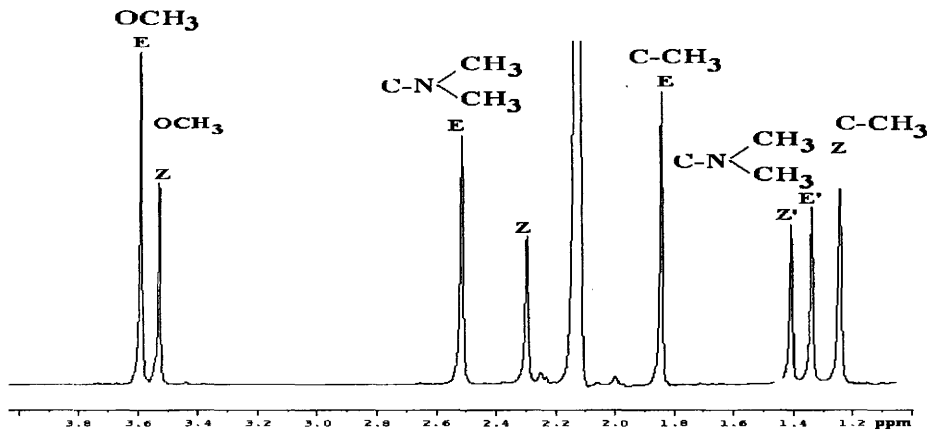

Figure 45. 1D ^{1}H NMR for MDACC in C_7D_8 at - 68°C.

1D ^{13}C NMR spectrum of MDACC in CD_2Cl_2 was acquired using Bruker-AV500MHz (Figure 46). At -48.0 °C the spectrum shows seven sets of peaks in the region 15 ppm – 180 ppm. The assignment is shown in Table 8. I would like to point out that carbon number two and three are the most interesting carbon in this molecule their chemical shifts difference is 102ppm! The justification of these assignments is discussed in the next section. The spectrum was collected by using the following parameters: ZgPg30 pulse program with P_1=12.8μs, SFO1= 125.7709968, SFO2=500.1326316MHz, NS=3072 scans, D1=0.5 sec, DE=4.5μs, DW=17.25μs, PL13=32dB, pl12=27dB, AQ=0.56sec, SWH=28985.51Hz, DS=2 scans, D11=0.03sec, D12=0.02 ms and TD=32k.

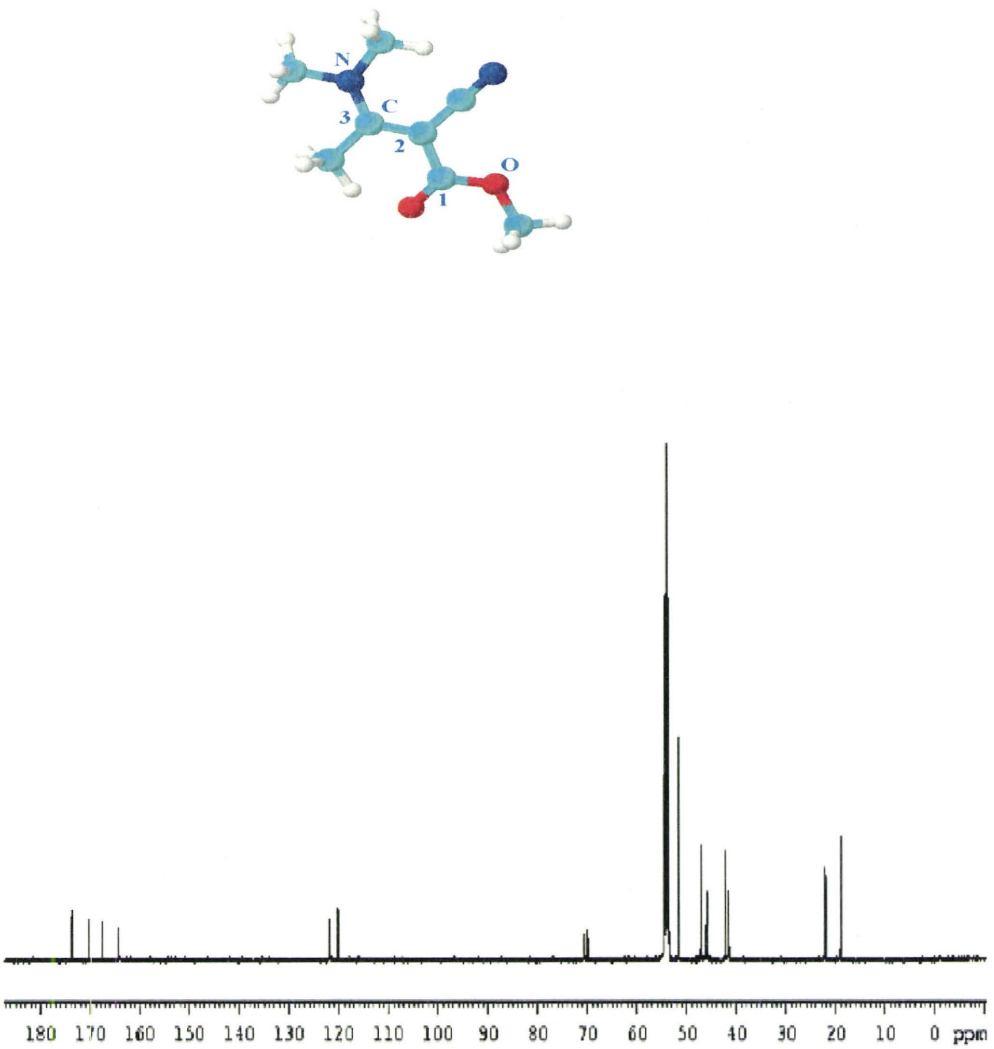

Figure 46. 1D ^{13}C solution NMR for MDACC in CD_2Cl_2 at -48.0 °C

Carbon number	Chemical shifts in ppm
3-E	173.8
3-Z	170.3
1-E	167.6
1-Z	164.2
Cyano-E	121.9
Cyano-Z	120.2
2-E	70.54
2-Z	69.91
O-CH_3	51.56
N-CH_3-E	47.07
N-CH_3-E'	45.89
N-CH_3-Z	42.12
N-CH_3-Z'	41.47
C-CH_3-E	22.01
C-CH_3-Z	18.89

Table 8. 1D ^{13}C NMR for MDACC in CD_2Cl_2 at -48.0 °C

3.2.a Cross Polarization Magic-Angle Spinning (CPMAS)

The purpose of this experiment was to identify the 1D ^{13}C NMR spectrum of the two configurations. Cross Polarization Magic-Angle Spinning (CPMAS) shows only one configuration of ^{13}C. X-ray crystallography is clearly shown the E –configuration is present at room temperature (X-ray result is shown at the end of this section). So the same X-ray quality of crystals was taken and CPMAS experiment was employed, then the resulting ^{13}C (Figure 47) spectrum should be in agreement with x-ray result. Thus, chemical shifts from CPMAS (which is corresponded to the E- configuration) were subtracted from the ^{13}C solution NMR spectrum. That successfully led to do the assignment for 1D^{13}C spectrum. CPMAS chemical shifts are given in Table 9.

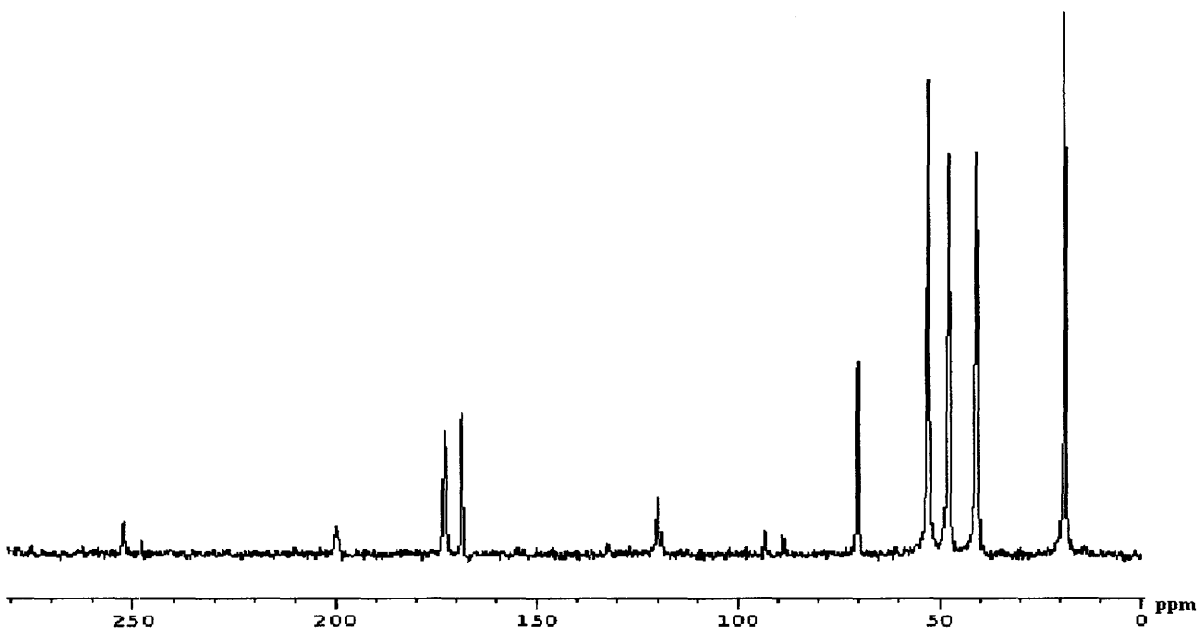

Figure 47. 1D ^{13}C-CPMAS solid state NMR

Carbon number	Chemical shifts in ppm
3-E	172.8
1-E	168.2
Cyano-E	120.1
2-E	70.23
O-CH_3-E	52.61
N-CH_3-E	47.54
N-CH_3-E'	40.49
C-CH_3-E	18.52

Table 9. CPMAS chemical shifts

3.2.b HMBC (Heteronuclear multiple bond correlation spectroscopy)

The HMBC experiment establishes multiple-bond correlations by taking advantage of the greater sensitivity associated with proton detection, and in essence is the HMQC sequence tuned to detect correlations via small couplings.[2;69] Owing to the close similarity of the two, only differences pertinent to HMBC will be presented here.

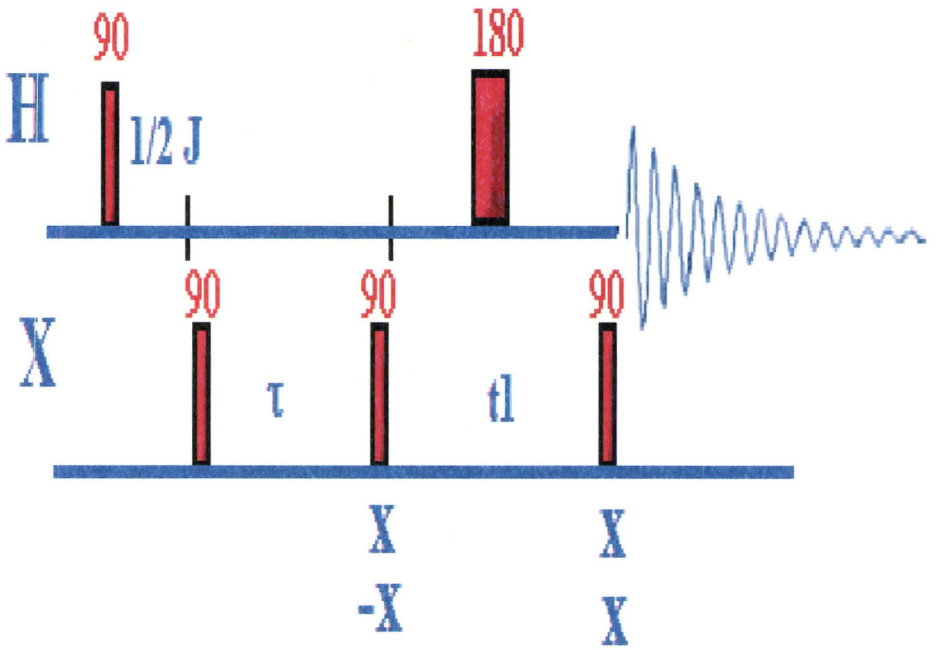

Figure 48. The HMBC pulse sequence

The HMBC experiment detects long range coupling between proton and carbon (two or three bonds away) with great sensitivity. The length of the tau delay can be adjusted to detect relatively large coupling constants (4-10 Hz) tau = 0.06 s or smaller couplings (2-7 Hz) tau = 0.1 s.

In this sequence, the first 90° pulse on Carbon-13 serves as a low-pass filter that suppresses one-bond correlation and passes the smaller coupling. This pulse creates multiple quantum coherence for the one-bond coupling which is removed from the spectra by alternating the phase of the Carbon-13 pulse. The second 90° pulse on C-13 creates multiple quantum coherence for the long-range couplings. After the evolution time t1, the magnetization is converted back into detectable single quantum proton magnetization. The carbon decoupler is never used in this sequence: therefore the protons displays homonuclear as well as heteronuclear couplings (Figure 48).

This technique is very valuable to detect indirectly quaternary carbons coupled to protons - specially useful if direct Carbon-13 is impossible to obtain due to low amount of material available. This very useful sequence provides information about the skeleton of a molecule. It could be an alternative to the 2D-INADEQUATE experiment (which is so insensitive). It is also very useful in carbohydrate area as a sequence analysis tool that provides unique information concerning connectivities across glycosidic linkages. Another area of interest for using HMBC is in the peptide-protein area - especially when applied to a 15N labeled protein - It is possible with this technique to get connectivities between the Nitrogen and the CH^{α} proton of the amino acid of the next residue.

The tuning of the experiment is achieved by setting the Δ preparation period to a sufficiently long time to allow the small long – range proton-carbon couplings to evolve to produce the anti-phase displacement of vectors required for the subsequent generation

of heteronuclear multiple-quantum coherence. Since long-range ^{1}H-^{13}C couplings are at least an order of magnitude smaller than one-bond couplings (often <5Hz), Δ should, in principle, be at least 100ms ($1/2^{n}J_{CH}$), although shorter delays are often used routinely to avoid relaxation losses. During this long Δ period, homonuclear ^{1}H-^{1}H couplings, which are of similar magnitude to the long-range heteronuclear couplings, also evolve and introduce phase distortions to the observed crosspeaks (these distortions are small enough to be ignored in HMQC because of the much smaller Δ periods used). Absolute-value presentations are therefore widely used for HMBC spectra to mask these phase errors and it is therefore a common place to acquire HMBC data set that are phase-modulated (N-type selection) as a function of τ. For sensitivity reasons, the refocusing period of HMBC is omitted in HMBC so that long-range heteronuclear couplings are antiphase at the start of t, precluding the application of ^{13}C-decoupling.

Although the Δ period is chosen according to long-range couplings, it may also happen to be a multiple of the appropriate setting for one-bond correlations, additionally causing these to appear. Since the FID is acquired without ^{13}C decoupling, these possess distinctive doublet structure in f_2 which aids their identification. These may be considered useful additions or unwanted interferences, depending on your point of view; while they simultaneously provide one-bond correlation, they may obscure or become confused with long-range correlations. Their suppression is at least partially afforded by the addition of a one-step low-pass J-filter (so-called because it retains or passes only those peaks arising from couplings that are smaller than a chosen cut-off value, here the one-bond coupling constant). Here, the Δ_1 period is set according to $^{1}J_{CH}$, whilst Δ_2 is set according to the long-range coupling. Alternation of the phase of the first carbon pulse without changing that of the receiver causes the signals originating from the one-bond

correlations to cancel on alternate on alternate scans. In practice, the suppressions is often not complete particularly when a wide range of J_{CH} values are present, and a purge scheme in addition to the low phase J-filter has been shown to provide improved suppression. [9]In routine studies one may omit all filtering schemes and accept the presence of breakthrough from one-bond couplings.

Without any doubt, the greatest problem associated with the HMBC sequence lies in the suppression of the parent ^{1}H-^{12}C signals which may otherwise mask the long-range satellites. Unlike HMQC, the BIRD sequence is not well suited to the removal of these resonances since this is also likely to lead to attenuation of the desired signals. Traditionally, the sequence has relied on the phase cycling alone to cancel the intense parent resonance, requiring a very stable spectrometer to be effective. Even so, bands of residual t-noise routinely plagued the original HMBC experiment and limited its use as a routine tool in organic chemistry.

The presence of long-range correlations in HMBC spectra is influenced by many factors, both experimental and structural, and an awareness of these points is important for the optimum application and interpretation of the experiment. Crosspeak intensities depend upon, among other things, both the magnitude of the long- range coupling and on the value selected for Δ, which should optimally be set to $1/2^{n}J_{CH}$ (crosspeak intensity α sin $\pi^{n}J_{CH}\Delta$). Long-range proton-carbon coupling over two or three bonds rarely exceed 25 Hz, and in the absence of unsaturation are more often less than 5 Hz indicating Δ should be 100 ms or more. Such long delays can lead to relaxation losses prior to detection, especially for larger molecules, so in practice a compromise is met with Δ being set to around 60-80 ms for routine applications. Since small organic molecules tend to have slower relaxation rates, longer delays can be used successfully in the search

for more connectivities through smaller couplings, with Δ taking values of up to 200ms. When using longer delays it is also becomes possible to detect peaks that arise from 4-bond correlations which are most likely to occur when the coupling pathway contains unsaturation or when it has the planar zig-zag (w-coupling) configuration, as commonly observed in long-range proton-proton couplings also. One should also recognize that three-bond couplings can be, and often are, greater in magnitude than two-bond couplings, displaying a Karplus –type relationship with the dihedral angle. Indeed, one of the limitations when using HMBC data the lack of differentiation between two-and three-bond connectivities. Furthermore, the lack of a correlation cannot on its own be taken as evidence for the nuclei in question being distance in the structure, since a variety of factors can contribute to $^{n}J_{CH}$ being close to zero. The most intense correlations are typically observed for methyl groups since magnetization is detected on three protons simultaneously and because they display simpler coupling structure, if any whereas the weakest correlations are generally associated with poorly resolved, complex proton multiplets.

Despite the lack of discrimination, protons can potentially correlate to a great number of carbon neighbors within two or three bonds, providing a mass of structural data on an unknown molecule. Connectivities may also be traced across heteroatom linkages where proton-proton couplings are usually negligibly small and in this the experiment is extremely effective at piecing together otherwise uncorrelated molecular fragments. Before justifying the ^{1}H assignment, I would like to address some points regarding to the importance of the 2D-HMBC experiment. First, COSY and TOCSY are powerful experiments that revealed the connectivity of two, three, and some times four and five bonds coupling. Unfortunately, there is no significant information that can be

collected from these experiments since all protons in this molecule are in methyl (CH_3) form. Second, 1D NOE could have been helpful in our case because we could measure the distance between the E and Z configuration of C-CH_3 and the ester group. But the E and Z chemical shifts are so close that when we tried to saturate one of them we end up flipping both signals. Third, 2D-NOESY would offer significant information, but the exchange was so strong therefore we end up getting Exsy crosspeaks instead.

Thus, the purpose of HMBC experiment was verifying the assignment of 1D ^{1}H NMR of MDACC. Please note that the assignment for ^{13}C was already recorded above from CPMAS so it is easy to do the assignment For 1D ^{1}H NMR by tracing ^{1}H- ^{13}C correlation. I would like to present some important examples of how HMBC was such a powerful technique for MDACC molecule (Figure 49). The small carbon peaks at 120 and 121 ppm show no correlation to any proton which is a tangible evidence that point out to the cyano group since it is 4 and 5 bond away from any proton methyls. The E configuration of O-CH_3 protons show a three bond correlation to the E configuration of carbon number one While, The Z configuration of O-CH_3 protons show three bond correlation to the Z configuration of carbon number one. The HMBC was done using these acquisition parameters. The pulse program is inv4gsipirnd, AQ-mod DQD, F2 dimension parameters TD 2048, NS=8, DS=64, SW=13.5465, SWH=6775.068, AQ=0.1511, RG=26008, DW=73.8, SFO1=500.1326316MHz. F1 dimension TD=256, SW=230.4626ppm, SWH=28985.508Hz, SFO2=125.7709968MHz. Processing parameter (F1) SI=1024, SF=500.1300053, offset=12.025, SR=5.30, wdw=sine.F1dimenion SI=1024, SF =125.7577913MHz, offset 220.251ppm, SR=-2208.67, WDW=SINE.

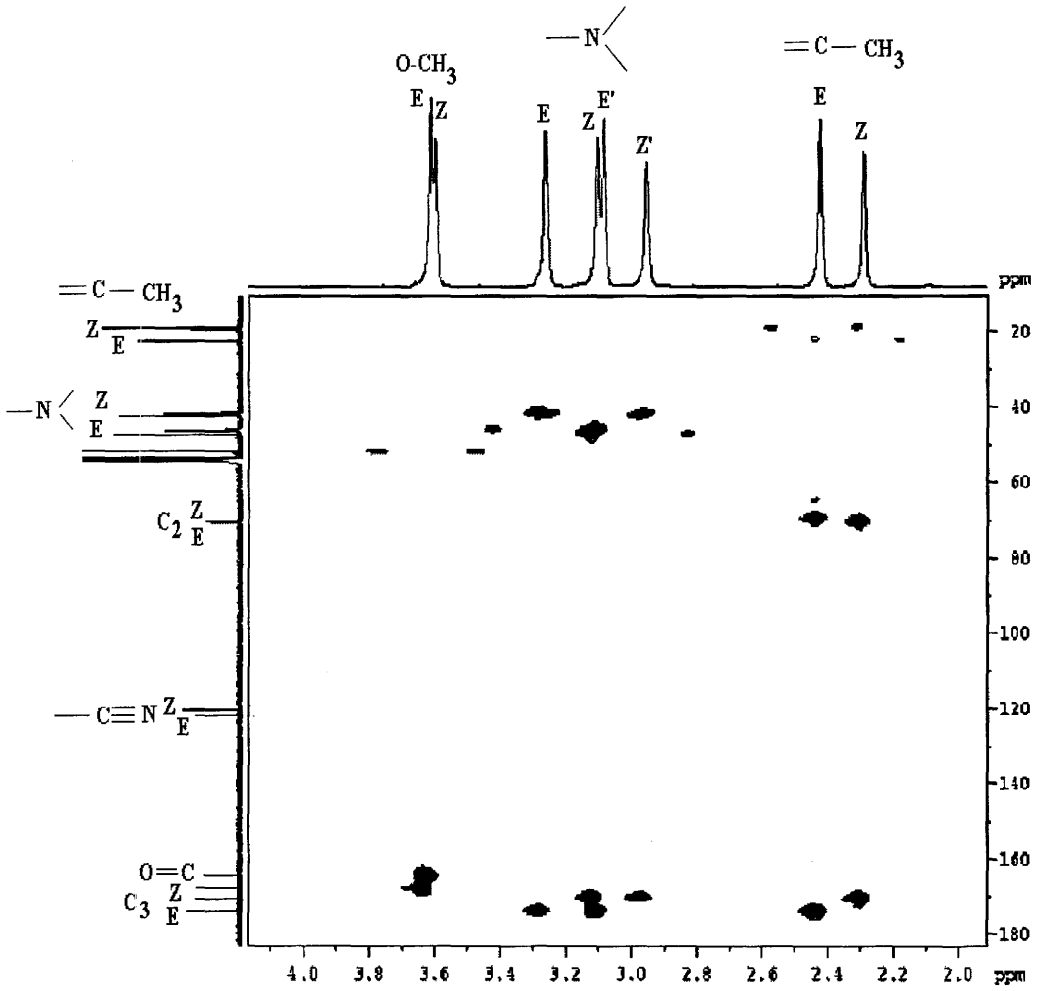

Figure 49. 2D HMBC for MDACC in CD_2Cl_2 at -45 °C

3.2.c X-ray

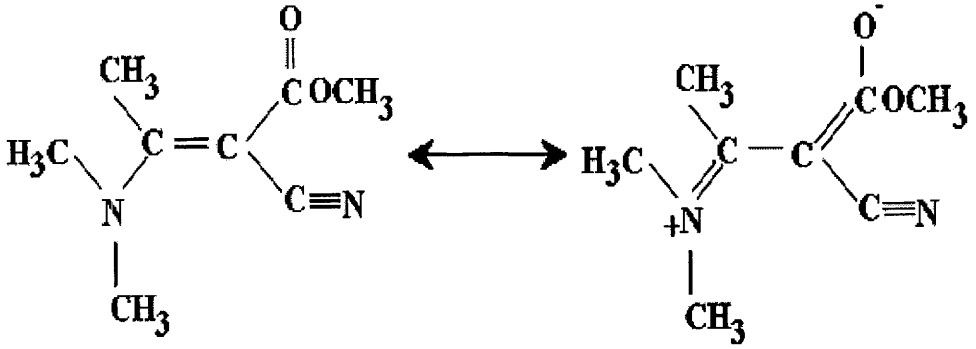

Figure 50. Resonance Structures of MDACC

The X-ray crystal structure of the MDACC has not been reported yet and is the subject of this section. The combined effects of the electron-withdrawing group and the electron-donating amino group serve to lengthen the central olefin bond of the MDACC from a normal value of 1.317 Å to the observed value of 1.406 Å.[70] Furthermore, the proposed resonance structure (Figure 50) agrees with the data obtained from the x-ray data. For example, the bond length between N4-C9 is 1.54 Å which is shorter than the normal value of 1.43 Å. The bond length between C1-C2 is 1.33 Å which is shorter than the normal value, 1.488 Å. The calculation numbers were obtained by Gaussian calculations, which will be discussed further in Section 4.9. The dihedral angle for C=C is -150.600 ° making it twisted (not planar). The C-N dihedral angle is -165.950 ° once again, making it twisted and not planar. This can be seen in Table 11.

Atoms	Bond length from X-Ray (Å)	Bond length from calculation (Å)
C(1)-O(12)	1.214	1.215
C(1)-O(9)	1.3494	1.322
C(1)-C(2)	1.456	1.455
C(2)-C(3	1.406	1.404
C(2)-C(10)	1.4214	1.427
C(3)-N(4)	1.3335	1.324
C(3)-C(7)	1.494	1.522
N(4)-C(5)	1.462	1.481
N(4)-C(6)	1.466	1.481
C(5)-H(5A)	0.960	0.980
C(5)-H(5B	0.970	0.970
C(5)-H(5C)	0.950	0.950
C(6)-H(6A)	1.000	1.0100
C(6)-H(6B)	0.910	0.900
C(6)-H(6C)	0.970	0.970
C(7)-H(7A)	0.890	0.890
C(7)-H(7B)	0.860	0.890
C(7)-H(7C)	0.96	0.970
C(8)-O(9)	1.427	1.432
C(8)-H(8A)	0.970	0.960
C(8)-H(8B)	0.950	0.950
C(8)-H(8C)	1.040	1.010
C(10)-N(11)	1.148	1.151

Table 10. Bond distances (Å) from X-ray data of MDACC versus the calculated.

Atoms	Torsion angle[°] from X-Ray	Torsion angle[°] from calculation
O(12)-C(1)-C(2)-C(3)	10.8	6.475
O(9)-C(1)-C(2)-C(3)	-171.35	-174.781
O(12)-C(1)-C(2)-C(10)	-175.38	-178.743
O(9)-C(1)-C(2)-C(10)	2.43	0.001
C(10)-C(2)-C(3)-N(4	27.2	19.026
C(1)-C(2)-C(3)-N(4)	-159.34	-166.392
C(10)-C(2)-C(3)-C(7)	-150.60	-158.872
C(1)-C(2)-C(3)-C(7)	22.9	15.707
C(2)-C(3)-N(4)-C(5)	17.3	27.253
C(7)-C(3)-N(4)-C(5)	-164.83	-154.733
C(2)-C(3)-N(4)-C(6)	-165.95	-160.408
C(7)-C(3)-N(4)-C(6)	11.9	17.606
O(12)-C(1)-O(9)-C(8)	3.9	-0.006
C(2)-C(1)-O(9)-C(8)	-174.02	-153.095
C(3)-C(2)-C(10)-N(11)	68	55.67
C(1)-C(2)-C(10)-N(11)	-106	-119.369

Table 11. Torsion Angles from X-ray data versus the calculated from MDACC

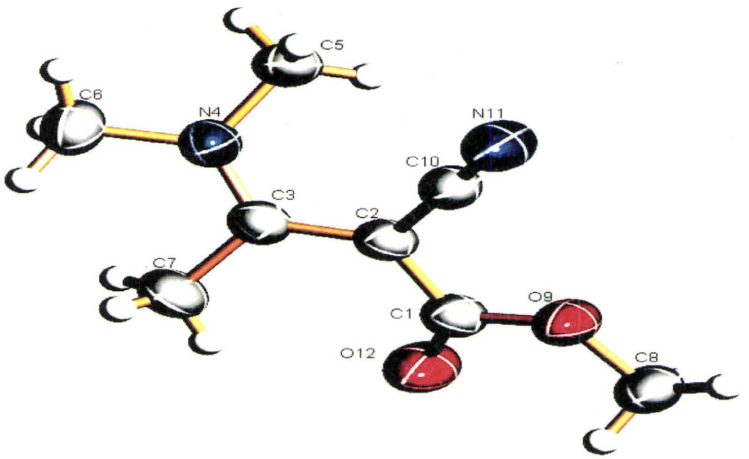

Figure 51. X-Ray Structure of MDACC

SUMMARY

A variety of 1D and 2D experiments were conducted in order to identify the structure of MDACC. These experiments include, 1D 1H spectra at several temperatures, 1D 13C, 1D CPMAS, 2D HMBC, and 2D EXSY. The x-ray data for the crystal structure of MDACC was in agreement with the proposed resonance structure.

Chapter 4

DYNAMICS

Solvent effects on the chemical exchange of the Push-Pull ethylene MDACC

Chemical exchange rates provide a sensitive probe of solvent effects in solution. The push-pull ethylene MDACC has three exchange processes E-Z, E-E', and Z-Z'. We have measured these rates in acetone-d_6, chloroform-d, tetrahydrofuran-d_8, toluene-d_8, methanol-d_4, acetonitrile-d_3, and methylene chloride-d_2. From this we obtain $\Delta H^{\ddagger}$, $\Delta S^{\ddagger}$, and $\Delta G^{\ddagger}$ of activation for each solvent. Different experiments were done to probe those parameters. For example, the temperature dependent 1D ^{1}H-NMR spectra of MDACC in different solvents were acquired using Bruker-AV500MHz at different temperature. The rates were obtained by using MEXICO program line shape analysis. This is very reliable at temperature before coalescence. 1H selective and non selective T_1 experiments were done using Bruker-AV500MHz. This is very powerful quantitative technique to probe the rate at low temperature. Exchange spectroscopy (EXSY) experiment is used here to prove qualitatively there is an exchange.

4.1 Exchange spectroscopy (EXSY)

Although the mechanisms of chemical exchange and the NOE are quite unrelated, they share in common the transfer of longitudinal magnetization and as such can be detected with the same 1D or 2D NMR experiments. In fact, the NOESY and EXSY pulse sequences are one and the same (Figure 52). The practical difference lies in the EXSY dependence on exchange rates rather than spin relaxation rates.[16;71;72]

Exchange experiments can be used both qualitatively, to map exchange pathways, and quantitatively to determine rate constants. In systems of multi-site exchange, the 2D EXSY experiment proves particularly powerful in the measurement of these for all pathways.[71;73] However, for either application the exchange processes studied must be slow on the NMR chemical shift timescale since the exchanging resonances must be resolved in order to observe transfer between them.[74] Furthermore, this exchange must not be too slow otherwise relaxation processes occurring during τ_m will remove all memory of the exchange process. Thus, magnetization transfer experiments are suitable for only a limited range of exchange rates and as a rule of thumb, these must be at least comparable to the longitudinal relaxation rates ($k_{ex} \geq 1/T_1$).In practice, this mean these experiments are sensitive to exchange processes with $k_{ex} \approx 10^2$-10^{-2} s^{-1}. The study of different nuclei provides a window on different rates within this range due to differences in relaxation times, with slower relaxing spins able to probe slower exchange processes. Fast exchange processes that lead to resonance coalescence can be studied by line shape analysis as mentioned above.

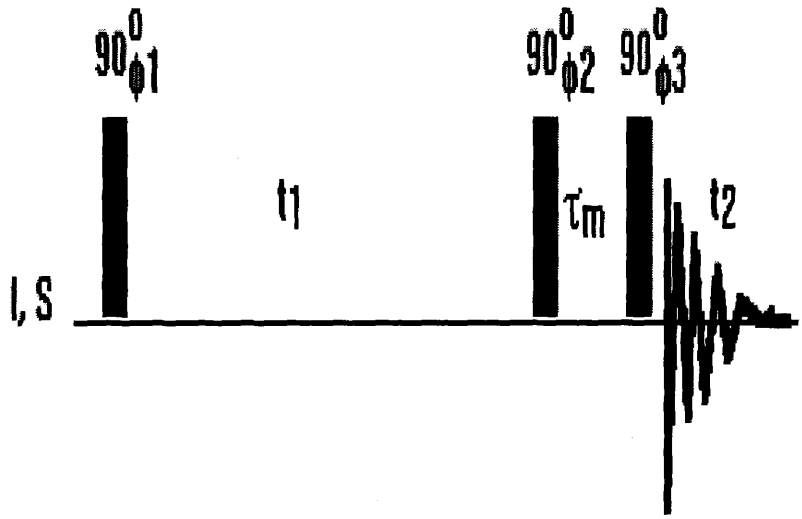

Figure 52. Pulse Sequence for EXSY/NOESY experiment

This pulse sequence for EXSY/NOESY can be explained as follows:

- Following the first 90° pulse, during the t1 time, the proton chemical shift evolution takes place (Figure 53).
- The second 90° pulse rotates one component along the z-axis. The length and sign of the vector along z oscillates with the proton chemical shift frequency.
- During the mixing time (τ) coupled spins exchange magnetization with each other, thereby transferring the chemical shift information from one proton to its coupling partner. Simultaneously the remaining component in the xy plane decays, often helped by a field gradient. If chemical exchange or rotation between non-equivalent sites takes place during (τ), this also leads to crosspeaks.
- The final 90° pulse tests the length of the vector along the z by rotating it into the x/y plane.

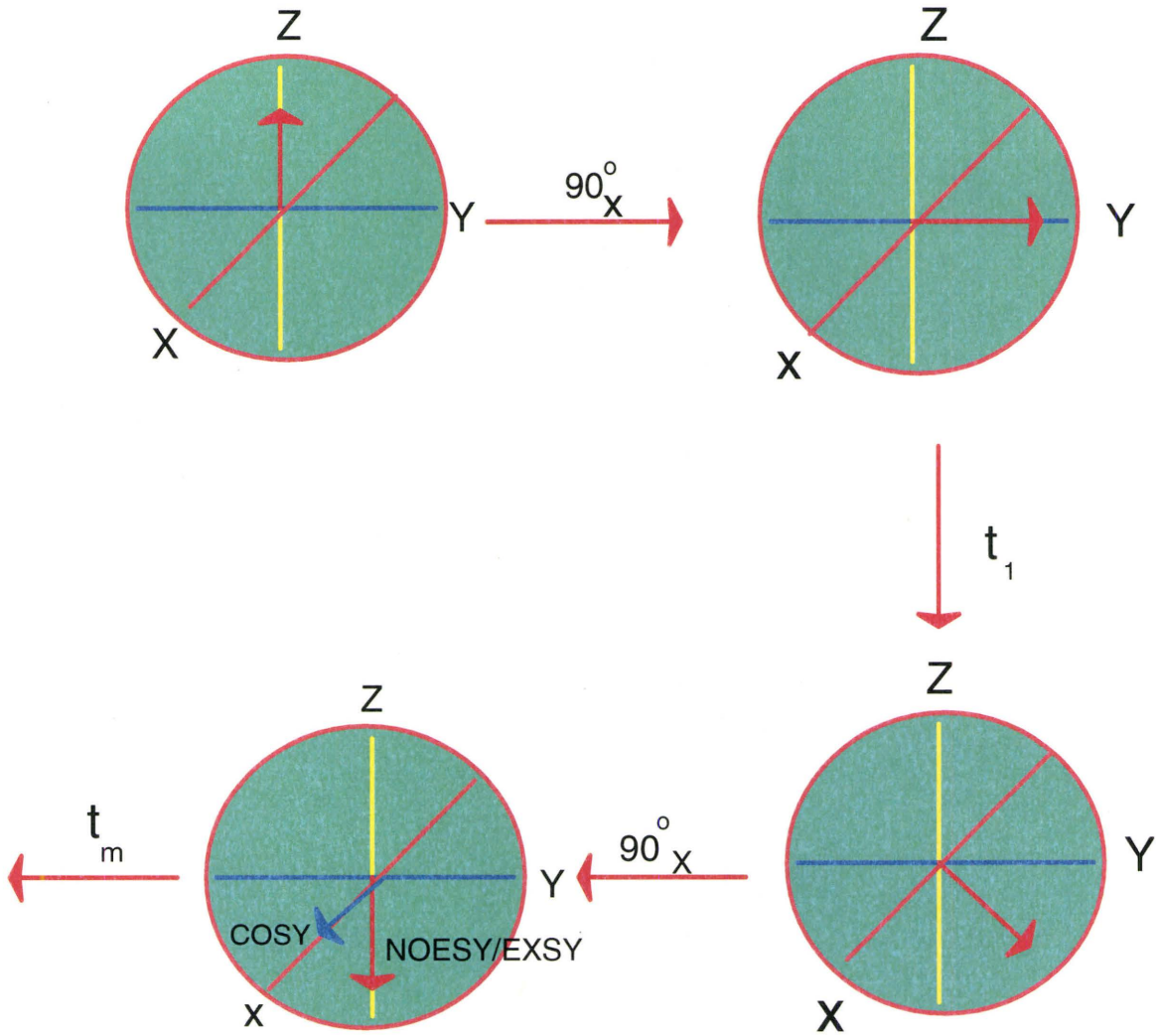

Figure 53. Vector Model for EXSY/NOESY experiment

2D EXSY is used to determine which nuclei are in chemical exchange.[71] Resonance of nuclei in chemical exchange will have a cross-peak between them. Thus, crosspeaks in a NOESY could be from chemical exchange or NOEs. However, chemical exchange peaks are always the same sign as the diagonal, NOEs are the opposite sign of the diagonal (positive NOE) for small molecules, but it has the same sign (negative NOE) for macromolecules (Table 12).

Sign of diagonal	Origin of Crosspeak	Sign of crosspeak
Positive	Positive NOE	Negative
Positive	Negative NOE	Positive
Positive	Chemical Exchange	Positive

Table 12. Differences between Exsy and Noesy crosspeaks

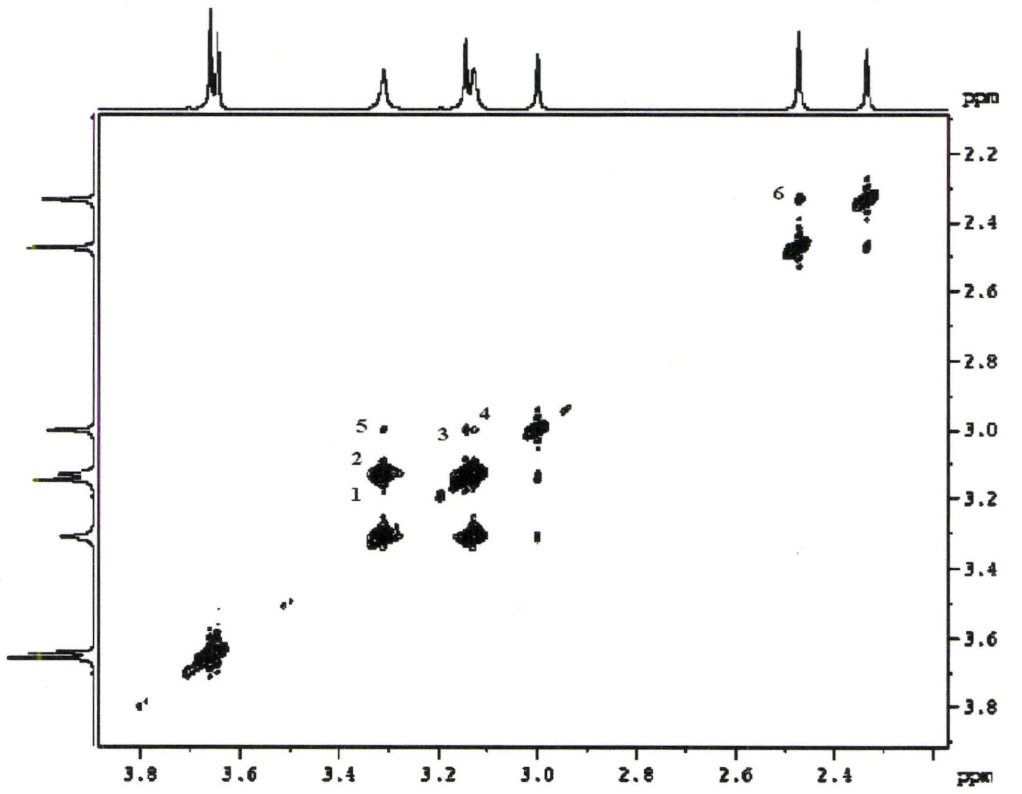

Figure 54. 2D EXSY for MDACC in CD_2Cl_2 at -40 °C

The 2D EXSY for MDACC in CD_2Cl_2 at -40 °C is displayed in Figure 54. For clarity, only cross-peaks above the diagonal are labeled; the cross-peaks below the diagonal are related by symmetry. Interpretation of the spectrum requires a consideration of the mechanistic details given in Figure 12. The C-methyl groups labeled E and F are inter-converted via C=C rotation and this gives rise to the crosspeak labeled 6 in Figure 54. Similarly, the crosspeaks labeled 2 and 3 arise due to C-N rotation in both the E and Z isomers of MDACC. A careful consideration of Figure 54 leads also to the crosspeaks labeled 1 and 4, which arise owing to C=C rotation as manifested by the exchange of N-methyl sites A with C and B with D, respectively. Since the chemical shifts of the N-methyl groups B and C are so similar, there is unfortunate overlap of cross-peaks 1 and 2, and 3 and 4. In addition, the 2D Exsy data may be collected at a variety of temperatures ranging from -55 °C to -20 °C. In the low temperatures limit, k_{EZ} and $k_{ZZ'}$ become too slow to yield kinetic data, whereas the cross-peak corresponding to $k_{EE'}$ is still large and visible. At higher temperature, $k_{EE'}$ becomes so fast that the A and B methyl signals coalesce into a single peak and obscure the kinetics of this process. The C=C and C-N (Z) rotational processes (k_{EZ} and $k_{ZZ'}$) are nicely visualized at the higher temperatures.

4.2 Selective and non-selective T1 experiments

Selective and non selective T1 experiments are very reliable technique used to probe kinetic parameter when the exchange is slow. Slow means that the exchange rate is much smaller than the frequency difference between the sites. In this situation, line shape analysis is not suitable since the appearance of the spectrum is a little bit

broadened by the exchange. So it is very difficult to ascribe the broadening to magnetic field inhomogeneities or exchange effect. Thus it is usually better to measure the rate from the effect of exchange on the spin-lattice relaxation.

The principle behind this experiment is not hard to understand. If the Z magnetization of a site is inverted, it will relax back to equilibrium through the spin – lattice relaxation mechanism. If there are two sites, an individual spin may exchange sites during the relaxation and carry its polarization. If one site is inverted selectively, then its spins may relax either by normal spin-lattice relaxation, or by exchange with the non-inverted site Figure 55 and 56. If the polarization of the two exchanging sites is different, the exchange will tend to average them. This leads to a faster return to equilibrium for the inverted site, and a transient dip in the other site, as in Figure 55. The top half of figure shows the normalized intensities of both C-methyl signals in MDACC following a non selective π pulse.[75] This is a standard inversion –recovery T_1 experiment. Both the methyl groups have roughly the same T_1, so their signals are superimposed as they both relax back to equilibrium. Their polarizations are the same, so exchange has essentially no effect o this experiment. If the T_1 values were different, the exchange will average them to some extent, so the decay rate in the lower part is not strictly T_1. The upper part of Figure 55 shows the intensities of the methyls following a selective inversion of one of the signals. The inverted site relaxes much more quickly at first, then at approximately the same rate as in the bottom part. The signal that was not inverted decreases in intensity at first, and then relaxes to equilibrium.[76] This transient behavior of the non-inverted site is characteristic of exchange. By using CIFIT program the out put of the non selective T_1 experiment gives $1/T_1$, then the value of $1/T_1$ plus the out put of selective T1 experiment gives the rate.[22] In the non-selective T1 we used the

same pulse sequence but the 180 is non-selective. The result of the non-selective experiment is shown in Figure 57 and 58. As you can see in Figure 58, both peaks were inverted.

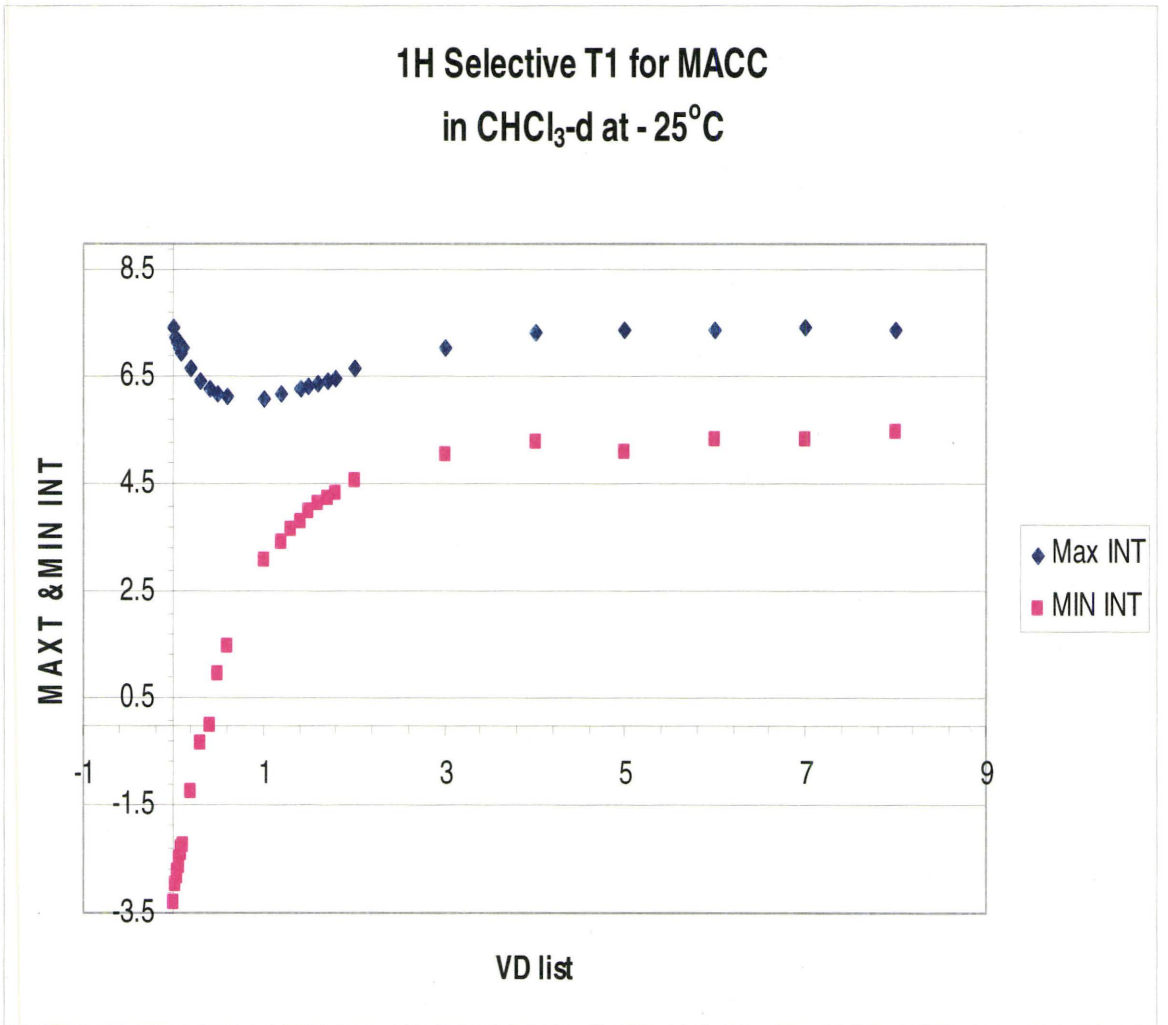

Figure 55. ^{1}H Selective T_1 for MDACC in chloroform at -25°C.

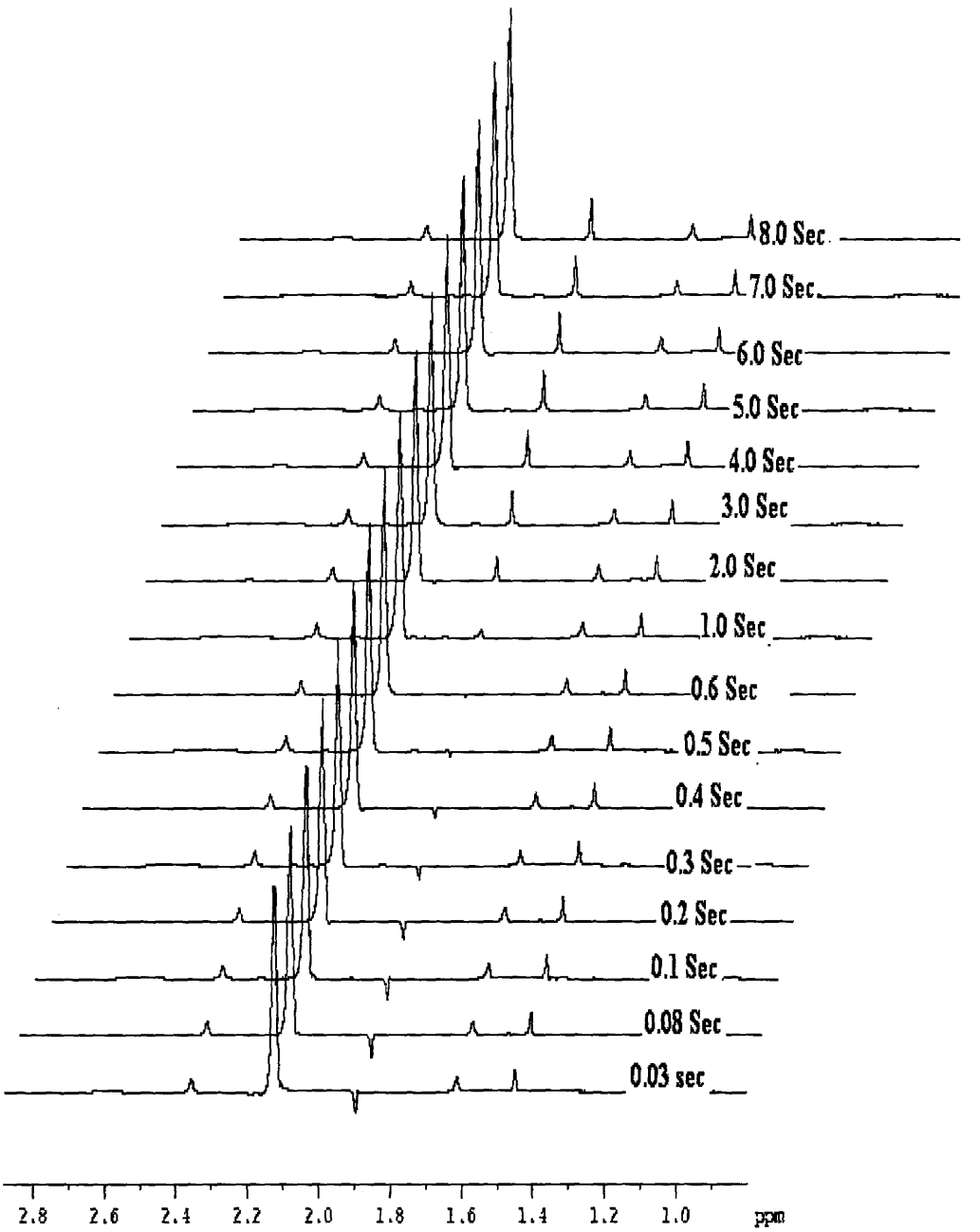
8.0 Sec
7.0 Sec
6.0 Sec
5.0 Sec
4.0 Sec
3.0 Sec
2.0 Sec
1.0 Sec
0.6 Sec
0.5 Sec
0.4 Sec
0.3 Sec
0.2 Sec
0.1 Sec
0.08 Sec
0.03 sec
2.8
2.6
2.4
2.2
2.0
1.8
1.6
1.4
1.2
1.0
ppm

Figure 56.

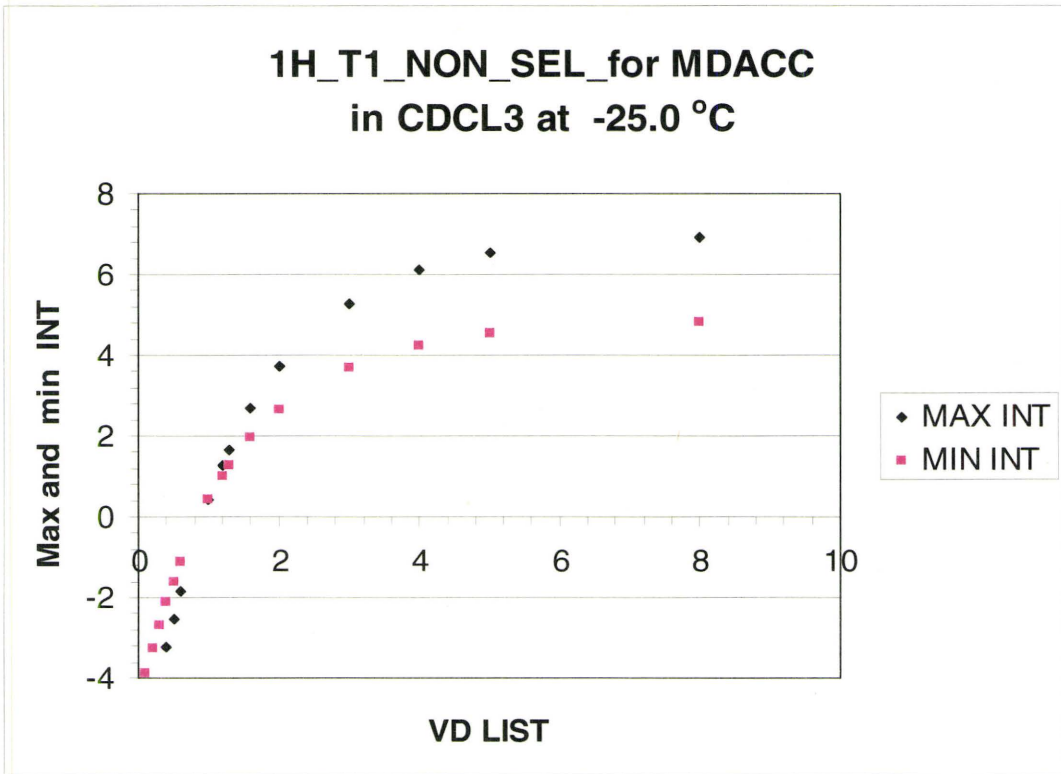
1H_T1_NON_SEL_for MDACC
in CDCL3 at -25.0 °C
Max and min INT
VD LIST
MAX INT
MIN INT
8
6
4
2
0
-2
-4
0
2
4
6
8
10

Figure 57.

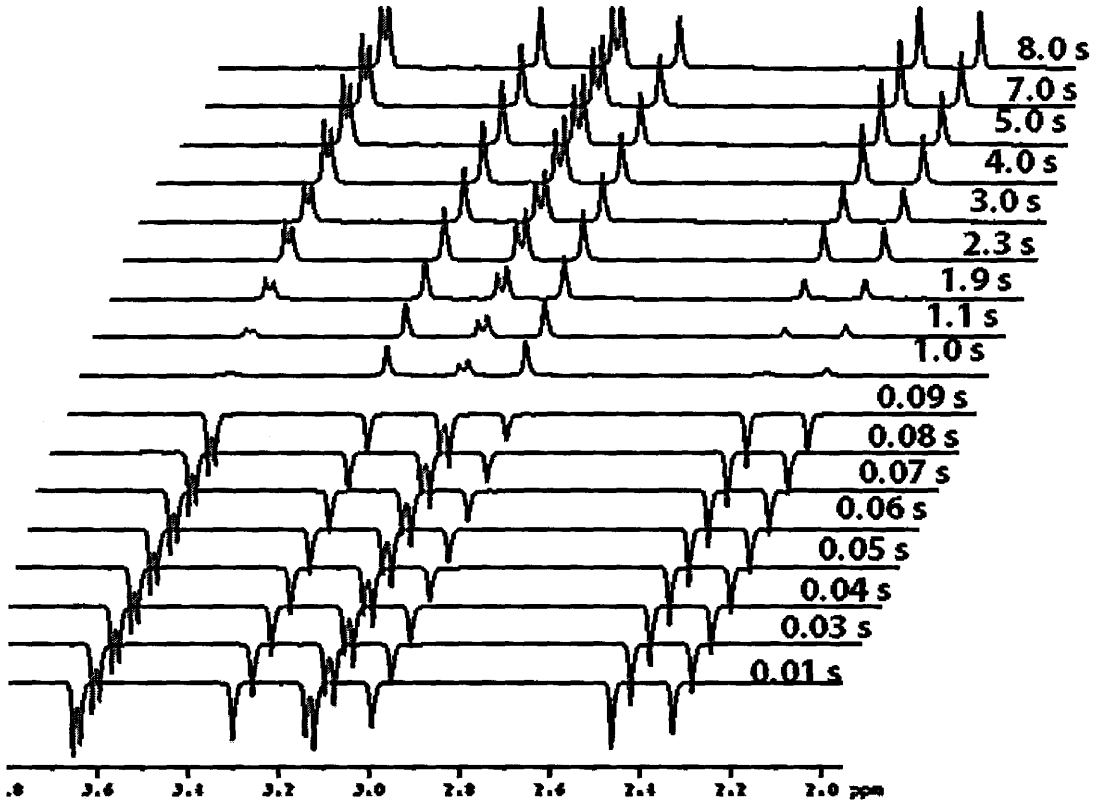
8.0 s
7.0 s
5.0 s
4.0 s
3.0 s
2.3 s
1.9 s
1.1 s
1.0 s
0.09 s
0.08 s
0.07 s
0.06 s
0.05 s
0.04 s
0.03 s
0.01 s
3.6
3.4
3.2
3.0
2.8
2.6
2.4
2.2
2.0 ppm

Figure 58.

Calculating activation parameters from rate data:

In a typical kinetic run, the reaction progress was followed by ^{1}H-NMR spectroscopy in which at least 20 data points were collected, where possible, Eyring plot. The Eyring plot comprises of eight data points. Three of these were recorded at the same temperature (300K), their average value being shown in the graph. The other five data points represent the rate constants as determined at 315K, 310K, 305K, 294K and 283K. The error bars shown in the Eyring plot are estimated quantities (±0.67% in X and ±0.30% in Y).

4.3 Kinetic Models and Thermodynamics

Chemical exchange does not only provide interesting spectroscopy, but also gives insights into molecular structure. Exchange involves the passing of the molecule through a transition state, at the top of a kinetic barrier. Measurements of the rate as a function of temperature or other parameters are one of the few methods of experimentally determining the height of the barrier. This measurement can then be compared to molecular structure calculations.[22]

The dependence of reaction rate, k, on temperature, T, was empirically described by Arrhenius in equation:

$$k = A \exp^{(-\Delta E\dagger / RT)}$$

Where A is the pre- exponential factor, R is the gas constant and $\Delta E^{\dagger}$ is the energy of activation. Later, Eyring put this relation on a firmer theoretical basis. Eyring's equation gives the rate constant as in equation:

$$k = \frac{k_B T}{h} \exp^{(-\Delta G^{\dagger}/RT)} \qquad [48]$$

$$= \frac{k_B}{h} \exp^{(\Delta S^{\dagger}/R - \Delta H/RT)}$$

In this equation, k_B is Boltzmann's constant, h is Planck's constant and $\Delta G^{\dagger}$ is free energy of activation.

The rate we measure is the rate of transfer from one site, A, to other, B. However, the system is in dynamic equilibrium, so there is a reverse rate as well as in the reaction below.

$$A \underset{k_r}{\overset{k_f}{\rightleftharpoons}} B$$

If the two sites do not have equal populations, then the ratio of the forward and reverse rates are related to the equilibrium constant, K, by:

$$K\frac{[B]}{[A]} = \frac{k_f}{k_r}$$

It is important to remember that the equilibrium constant itself is temperature – dependent, through the relation to the standard free energy difference between the two sites, ΔG^0

$$K = e^{-\Delta G^0/RT}$$

In order to analyze experimental data, it is customary to plot the natural logarithm of k/T against 1/T, an Eyring plot (Figure 59). The slope and the intercept of the straight line are given by equation below, in which log means natural logarithm. The constant term in

the intercept (if the rate is in s^{-1}), is obtained from $K_B/h=2.0842\times10^{10}$ $s^{-1}K^{-1}$,and that give natural logarithm of 23.77024.

Slope= $\Delta H^{\dagger}/R$

$$\text{intercept} = \ln\left(\frac{k_B}{h}\right) + \Delta S^{\dagger} / R.$$

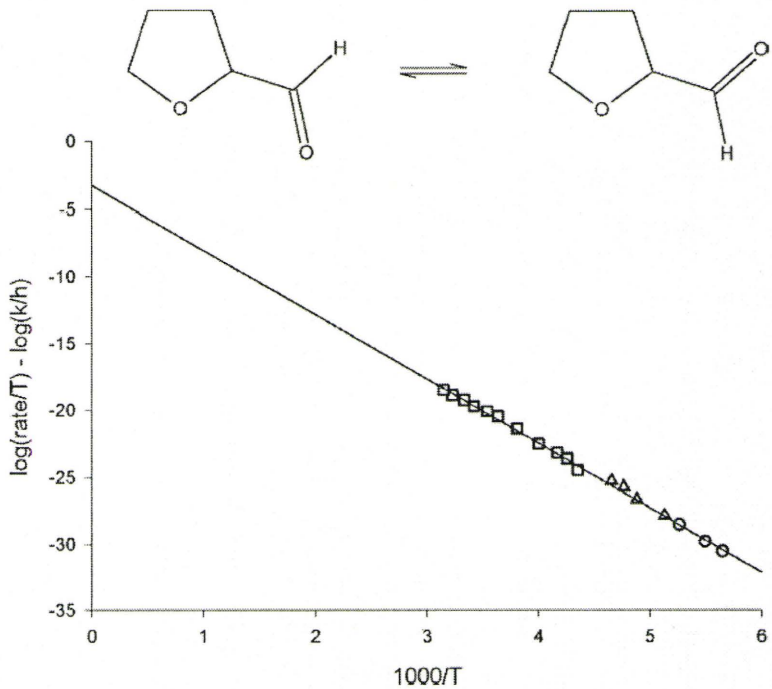

Figure 59[22]. An example of the plot for exchange of the aldehyde group in furfural between the O-O cis and trans conformation. The constant term has been subtracted, so the y-axis intercept gives the entropy directly[22].

From temperature-based measurements, the problem of determining the entropy and enthalpy of activation is illustrated in the Fig. above. It is common to quote the free energy of activation, which is equivalent to quoting the rate, since all the other terms are constants. For comparison purposes, the free energy of activation is often converted to a value appropriate to 298 K.

The internal rotation about the amide bond is an equilibrium process. The Eyring absolute rate theory can be used to calculate activation parameters. The rate constant for the exchange of methyl groups is:

$$k = k_B T / h * \exp(-\Delta G^{\ddagger}/RT) \quad [49]$$

$$k = k_B T / h * \exp(\Delta S^{\ddagger}/R) * \exp(-\Delta H^{\ddagger}/RT) \quad [50]$$

where k_B is Boltzmann's constant, h is Planck's constant, κ is the transmission coefficient (the fraction of reactant reaching the transition state that goes on to form product--normally assumed to be one), and $\Delta G^{\ddagger}$, $\Delta H^{\ddagger}$, and $\Delta S^{\ddagger}$ are the free energy of activation, the enthalpy of activation, and the entropy of activation respectively.

From the linear plot of ln(k/T) versus 1/T, the entropy and enthalpy of activation can be calculated:

$$\ln(k/T) = \{\ln(k_B / h) + \Delta S^{\ddagger}/R\} - \Delta H^{\ddagger}/R * (1/T) \quad [51]$$

4.4 Results and experimental data

The dynamic processes of MDACC in a variety of solvents were studied through 1D-^{1}H NMR. The temperature dependent proton spectra are reproduced in Figure 61. The spectra of CD_2Cl_2 at a temperature of -60° C (Figure 60) exhibits pairs of signals for each equivalent group of protons. It should be noted that, at this temperature, rotation about the C-N bond is slow and the two N-methyl groups are non-equivalent. The relative populations of the two isomers are immediately obtained by integration of the two completely resolved C-methyl absorptions - the assignments were justified earlier. As the temperature increases, three distinct coalescences of N-methyl, O-methyl, and C-methyl absorptions occur which must correspond to three different kinetic processes, namely rotation about the C-N bonds and rotation about the carbon-carbon double bond. Kinetic parameters for each solvent of MDACC were calculated by using Eyring plot. The rate of reaction for each solvent at a specific temperature was obtained by using the MEXICO program, and the low temperature rate was obtained by using the CIFIT program.

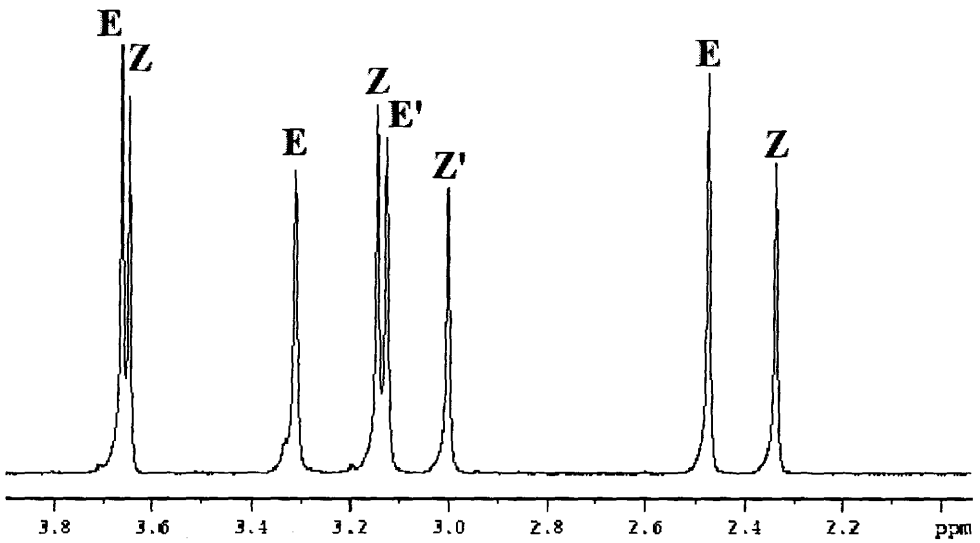

Figure 60. MDACC in CD_2Cl_2 at -60.0 C°

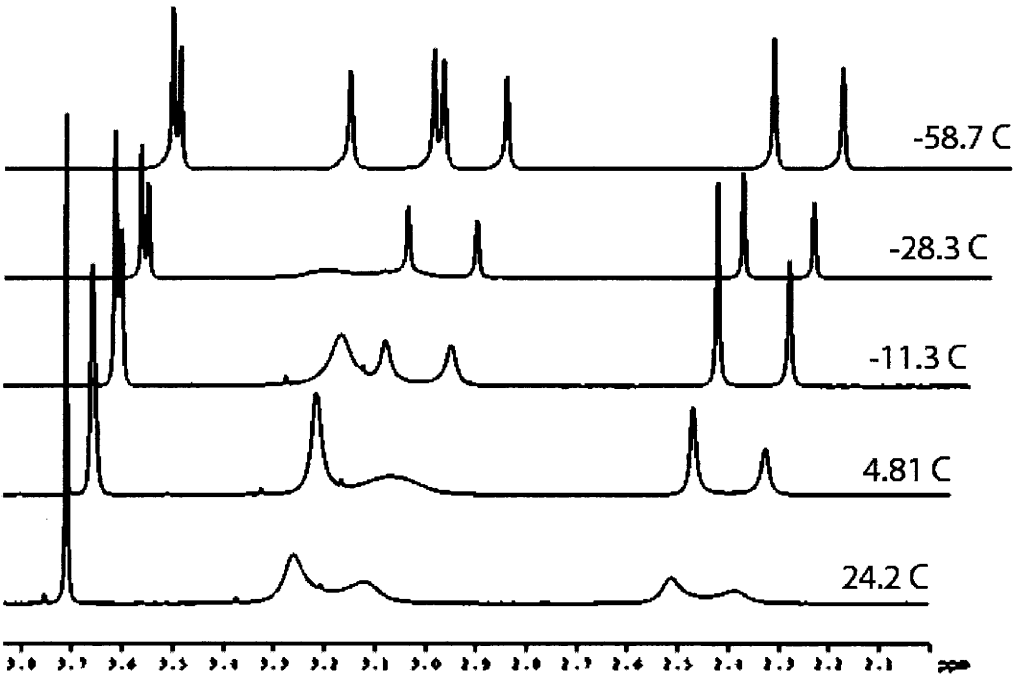

Figure 61. MDACC in CD_2Cl_2 at different temperatures

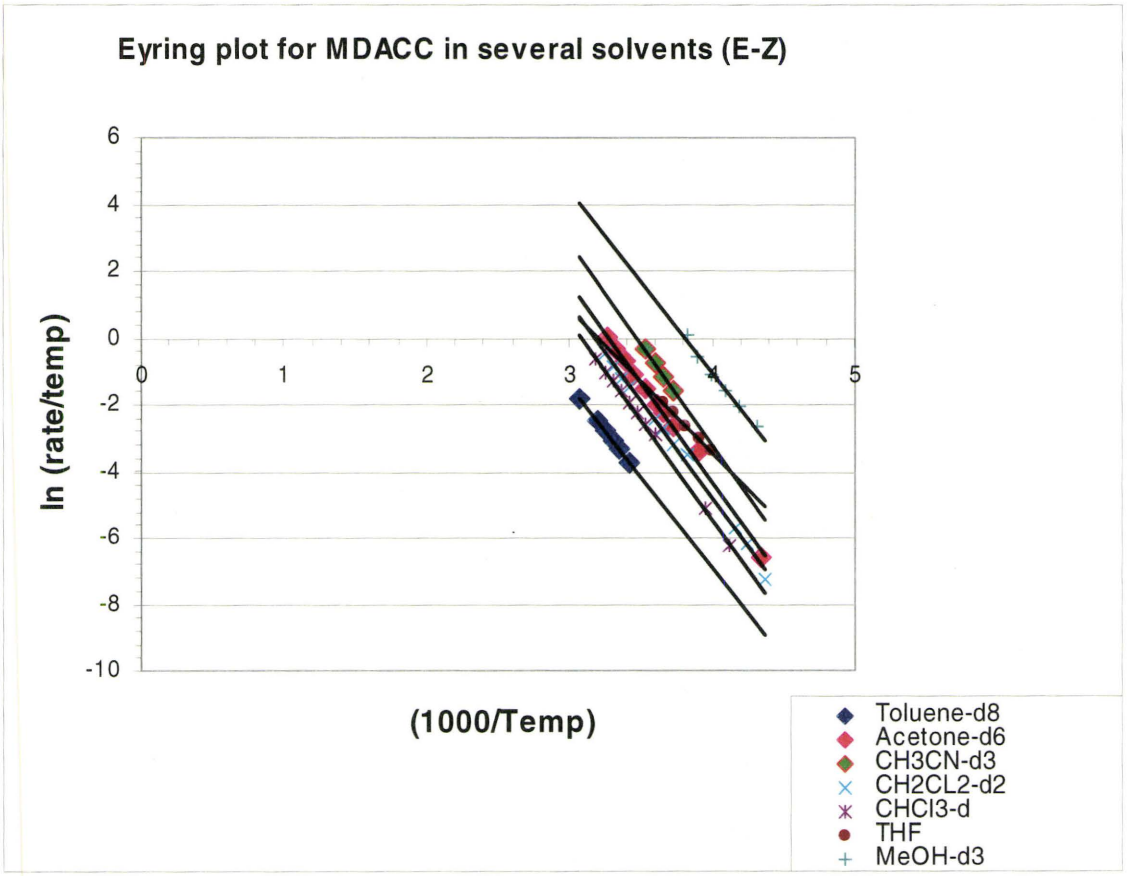
Eyring plot for MDACC in several solvents (E-Z)
ln (rate/temp)
(1000/Temp)
6
4
2
0
-2
-4
-6
-8
-10
0
1
2
3
4
5
Toluene-d8
Acetone-d6
CH3CN-d3
CH2CL2-d2
CHCl3-d
THF
MeOH-d3

Figure 62

Solvent	ε	$\Delta H^{\ddagger}$ kJ/mol	$\Delta S^{\ddagger}$ J/mol K	$\Delta G^{\ddagger}$ kJ/mol
Toluene-d_8	2.41	46	-68	67
Chloroform-d	4.81	44	-66	63
Tetrahydrofuran-d_8	7.5	49	-56	65
Methylene chloride-d_2	9.01	46	-49	61
Acetone-d_6	20.7	50	-30	60
Methanol-d_4	32.7	45	-24	52
Acetonitrile-d_3	37.5	49	-21	52

Table 13. Kinetics Data for E- Z configuration of MDACC in a variety of solvents.

4.5 Rotation about C=C bond

In the first dynamic NMR studies of push-pull ethylenes, a strong effect of solvent polarity on the C=C barriers was noted. According to Kende et al. found that $\Delta G^{\ddagger} = 74.4$ kJ/mol in N, N dimethyl formamide ($\varepsilon = 38$). Similar observations have been made by many other workers, and they have been seen as a strong support for a zwitterionic transition state. Similarly, Shvo et al. found linear correlations between natural log k_{298} and the polarity parameters for three compounds. According to Table 13 (above), we found that the solvent polarity is linearly proportional with the entropy of activation. This is particularly interesting since it has never before been noted. The activation entropy ($\Delta S^{\ddagger}$) to C=C rotation in MDACC is negative, since the increase in polarity in the transition state should increase the order in the solvated structure. The effect should increase with increasing difference in polarity between ground and transition states, and also with increasing solvent polarity. The ground state is less polar than the transition state to C=C rotation, and negative $\Delta S^{\ddagger}$ is observed. The enthalpy remained relatively constant while on the other hand, the rate of reaction varied for each solvent. The rate of reaction ranges from 52 – 67 kJ/mol (Table 13). Therefore, it is quite evident that as the solvent polarity increases, the entropy of activation increases as well (Figure 62). Raw data can be found in the appendix.

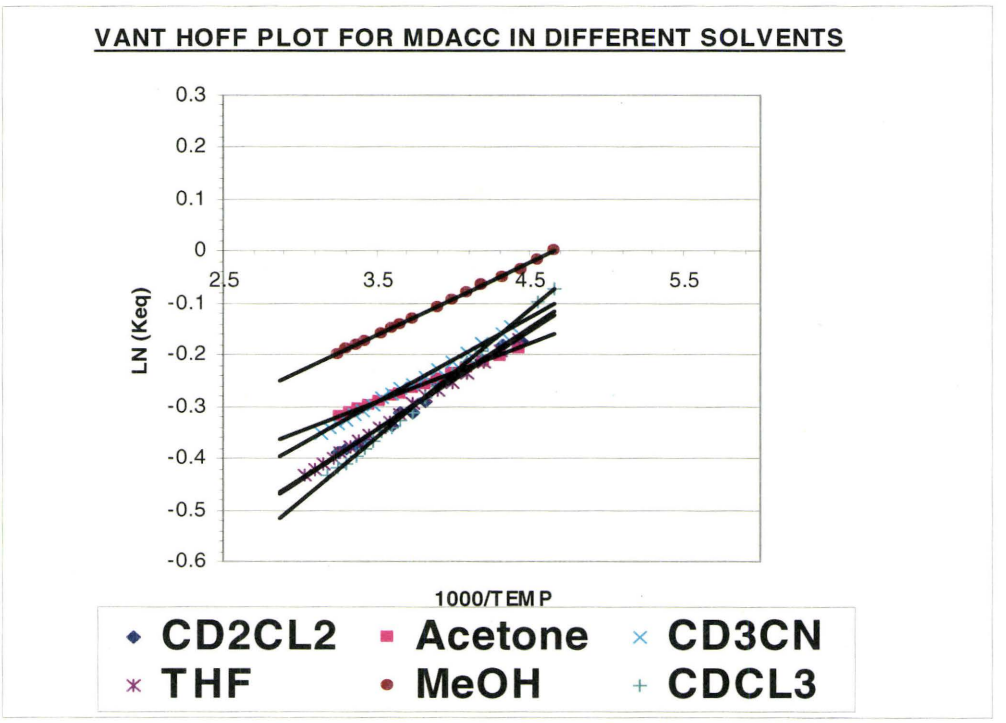

Figure 63. Thermodynamic data for MDACC in different solvents.

4.6 Equilibrium Thermodynamic

If two species that are in equilibrium have different thermodynamic stabilities, then variable-temperature NMR spectra for such species, undergoing sufficiently slow exchange that separate resonances for both species may be observed and can be used to determine equilibrium constant K_{eq} for these equilibria. Since the equilibrium constants should be temperature dependent, their measurement (from ratio of integrals in the spectra) as a function of temperature provides a means of measuring equilibrium thermodynamics from the following equations:

$$\Delta G^{\circ} = -RT \ln K_{eq} \qquad [52]$$

$$\Delta G^{\circ} = \Delta H^{\circ} - T\Delta S^{\circ} \qquad [53]$$

$$\ln K_{eq} = -\frac{\Delta H^{\circ}}{RT} + \frac{\Delta S^{\circ}}{R} \qquad [54]$$

Hence, in a plot of ln K_{eq} vs. 1/T (Figure 63), the slope is - $\Delta H^{o}/R$ and the intercept is $\Delta S^{o}/R$. Analogous equilibrium and activation thermodynamic quantities have similar magnitudes of uncertainties.

Since the equilibrium constant for MDACC in different solvents is less than one we would expect it to increase with temperature, but in our case it decreases! This can been seen in the Van't Hoff plot where the slope is positive, indicating that going from the major site (lower free energy) to the minor site is exothermic. This means that entropy is important. Even though one would lose enthalpy, the entropy gained was significant enough to drive the reaction. Raw data can be found in the appendix.

4.7 Rotation about C-N bond

Two kinetic processes arise from the rotation around C-N bond, the E-E' and Z-Z'. The most important parameter of the solvent dynamic effect for MDACC dependent happens to be $\Delta S^{\ddagger}$. Unlike the $\Delta S^{\ddagger}$ of rotation around the C=C, the $\Delta S^{\ddagger}$ for C-N is positive. So, this means that the ground state is more polar than the transition state since $\Delta S^{\ddagger}$ is increasing with the solvent polarity (Table 14 and 15). These trends can be clearly seen in the following two tables of E-E' and Z-Z'(Figure 64 and 65). The equilibrium constant is equal to one since they are equally populated. The $\Delta H^{\ddagger}$ for E-E' ranges between 48 – 58 kJ/mol while for Z-Z' the range is slightly higher, 63 – 78 kJ/mol. The dynamic effects of the solvent on MDACC for E-E' and Z-Z' remain relatively constant as can be seen from the table below, the range for $\Delta G^{\ddagger}$ Z-Z' is 51 – 54 kJ/mol and $\Delta G^{\ddagger}$ for E-E' is 46 - 49.6 kJ/mol. The rate of C-N rotation is much smaller than the rate of C=C rotation. Raw data can be found in the appendix.

Solvent	ε	$\Delta H^{\ddagger}$ kJ/mol	$\Delta S^{\ddagger}$ J/mol K	$\Delta G^{\ddagger}$ kJ/mol
Toluene-d_8	2.41	63	32	53
Chloroform-d	4.81	68	43	55
Tetrahydrofuran-d_8	7.5	69	51	53
Methylene chloride-d_2	9.01	73	64	54
Acetone-d_6	20.7	73	68	53
Methanol-d_4	32.7	77	88	52
Acetonitrile-d_3	37.5	78	92	51

Table 14. Kinetic Data for MDACC Z-Z' Conformation

Solvent	ε	$\Delta H^{\ddagger}$ kJ/mol	$\Delta S^{\ddagger}$ J/mol K	$\Delta G^{\ddagger}$ kJ/mol
Toluene-d_8	2.41	48.9	3.38	47
Chloroform-d	4.81	54.98	14.0	49.6
Tetrahydrofuran-d_8	7.50	53.1	16.0	48.0
Methylene chloride-d_2	9.01	55.0	22.9	48.6
Acetone-d_6	20.70	55.7	25.5	48.1
Methanol-d_4	32.70	56.0	36.0	46.0
Acetonitrile-d_3	37.5	58.0	41.0	46.7

Table 15. Kinetic Data for MDACC E_E' Conformation

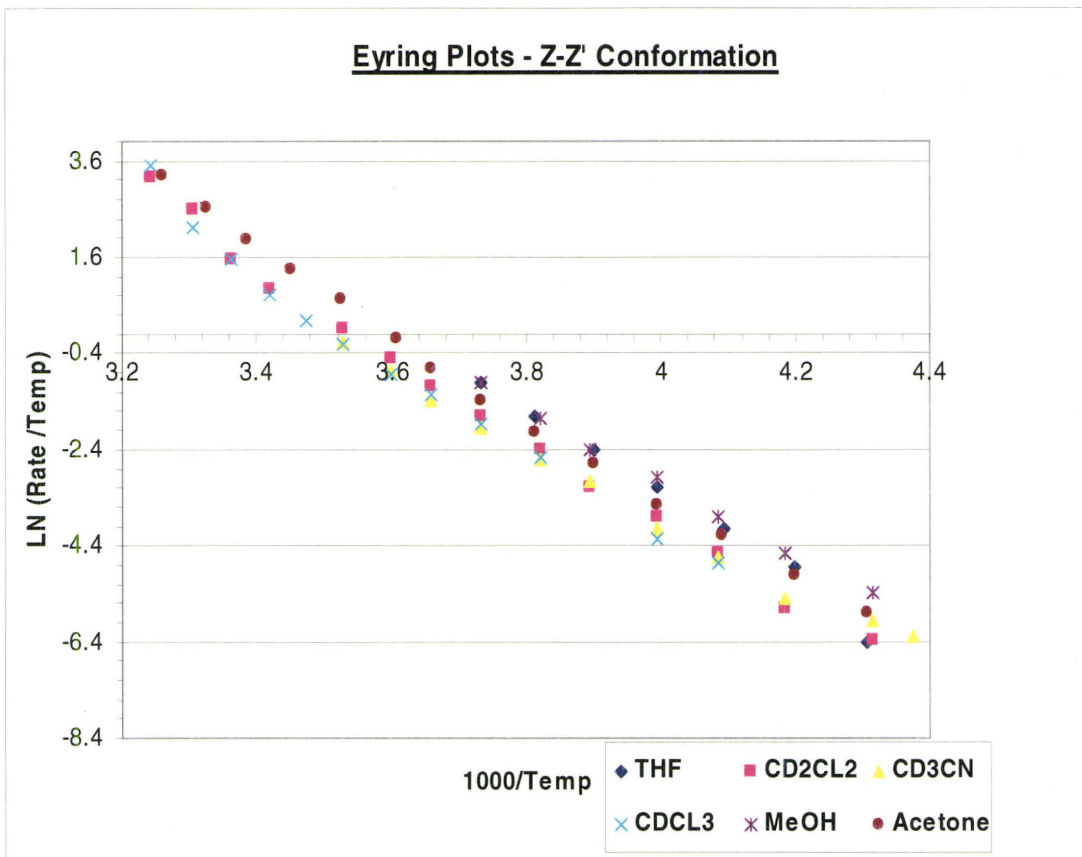
Eyring Plots - Z-Z' Conformation
3.6
1.6
-0.4
-2.4
-4.4
-6.4
-8.4
LN (Rate /Temp)
3.2
3.4
3.6
3.8
4
4.2
4.4
1000/Temp
THF
CD2CL2
CD3CN
CDCL3
MeOH
Acetone

Figure 64

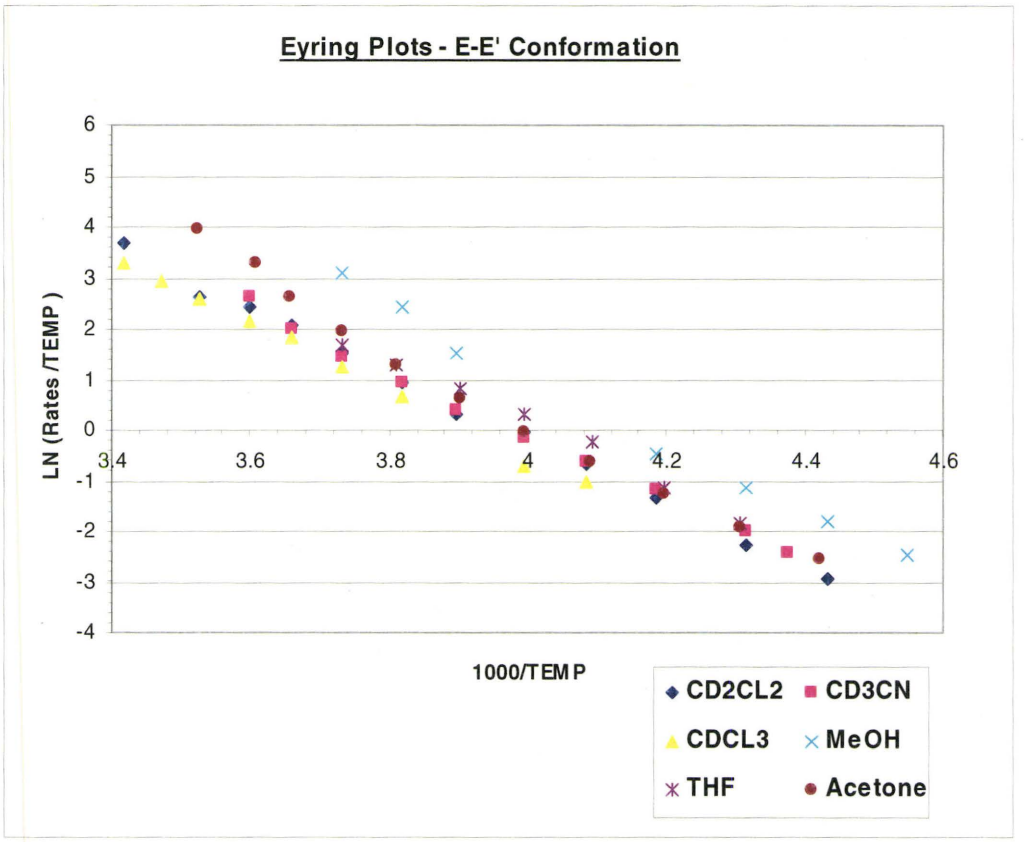
Eyring Plots - E-E' Conformation
LN (Rates /TEMP)
6
5
4
3
2
1
0
-1
-2
-3
-4
3.4
3.6
3.8
4
4.2
4.4
4.6
1000/TEMP
CD2CL2
CD3CN
CDCL3
MeOH
THF
Acetone

Figure 65

4.8 Gaussian calculation

The purpose of these calculations is to compare them with the experimental calculations. As can be seen from the Tables 16 a,b below, the calculated parameters show that the $\Delta H^{\ddagger}$ For E configuration is lower than the Z configuration. Therefore, the E configuration is the minor site while the Z configuration is the major site which does not agree with the experimental calculations (Figure 66). This could be due to many reasons:

1.) The calculation was done in a gas phase while the experimental calculation was done in liquid state.

2.) Temperature pressure and other conditions are not taking into account in the calculated spectrum

So the experimental data are more reliable and considered in this thesis

	Ground State Energy (kJ/mol)		Transition State Energy (kJ/mol)		
Basis Set	Z	E	E-E'	Z-Z'	E-Z
RHF/6-31G(d)	-1492581.58	-1492583.49	-1492527.54	-1492492.04	-1492464.99
RHF/6-31G(d,P)	-1492631.69	-1492633.74	-1492555.62	-1492547.74	-1492515.82
RHF/6-31+G(d)	-1492613.20	-1492614.25	-1492563.50	-1492528.41	-1492564.91
RHF/6-31+G(d,p)	-1492662.44	-1492663.69	-1492612.76	-1492587.09	-1492553.55
RHF/6-311+G(d,p)	-1492966.14	-1492966.98	-1492911.52	-1492883.14	
RHF/6-311+G(2d,p)	-1493011.71	-1493011.98		-1492930.41	
DFT-RB3LyP\6-31G(d,p)	-1501731.21	-1501733.06			
DFT+CdCl3-d-2	-1501738.07	-1501746.88			
DFT+CdCl3-d-1	-1501694.79	-1501711.31			
DFT+CdCl3-d-3	-1501752.94	-1501766.67			
DFT+CdCl3-4		-1501810.40			
DFT+Cd3CN		-1501760.76			
RHF/6-311+G(2df,2p)	-1493079.44			-1492996.85	
RHF/6-311+G(3df,2pd)					

Table 16a. Gaussian Calculations

	Total Dipole Moment (Debye)		Difference in Ground State (kJ/mol)	Barrier (kJ/mol)		
Basis Set	E	Z	E-Z	Z-Z'	(E-E')-(E)	(E-Z)-(E)
RHF/6-31G(d)			-1.91	-89.54	-55.95	118.50
RHF/6-31G(d,P)			-2.05	-83.95	78.12	117.93
RHF/6-31+G(d)			-1.05	-82.99	-50.75	60.69
RHF/6-31+G(d,p)			-1.26	-82.99	50.93	110.15
RHF/6-311+G(d,p)			-0.83	-82.99	55.45	
RHF/6-311+G(2d,p)			-0.27	-81.30		
DFT-RB3LyP\6-31G(d,p)	4.85	6.01	-1.85			
DFT+CdCl3-d-2	6.25	7.50	-8.81			
DFT+CdCl3-d-1	6.24	6.99	-16.52			
DFT+CdCl3-d-3	6.77	7.43	-15.73			
DFT+CdCl3-4	6.38					
DFT+Cd3CN						
RHF/6-311+G(2df,2p)						
RHF/6-311+G(3df,2pd)						

Table 16b. Gaussian Calculations

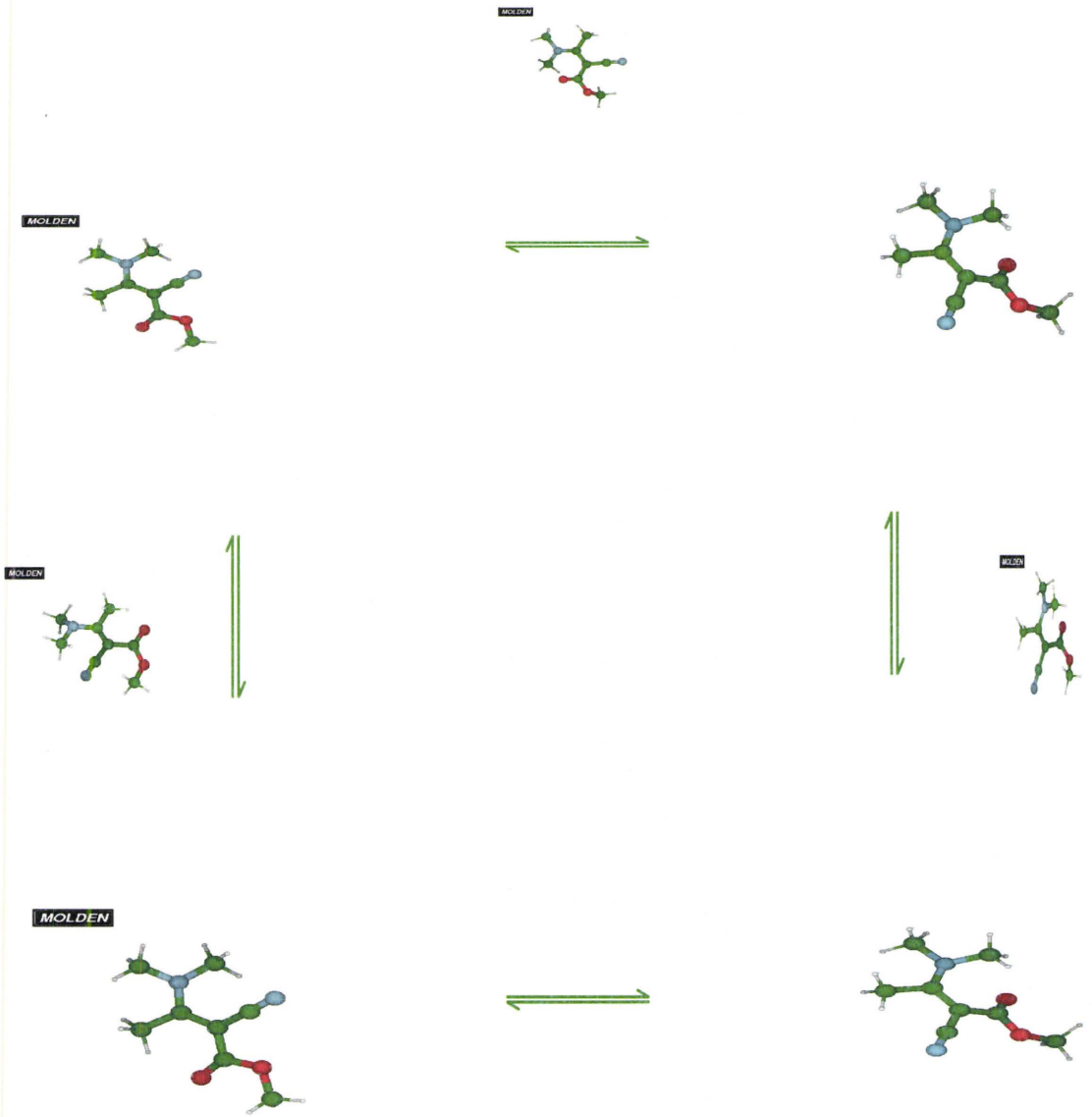

Figure 66. Gaussian conformations for MDACC

Chapter 5

CONCLUSION

Push-pull ethylenes are excellent systems to investigate. MDACC is just one example of such a system. These types of molecules can contain one or more electron donating groups at one end of the C=C bond and one or more electron-accepting groups at the other. The dynamic processes of these molecules are particularly interesting to study by variable temperature NMR spectroscopy. Using programs like MEXICO and CIFIT, 1D ^{1}H line shapes can be simulated and then compared to the experimental data. The rate can be determined once both the simulated and the experimental lineshape match. MDACC experiences a strong effect of solvent polarity on the C=C barriers. Three exchange processes exist for MDACC, the E-Z, Z-Z', and E-E' process. In all these processes, as the polarity increases, the entropy of activations increases. The rotation between the C-N and the C=C bond occurs through a step wise mechanism (non-concerted mechanism). Two reasons why this occurred was apparent through EXSY, since the intensity of n-methyl cross peak varies with different mixing time (Figure 52) and second, the rates from C=C rotation (E-Z) and C-N rotations (E-E' and Z-Z') are different at the same temperature. In all of our investigations, whether through NMR, x-ray, and molecular modeling, the E configuration is the major site while the Z configuration is the minor site in solution. Since the equilibrium constant is less than 1 for the E-Z' process, one would expect that it would increase with temperature. However, the opposite is true. This was seen in the Van't Hoff plot, where the slope was positive. This indicates that the reaction is entropy driven and that going from the major

site to the minor site is exothermic. The x-ray data for the crystal structure of MDACC was in agreement with the proposed resonance structure.

5.1 Future work

Small amounts of acids in halogenated solvents, or acidic impurities, would be tested by adding small quantity of a base such as 2, 4-lutidine to obtain reliable rate constants. Addition of different substituents such as phenyl, thiol, etc and observe the rate. A coupled HSQC and NOESY experiment would be helpful to identify E-Z assignments.

Appendix

Table 1. Crystal data and structure refinement for MDACC

Empirical formula	$C_8 H_{12} N_2 O_2$	
Formula weight	168.20	
Temperature	295(2) K	
Wavelength	1.54178 Å	
Crystal system	Monoclinic	
Space group	$P2_1$	
Unit cell dimensions	a = 3.98380(10) Å	α= 90°.
	b = 10.8370(2) Å	β= 91.6640(10)°.
	c = 10.1709(2) Å	γ = 90°.
Volume	438.917(16) $Å^3$	
Z	2	
Density (calculated)	1.273 Mg/m^3	
Absorption coefficient	0.766 mm^{-1}	
F(000)	180	
Crystal size	0.60 x 0.40 x 0.20 mm^3	
Theta range for data collection	4.35 to 68.16°.	
Index ranges	-4<=h<=4, -11<=k<=12, -12<=l<=11	
Reflections collected	2329	
Independent reflections	1311 [R(int) = 0.0212]	
Completeness to theta = 68.16°	94.6 %	
Absorption correction	SADABS	
Refinement method	Full-matrix least-squares on F^2	
Data / restraints / parameters	1311 / 1 / 158	
Goodness-of-fit on F^2	1.051	
Final R indices [I>2sigma(I)]	R1 = 0.0284, wR2 = 0.0808	
R indices (all data)	R1 = 0.0287, wR2 = 0.0814	
Absolute structure parameter	-0.1(2)	
Extinction coefficient	0.023(3)	
Largest diff. peak and hole	0.098 and -0.109 $e.Å^{-3}$	

Table 2. Atomic coordinates (x 10^4) and equivalent isotropic displacement parameters ($Å^2$x 10^3) for MDACC. U(eq) is defined as one third of the trace of the orthogonalized U^{ij} tensor.

	x	y	z	U(eq)
C(1)	1686(4)	3595(1)	7825(2)	47(1)
C(2)	2602(3)	4775(1)	7254(1)	43(1)
C(3)	2999(3)	5867(1)	7989(1)	43(1)
N(4)	2835(3)	6982(1)	7438(1)	47(1)
C(5)	1352(4)	7206(2)	6127(2)	52(1)
C(6)	3977(5)	8099(2)	8131(2)	61(1)
C(7)	3755(5)	5814(2)	9435(2)	61(1)
C(8)	802(5)	1487(2)	7326(2)	60(1)
O(9)	1944(3)	2677(1)	6937(1)	55(1)
C(10)	3429(3)	4745(1)	5904(1)	45(1)
N(11)	4248(4)	4728(1)	4831(1)	60(1)
O(12)	705(4)	3404(1)	8926(1)	67(1)

Table 3. Bond lengths [Å] and angles [°] for MDACC.

C(1)-O(12)	1.214(2)	C(8)-H(8A)	0.97(4)
C(1)-O(9)	1.3494(19)	C(8)-H(8B)	0.95(3)
C(1)-C(2)	1.456(2)	C(8)-H(8C)	1.04(3)
C(2)-C(3)	1.406(2)	C(10)-N(11)	1.1484(18)
C(2)-C(10)	1.4214(18)		
C(3)-N(4)	1.3335(19)	O(12)-C(1)-O(9)	121.62(14)
C(3)-C(7)	1.494(2)	O(12)-C(1)-C(2)	127.48(14)
N(4)-C(5)	1.462(2)	O(9)-C(1)-C(2)	110.86(12)
N(4)-C(6)	1.466(2)	C(3)-C(2)-C(10)	120.44(13)
C(5)-H(5A)	0.96(2)	C(3)-C(2)-C(1)	123.58(12)
C(5)-H(5B)	0.97(2)	C(10)-C(2)-C(1)	115.68(13)
C(5)-H(5C)	0.95(2)	N(4)-C(3)-C(2)	122.43(12)
C(6)-H(6A)	1.00(3)	N(4)-C(3)-C(7)	117.06(14)
C(6)-H(6B)	0.91(3)	C(2)-C(3)-C(7)	120.48(14)
C(6)-H(6C)	0.97(3)	C(3)-N(4)-C(5)	123.18(12)
C(7)-H(7A)	0.89(3)	C(3)-N(4)-C(6)	122.37(13)
C(7)-H(7B)	0.86(3)	C(5)-N(4)-C(6)	114.38(13)
C(7)-H(7C)	0.96(3)	N(4)-C(5)-H(5A)	108.4(11)
C(8)-O(9)	1.427(2)	N(4)-C(5)-H(5B)	107.4(13)

H(5A)-C(5)-H(5B)	111.0(18)
N(4)-C(5)-H(5C)	111.4(12)
H(5A)-C(5)-H(5C)	111.5(17)
H(5B)-C(5)-H(5C)	107.2(19)
N(4)-C(6)-H(6A)	111.4(18)
N(4)-C(6)-H(6B)	111(2)
H(6A)-C(6)-H(6B)	95(3)
N(4)-C(6)-H(6C)	106.4(17)
H(6A)-C(6)-H(6C)	122(2)
H(6B)-C(6)-H(6C)	111(3)
C(3)-C(7)-H(7A)	113.3(18)
C(3)-C(7)-H(7B)	117.1(18)
H(7A)-C(7)-H(7B)	103(3)
C(3)-C(7)-H(7C)	113.6(16)
H(7A)-C(7)-H(7C)	103(3)
H(7B)-C(7)-H(7C)	106(3)
O(9)-C(8)-H(8A)	113(2)
O(9)-C(8)-H(8B)	107.5(18)
H(8A)-C(8)-H(8B)	106(3)
O(9)-C(8)-H(8C)	103.8(17)
H(8A)-C(8)-H(8C)	110(2)
H(8B)-C(8)-H(8C)	117(2)
C(1)-O(9)-C(8)	116.73(12)
N(11)-C(10)-C(2)	176.88(15)

Table 4. Anisotropic displacement parameters ($Å^2 x\ 10^3$) for MDACC. The anisotropic displacement factor exponent takes the form: $-2\pi^2[\ h^2\ a^{*2}U^{11} + ...\ + 2\ h\ k\ a^*\ b^*\ U^{12}\ ]$

	U^{11}	U^{22}	U^{33}	U^{23}	U^{13}	U^{12}
C(1)	57(1)	47(1)	37(1)	1(1)	2(1)	4(1)
C(2)	51(1)	45(1)	33(1)	1(1)	2(1)	2(1)
C(3)	46(1)	47(1)	35(1)	-3(1)	2(1)	2(1)
N(4)	56(1)	46(1)	39(1)	-5(1)	2(1)	-1(1)
C(5)	62(1)	47(1)	46(1)	3(1)	-2(1)	5(1)
C(6)	77(1)	51(1)	54(1)	-11(1)	7(1)	-9(1)
C(7)	81(1)	65(1)	36(1)	-3(1)	-5(1)	0(1)
C(8)	82(1)	45(1)	52(1)	3(1)	4(1)	-6(1)
O(9)	80(1)	43(1)	43(1)	1(1)	9(1)	-3(1)
C(10)	54(1)	40(1)	40(1)	-1(1)	5(1)	0(1)
N(11)	87(1)	51(1)	44(1)	-1(1)	19(1)	1(1)
O(12)	102(1)	58(1)	42(1)	3(1)	19(1)	-9(1)

Table 5. Hydrogen coordinates (x 10^4) and isotropic displacement parameters ($Å^2$x 10^3) for MDACC.

	x	y	z	U(eq)
H(5A)	-280(40)	6570(20)	5941(18)	48(4)
H(5B)	310(60)	8010(20)	6140(20)	64(5)
H(5C)	3020(50)	7230(19)	5480(19)	54(5)
H(6A)	5650(70)	7900(30)	8850(30)	97(8)
H(6B)	2390(80)	8380(30)	8680(30)	96(9)
H(6C)	4410(70)	8710(30)	7460(30)	89(8)
H(7A)	5910(80)	5970(30)	9650(30)	94(8)
H(7B)	3400(70)	5120(30)	9820(30)	88(8)
H(7C)	2580(70)	6420(30)	9930(30)	91(7)
H(8A)	-1610(90)	1460(30)	7450(30)	111(9)
H(8B)	1830(70)	1310(30)	8160(30)	93(8)
H(8C)	1440(70)	910(30)	6550(30)	97(8)

Table 6. Torsion angles [°] for MDACC.

O(12)-C(1)-C(2)-C(3)	10.8(2)
O(9)-C(1)-C(2)-C(3)	-171.35(12)
O(12)-C(1)-C(2)-C(10)	-175.38(16)
O(9)-C(1)-C(2)-C(10)	2.43(18)
C(10)-C(2)-C(3)-N(4)	27.2(2)
C(1)-C(2)-C(3)-N(4)	-159.34(13)
C(10)-C(2)-C(3)-C(7)	-150.60(15)
C(1)-C(2)-C(3)-C(7)	22.9(2)
C(2)-C(3)-N(4)-C(5)	17.3(2)
C(7)-C(3)-N(4)-C(5)	-164.83(15)
C(2)-C(3)-N(4)-C(6)	-165.95(15)
C(7)-C(3)-N(4)-C(6)	11.9(2)
O(12)-C(1)-O(9)-C(8)	3.9(2)
C(2)-C(1)-O(9)-C(8)	-174.02(13)
C(3)-C(2)-C(10)-N(11)	68(3)
C(1)-C(2)-C(10)-N(11)	-106(3)

50% probability thermal ellipsoid plot of MDACC showing atom labels. Hydrogen atoms are shown as arbitrary sized spheres.

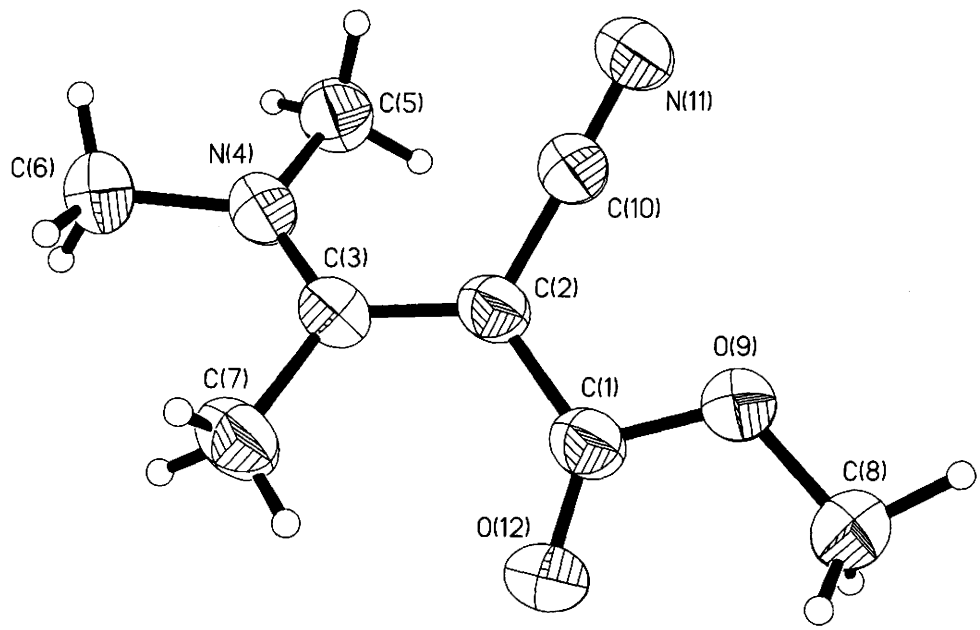

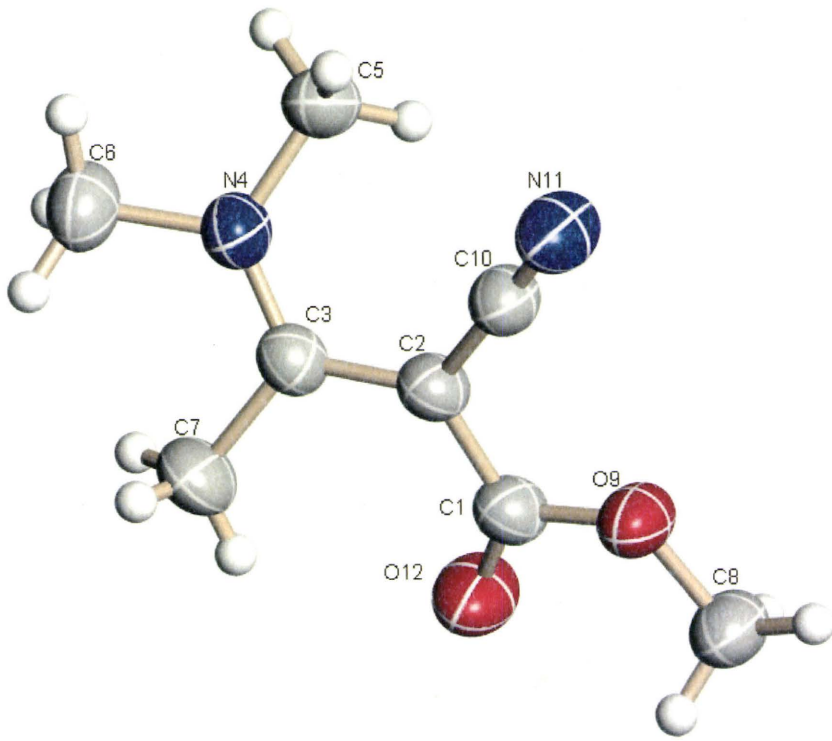
C5
C6
N4
N11
C10
C3
C2
C7
O9
C1
O12
C8

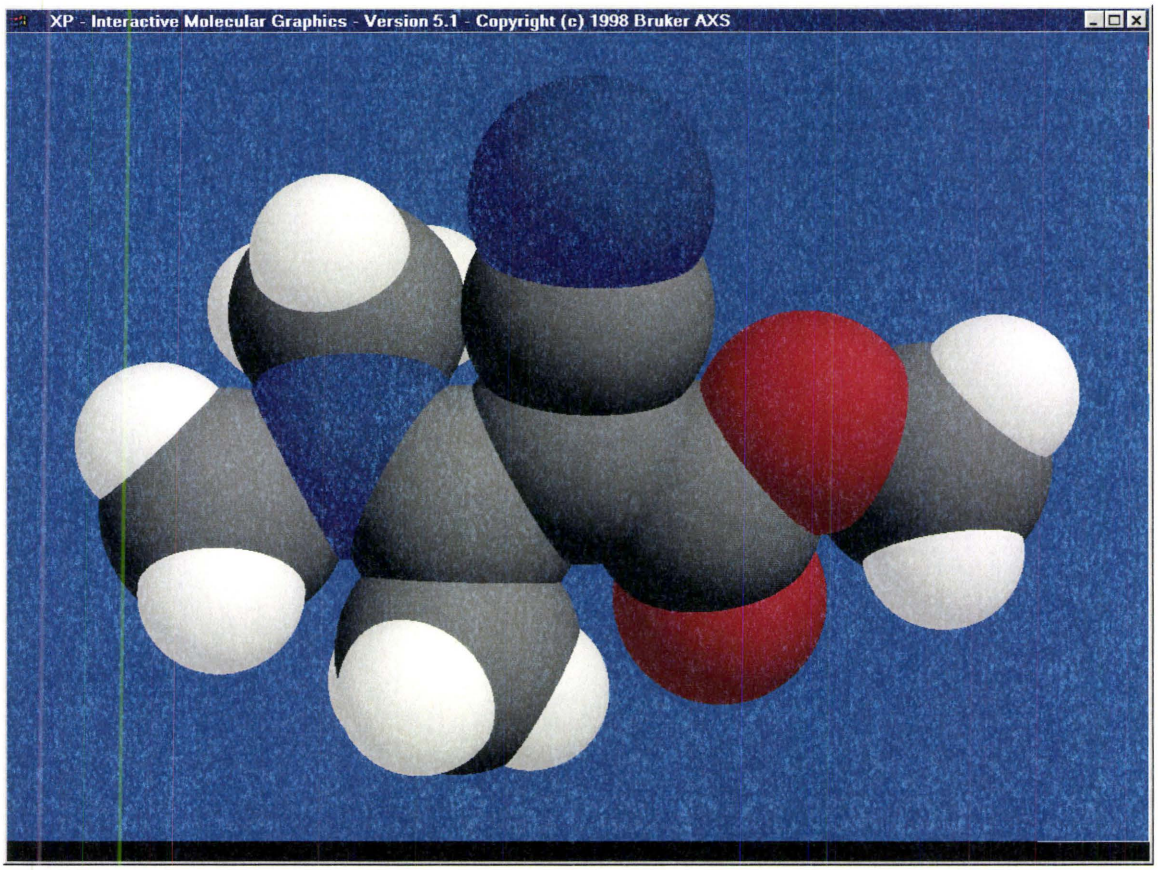
XP - Interactive Molecular Graphics - Version 5.1 - Copyright (c) 1998 Bruker AXS

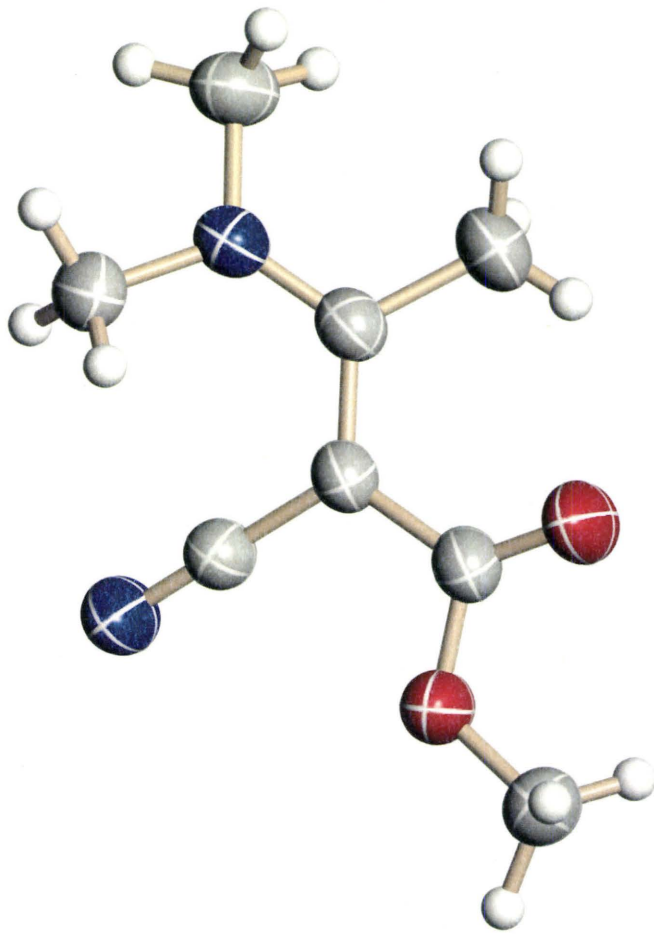

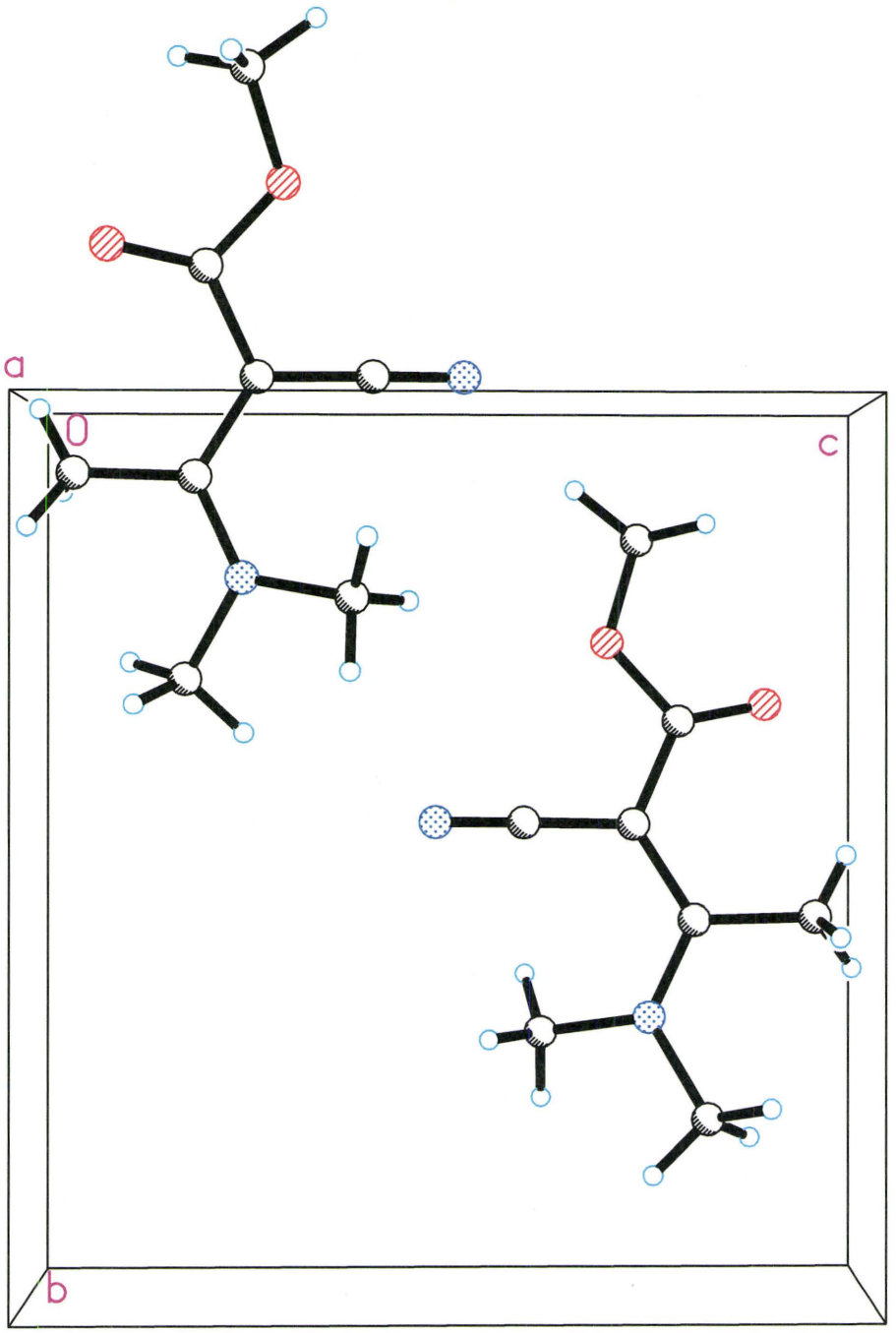
a
0
c
b

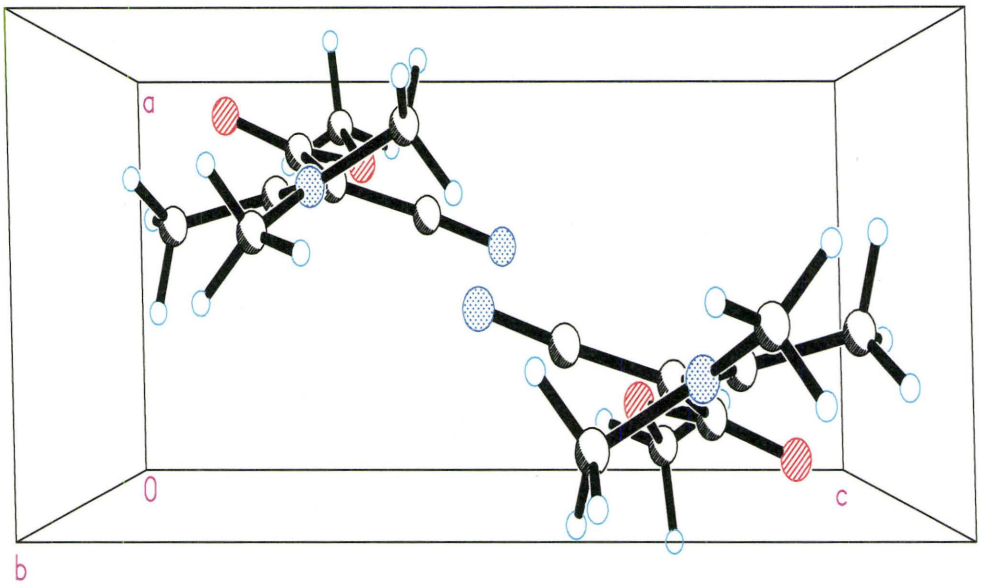
a
0
b
c

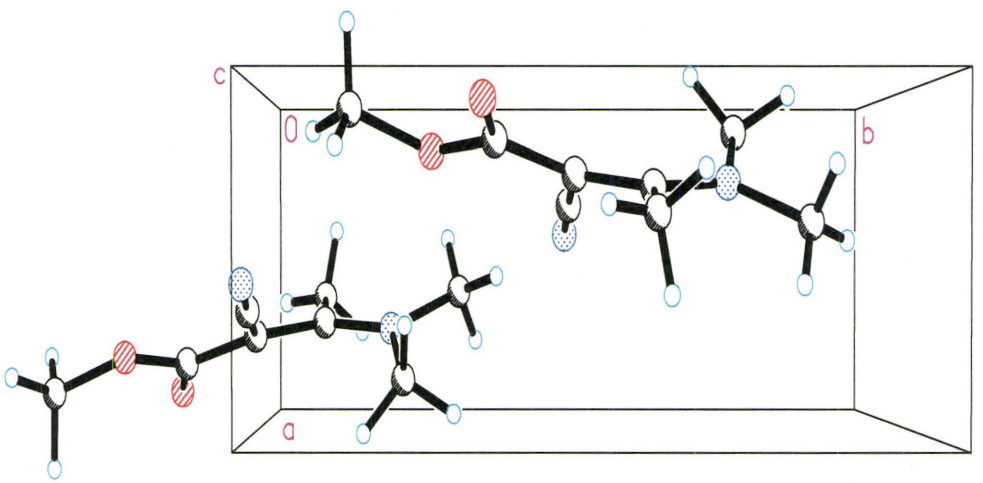
c
0
b
a

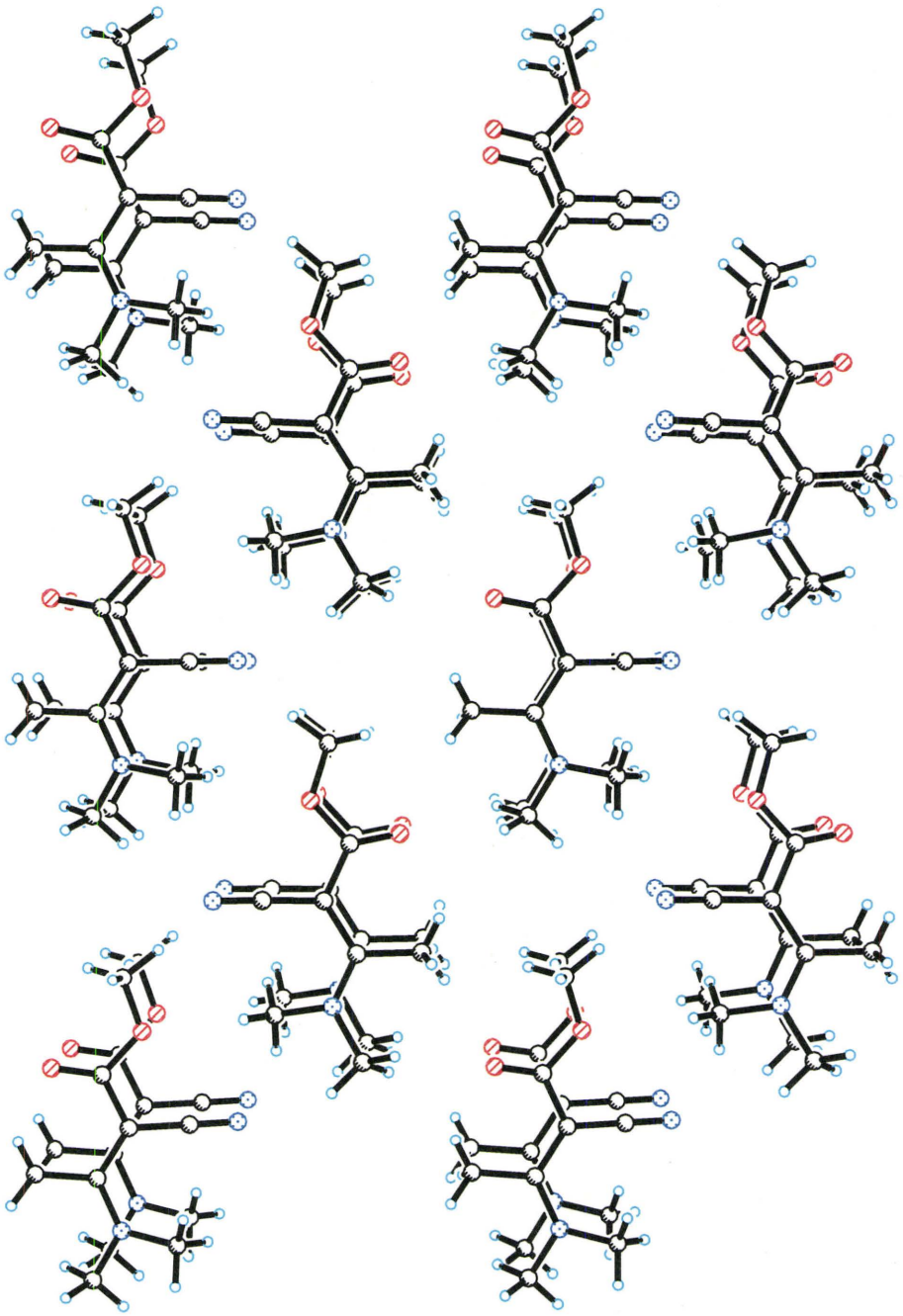

Table 7a – Eyring Raw Data for MDACC in different solvents E – Z configuration

1000/Temp K	LN(rate/temp) Toluene	LN(rate/temp) C_3D_6O	LN(rate/temp) CD_3CN	LN(rate/temp) CD_2Cl_2
3.424	-3.760			
3.347	-3.320			
3.304	-3.073			
3.253	-2.781			
3.189	-2.470			
3.069	-1.802			
3.900		-3.383		
4.339		-6.595		
3.732		-2.673		
3.656		-2.240		
3.606		-2.019		
3.522		-1.521		
3.451		-1.115		
3.383		-0.678		
3.323		-0.312		
3.259		0.007		
3.730			-1.583	
3.658			-1.144	
3.597			-0.753	
3.526			-0.349	
4.371				-7.265
4.162				-5.675
4.239				-6.156
3.818				-3.514
3.730				-3.206
3.658				-2.706
3.597				-2.424
3.418				-1.483
3.363				-1.195
3.305				-0.875
3.243				-0.442

Table 7b. Eyring Raw Data for MDACC in different solvents E – Z configuration

1000/Temp K	LN(rate/temp) $CdCl_3$	LN(rate/temp) THF	LN(rate/temp) MeOd
4.119	-6.264		
3.956	-5.128		
3.597	-2.921		
3.526	-2.568		
3.471	-2.252		
3.418	-1.936		
3.363	-1.601		
3.305	-1.293		
3.243	-1.021		
3.183	-0.636		
3.992		-3.348	
3.900		-3.016	
3.810		-2.638	
3.732		-2.250	
3.656		-1.914	
4.314			-2.673
4.183			-2.075
4.084			-1.559
3.994			-1.116
3.894			-0.537
3.818			0.102

Table 8a. Eyring plot data for MDACC Z-Z' conformation in different solvents

1000/Temp	LN (rate/Temp)) THF	LN(rate/Temp) CD_2Cl_2	Ln(rate/Temp) CD_3CN
4.802			
4.306	-6.413		
4.197	-4.853		
4.092	-4.048		
3.993	-3.203		
3.901	-2.411		
3.81	-1.696		
3.732	-1.005		
4.315		-6.36195	
4.183		-5.69982	
4.084		-4.54513	
3.994		-3.80009	
3.895		-3.17786	
3.819		-2.42267	
3.731		-1.71997	
3.658		-1.08896	
3.598		-0.49164	
3.527		0.105184	
3.418		0.934749	
3.363		1.563502	
3.305		2.581803	
3.243		3.255961	
4.375			-6.299
4.315			-5.973
4.183			-5.487
4.084			-4.625
3.994			-4.041
3.895			-3.063
3.819			-2.602
3.731			-1.954
3.658			-1.362
3.598			-0.76
3.527			-0.167

Table 8b. Eyring plot data for MDACC Z-Z' conformation in different solvents

1000/Temp	LN(rate/Temp) CDCl3	LN(rate/Temp) methanol-d_4	LN(rate/Temp) acetone-d_6
3.184	4.215		
3.243	3.503		
3.305	2.238		
3.363	1.549		
3.418	0.815		
3.472	0.292		
3.527	-0.22		
3.598	-0.828		
3.658	-1.262		
3.731	-1.856		
3.819	-2.569		
3.994	-4.279		
4.084	-4.783		
4.315		-5.378	
4.183		-4.56	
4.084		-3.814	
3.994		-2.973	
3.895		-2.413	
3.819		-1.761	
3.731		-0.986	
4.42			-6.338
4.306			-5.804
4.197			-5.003
4.089			-4.164
3.993			-3.549
3.901			-2.691
3.81			-2.044
3.732			-1.371
3.657			-0.698
3.607			-0.103
3.523			0.732
3.451			1.334
3.384			1.961
3.324			2.636
3.26			3.31

Table 9a. Eyring plot data for MDACC in different solvents E-E'

1000/Temp K	LN(rate/Temp) methylenechloride-d_2	LN(rate/Temp) acetonitrile-d_3	LN(rate/Temp chloroform-d
4.434	-2.951		
4.315	-2.268		
4.183	-1.334		
4.084	-0.664		
3.994	-0.042		
3.895	0.31		
3.819	0.947		
3.731	1.536		
3.658	2.067		
3.598	2.429		
3.527	2.644		
3.418	3.671		
4.375		-2.426	
4.315		-1.989	
4.183		-1.173	
4.084		-0.633	
3.994		-0.162	
3.895		0.403	
3.819		0.932	
3.731		1.438	
3.658		1.993	
3.598		2.615	
3.184			5.013
3.243			4.311
3.305			4.086
3.363			3.721
3.418			3.311
3.472			2.957
3.527			2.601
3.598			2.159
3.658			1.828
3.731			1.239
3.819			0.672
3.994			-0.703
4.084			-1.006

Table 9b. Eyring plot data for MDACC in different solvents E-E'

1000/Temp K	LN(rate/Temp methanol-d4	LN(rate/Temp) tetrahydrofuran-d_8	LN(rate/Temp) acetone-d6
4.549	-2.462		
4.434	-1.795		
4.315	-1.128		
4.183	-0.466		
3.895	1.542		
3.819	2.4386		
3.731	3.108		
4.306		-1.833	
4.197		-1.147	
4.092		-0.225	
3.993		0.326	
3.901		0.828	
3.81		1.291	
3.732		1.678	
4.42			-2.531
4.306			-1.922
4.197			-1.254
4.089			-0.632
3.993			-0.043
3.901			0.627
3.81			1.297
3.732			1.969
3.657			2.627
3.607			3.306
3.523			3.975

Table 10a. Raw Data Van't Hoff Plot for MDACC in different solvents

1000/Temp K	ln(K) CD_2Cl_2	ln(K) Acetone	ln(K) CD_3CN
4.433	-0.174		
4.314	-0.181		
4.183	-0.210		
4.084	-0.218		
3.994	-0.243		
3.894	-0.254		
3.818	-0.291		
3.730	-0.311		
3.658	-0.311		
3.597	-0.336		
3.418	-0.368		
3.363	-0.375		
3.305	-0.381		
3.243	-0.389		
4.419		-0.188	
4.305		-0.201	
4.197		-0.213	
4.089		-0.225	
3.992		-0.236	
3.900		-0.247	
3.810		-0.257	
3.732		-0.266	
3.656		-0.274	
3.606		-0.281	
3.522		-0.290	
3.451		-0.297	
3.383		-0.305	
3.323		-0.313	
3.259		-0.320	
4.375			-0.143
4.314			-0.158
4.183			-0.176
4.084			-0.194
3.994			-0.213
3.894			-0.226
3.818			-0.243
3.730			-0.257
3.658			-0.266
3.597			-0.274
3.526			-0.282
3.470			-0.296
3.411			-0.306

3.354			-0.316
3.298			-0.325
3.245			-0.334
3.193			-0.342
3.143			-0.351

Table 10b. Raw Data Van't Hoff Plot for MDACC in different solvents

1000/Temp K	ln(K) THF	ln(K) MeOH	ln(K) $CDCl_3$
4.41989	-0.169		
4.305705	-0.191		
4.197272	-0.211		
4.089143	-0.235		
3.992813	-0.252		
3.900917	-0.267		
3.81025	-0.281		
3.73204	-0.294		
3.656976	-0.314		
3.591309	-0.3291		
3.520507	-0.342		
3.451251	-0.355		
3.383522	-0.366		
3.323916	-0.378		
3.259984	-0.390		
3.219057	-0.398		
3.152088	-0.410		
3.101256	-0.420		
3.034441	-0.433		
4.548556		-0.017	
4.433607		-0.033	
4.314995		-0.048	
4.183225		-0.064	
4.084133		-0.080	
3.994408		-0.093	
3.894839		-0.109	
3.730647		-0.130	
3.658314		-0.140	
3.597769		-0.148	
3.526715		-0.158	
3.418219		-0.173	
3.36304		-0.181	
3.305239		-0.189	
3.243068		-0.1981	
4.663092		-0.0001	
4.548556			-0.098

4.663092			-0.070
4.183225			-0.190
4.084133			-0.214
3.994408			-0.237
3.894839			-0.262
3.81898			-0.282
3.730647			-0.311
3.597769			-0.340
3.526715			-0.349
3.418219			-0.381
3.47162			-0.365
3.36304			-0.397
3.305239			-0.40947313
3.243068			-0.41703174
3.183699			-0.43386458
3.658314			-0.32850407

List of acronym

acronym	meaning
NMR	Nuclear magnetic resonance
FID	Free induction decay
MDACC	Methyl 3-dimethylamino-2-cyanocrotonate
CIFIT	Selective Inversion Fit
MEXICO	McMaster Exchange on coupled systems
FT	Fourier Transform
RF	Radio-Frequency
DNMR	Dynamic Nuclear Magnetic Resonance
HMBC	Heteronuclear Multiple Bond Correlation
HMQC	Heteronuclear multiple Quantum coherence
BIRD	Bilinear rotation decoupling
CP MAS	Cross polarization magic angle spinning
EXSY	Exchange Spectroscopy
NOESY	Nuclear over Houser effect spectroscopy
NOE	Nuclear over Houser effect

Reference List

(1) Timothy D.W.Claridge *High-Resolution NMR Techniques in Organic Chemistry*; Pergamon: Oxford, 1999.

(2) Nelson, J. H. *Nuclear Magnetic Resonance Spectroscopy*; Prentice Hall: New Jersey, 2003.

(3) Zheng, Z.; Mayne, C. L.; Grant, D. M. *J.Magn.Reson.* **1993**, *103 A*, 268-281.

(4) Arata, Y.; Fukumi, T.; Fujiwara, S. *J.Chem.Phys.* **1969**, *51*, 859-862.

(5) Weinberg, I.; Zimmerman, J. R. *J.Chem.Phys.* **1955**, *23*, 748-749.

(6) Wishart, D. S.; Bigam, C. G.; Yao, J.; Abildgaard, F.; Dyson, H. J.; Oldfield, E.; Markley, J. L.; Sykes, B. D. *Journal of Biomolecular NMR* **1995**, *6*, 135-140.

(7) Macomber, R. S. *A Complete Introduction to Modern NMR Spectrometry*; John Wiley: New York, 1998.

(8) Bain, A. D. Early Development of Homonuclear 2D NMR (from the outside); In *The Encyclopedia of NMR*; Grant, D. M., Harris, R. K., eds. John Wiley: Chichester, 1996; pp 198-199.

(9) Derome, A. E. *Modern NMR Techniques for Chemistry Research*; Pergamon Press: Oxford, 1988.

(10) Nakanishi, K. *One-dimensional and two-dimensional nmr spectra by modern pulse techniques*; University Science Books: Mill Valley, California, 1990.

(11) Tonelli, A. E. *NMR Spectroscopy and Polymer Microstructure. The Conformational Connection*; VCH Publishers: New York, 1989.

(12) Pople, J. A.; Schneider, W. G.; Bernstein, H. J. *High-Resolution Nuclear Magnetic Resonance*; McGraw-Hill Book Company, Inc.: New York, 1959.

(13) Kasler, F. *Quantitative Analysis by NMR*; Academic Press: New York, 1973.

(14) Bax, A. Two-dimensional NMR spectroscopy; In *Topics in carbon-13 NMR spectroscopy*; Levy, G. C., ed. John Wiley: New York, 1984; pp 199-238.

(15) Jackman, L. M.; Cotton, F. A. *Dynamic Nuclear Magnetic Resonance Spectroscopy*; Academic Press: New York, 1975.

(16) Sandstrom, J. *Dynamic NMR Spectroscopy*; Academic Press: London, 1982.

(17) Bain, A. D.; Duns, G. J.; Rathgeb, F.; Vanderkloet, J. *J.Phys.Chem.* **1995**, *99*, 17338-17343.

(18) Inglefield, P. T.; Krakower, E.; Reeves, L. W.; Stewart, R. *Mol.Phys.* **1968**, *15*, 65-86.

(19) Kaplan, J. I.; Fraenkel, G. *NMR of Chemically Exchanging Systems*; Academic Press: New York, 1980.

(20) Gutowsky, H. S.; Saika, A. *J.Chem.Phys.* **1953**, *21*, 1688-1694.

(21) Fauconnier, T.; Bain, A. D.; Hazendonk, P.; Bell, R. A.; Lock, C. J. L. *Can.J.Chem.* **1998**, *76*, 426-430.

(22) Bain, A. D. *Prog.Nucl.Magn.Reson.Spectrosc.* **2003**, *43*, 63-103.

(23) Solomon, I. *Phys.Rev.* **1955**, *99*, 559-565.

(24) Mackor, E. L.; MacLean, C. *Prog.Nucl.Magn.Reson.Spectrosc.* **1967**, *3*, 129-157.

(25) Kaplan, J. I. *J.Chem.Phys.* **1958**, *29*, 462.

(26) Schotland, J.; Leigh, J. S. *J.Magn.Reson.* **1983**, *51*, 48-55.

(27) Shvo, Y.; Shanan-Atidi, H. *J.Am.Chem.Soc.* **1969**, *91*, 6689-6696.

(28) Shvo, Y.; Shanan-Atidi, H. *J.Am.Chem.Soc.* **1969**, *91*, 6683-6689.

(29) Shanan-Atidi, H.; Bar-Eli, K. H. *J.Phys.Chem.* **1970**, *74*, 961-963.

(30) Dwyer, T.; Norman, J. E.; Jasien, P. G. *J.Chem.Ed.* **1998**, *75*, 1635-1640.

(31) Wiberg, K. B.; Wong, M. W. *J.Am.Chem.Soc.* **1993**, *115*, 1078-1084.

(32) Drakenberg, T.; Dahlqvist, K.-I.; Forsen, S. *J.Phys.Chem.* **1972**, *76*, 2178-2190.

(33) Abraham, M. H.; Grellier, P. L.; Abboud, J. M.; Doherty, R. M.; Taft, R. W. *Can.J.Chem.* **1988**, *66*, 2673-2686.

(34) Laszlo, P. *Prog.Nucl.Magn.Reson.Spectrosc.* **1967**, *3*, 231-402.

(35) Knuttel, A.; Balaban, R. S. *J.Magn.Reson.* **1991**, *95*, 309-319.

(36) Arnold, J. T. *Phys.Rev.* **1956**, *102*, 136-150.

(37) Bain, A. D. Manual for the SIMPLTN program. 1995.
Ref Type: Unpublished Work

(38) Allman, T.; Bain, A. D.; Garbow, J. R. *J.Magn.Reson.* **1996**, *123 A*, 26-31.

(39) Smith, S. A.; Levante, T. O.; Meier, B. H.; Ernst, R. R. *J.Magn.Reson.* **1994**, *106 A*, 75-105.

(40) Friebolin, H. *Basic One- and Two-dimensional NMR Spectroscopy*; VCH: Weinheim, 1993.

(41) Bain, A. D. Radiofrequency Pulses: Response of Nuclear Spins; In *The Encyclopedia of NMR*; Grant, D. M., Harris, R. K., eds. John Wiley: Chichester, 1996; pp 3944-3949.

(42) Claridge, T. D. W. *High Resolution NMR Techniques in Organic Chemistry*; Pergamon Press: Oxford, 1999.

(43) Bodenhausen, G.; Freeman, R. *J.Am.Chem.Soc.* **1978**, *100*, 320-321.

(44) Ernst, R. R.; Bodenhausen, G.; Wokaun, A. *Principles of Nuclear Magnetic Resonance in One and Two Dimensions*; Clarendon Press: Oxford, 1987.

(45) Cowan, B. P. Nuclear magnetic resonance and relaxation. 117-121. 1997. Cambridge, Cambridge University Press.
Ref Type: Serial (Book,Monograph)

(46) Torchia, D. A.; Szabo, A. *J.Magn.Reson.* **1982**, *49*, 107-121.

(47) Jackman, L. M. Rotation about partial double bonds in organic molecules; In *Dynamic Nuclear Magnetic Resonance Spectroscopy*; Jackman, L. M., Cotton, F. A., eds. Academic Press: New York, 1975; pp 203-252.

(48) Bain, A. D. Magnetic Resonance: Chemical Exchange Effects in NMR; In *Encyclopedia of Spectroscopy and Spectrometry*; Lindon, J., Tranter, G., Holmes, J., eds. Academic Press: London, 2000.

(49) Bain, A. D. NMR methods for studying exchanging systems; In *Encyclopedia of Chemical Physics and Physical Chemistry*; Moore, J. H., Spencer, N. D., eds. Institute of Physics: Philadelphia, 2001; pp 1847-1869.

(50) Mladenov, G.; Dimitrov, V. S. *Magn.Reson.Chem.* **2001**, *39*, 672-680.

(51) Vasavada, K. V.; Kaplan, J. I. *J.Magn.Reson.* **1985**, *62*, 37-41.

(52) Sandstrom, J. *Top.Stereochem.* **1983**, *14*, 83-181.

(53) Alkorta, I.; Wentrup, C.; Elguero, J. *J.Molec.Struct.(Theochem)* **2002**, *585*, 27-34.

(54) Bernhardt, P. V.; Koch, R.; Moloney, D. W. J.; Shtaiwi, M.; Wentrup, C. *J.Chem.Soc.Perkin Trans.2* **2002**, 515-523.

(55) Pappalardo, R. R.; Marcos, E. S.; Ruiz-Lopez, M. F.; Rinaldi, D.; Rivail, J.-L. *J.Am.Chem.Soc.* **1993**, *115*, 3722-3730.

(56) Smith, M. A.; Jasien, P. G. *J.Molec.Struct.(Theochem)* **1998**, *429*, 131-141.

(57) Mannschreck, A.; Koelle, U. *Tetrahedron Lett.* **1967**, *10*, 863-867.

(58) Shvo, Y.; Taylor, E. C.; Bartulin, J. *Tetrahedron Lett.* **1967**, *34*, 3259-3265.

(59) Osman, R.; Shvo, Y. *Tetrahedron* **1978**, *34*, 2321-2325.

(60) Koelle, U.; KOLB, B.; Mannschreck *Chem.Ber.* **1980**, *113*, 2545.

(61) Uray, G.; Wolfbeis, O. S.; Junek, H. *J.Molec.Struct.* **1979**, *54*, 77.

(62) Bakhmutov, V. I.; Burmistrov, V. A. *Org.Magn.Reson.* **1979**, *12*, 185.

(63) Bloch, F.; Hansen, W. W.; Packard, M. E. *Phys.Rev.* **1946**, *69*, 127.

(64) Bloch, F.; Siegert, A. *Phys.Rev.* **1940**, *57*, 522-527.

(65) Bloch, F.; Hansen, P. E.; Packard, M. E. *Phys.Rev.* **1946**, *70*, 474-485.

(66) Bodenhausen, G.; Ernst, R. R. *J.Am.Chem.Soc.* **1982**, *104*, 1304-1309.

(67) Bain, A. D.; Cramer, J. A. *J.Magn.Reson.* **1996**, *118 A*, 21-27.

(68) Bain, A. D.; Cramer, J. A. *J.Phys.Chem.* **1993**, *97*, 2884-2887.

(69) Ding, K. *Magn.Reson.Chem.* **2000**, *38*, 321-323.

(70) Adhikesavalu, D.; Kamath, N. U.; Venkatesan, K. *Proceedings of the Indian Academy of Sciences (Chemical Sciences)* **1983**, *92*, 449-456.

(71) Perrin, C. L.; Dwyer, T. *Chem.Rev.* **1990**, *90*, 935-967.

(72) Orrell, K. G.; Sik, V. *Annu.Rep.NMR Spectrosc.* **1993**, *27*, 103-171.

(73) Aguirre, G.; Somanathan, R.; Hellberg, L.; Dwyer, T.; North, R. *Magn.Reson.Chem.* **2003**, *41*, 131-134.

(74) Jeener, J.; Meier, B. H.; Bachmann, P.; Ernst, R. R. *J.Chem.Phys.* **1979**, *71*, 4546-4553.

(75) Rossi, C. Selective relaxation techniques in biological NMR; In *Encyclopedia of Nuclear Magnetic Resonance*; 1996; pp 4237-4246.

(76) Freeman, R.; Wittekoek, S. *J.Magn.Reson.* **1969**, *1*, 238-276.